JPL Publication 95-3

An Atlas of Monthly Mean Distributions of SSMI Surface Wind Speed, AVHRR/2 Sea Surface Temperature, AMI Surface Wind Velocity, TOPEX/POSEIDON Sea Surface Height, and ECMWF Surface Wind Velocity During 1993

D. Halpern
L. Fu
W. Knauss
G. Pihos
Jet Propulsion Laboratory
Pasadena, California

O. Brown
University of Miami
Miami, Florida

M. Freilich
Oregon State University
Corvallis, Oregon

F. Wentz
Remote Sensing Systems
Santa Rosa, California

January 1995

National Aeronautics and
Space Administration

Jet Propulsion Laboratory
California Institute of Technology
Pasadena, California

The research described in this publication was carried out, in part, by the Jet Propulsion Laboratory, California Institute of Technology, under a contract with the National Aeronautics and Space Administration.

ACKNOWLEDGMENTS

Many people contributed to the preparation of the data sets displayed in the atlas, and we thank them for their tremendous support. James Brown (RSMAS) and Joanie Splain (RSMAS) participated in processing the SST data. Dr. Scott Dunbar (JPL) processed the AMI wind data. Akiko Hayashi (JPL) processed the TOPEX/POSEIDON data. Charles Walton (NESDIS) kindly sent validation results of the SST data product. We are extremely grateful to NASA (NAGW-273 (OB), NAGW-3062 (MF), JPL Contract 959351 (MF), UPN 578-22-24 (LF, GP), UPN 428-82-19 (DH, WK), NASW-4714 (FW)), particularly Martha Maiden (NASA Headquarters), and to ONR (N00014-89-J-1144 (OB)) for their continued support of our research.

CONTENTS

ABSTRACT

The following monthly mean global distributions for 1993 are presented with a common color scale and geographical map: 10-m height wind speed estimated from the Special Sensor Microwave Imager (SSMI) on a United States (U.S.) Air Force Defense Meteorological Satellite Program (DMSP) spacecraft; sea surface temperature estimated from the Advanced Very High Resolution Radiometer (AVHRR/2) on a U.S. National Oceanic and Atmospheric Administration (NOAA) satellite; 10-m height wind speed and direction estimated from the Active Microwave Instrument (AMI) on the European Space Agency (ESA) European Remote Sensing (ERS-1) satellite; sea surface height estimated from the joint U.S. - France Topography Experiment (TOPEX)/POSEIDON spacecraft; and 10-m height wind speed and direction produced by the European Center for Medium-Range Weather Forecasting (ECMWF). Charts of annual mean, monthly mean, and sampling distributions are displayed.

1 INTRODUCTION

This is the seventh volume of a series of annual summaries (Halpern *et al.*, 1991, 1992a, 1992b, 1993a, 1993b, 1994) of global distributions of surface oceanographic variables.

Progress in climate research depends on the availability of a variety of geophysical data sets to describe the boundary conditions and forcing functions of the climate system. The importance of long-period global data sets is highlighted in the United States (U.S.) National Aeronautics and Space Administration (NASA) Earth Observing System (EOS) and the U.S. Committee on Earth and Environmental Sciences (CEES) Global Change Research Program. The unique perspective from space provides the opportunity for observations well suited for the global ocean, which is an essential component of the climatic system and which remains severely undersampled.

Stommel and Fieux (1978), in their guide to oceanographic atlases, stated that "the oceanographic atlas is one of the main tools of the oceanographer." Because of the scarcity of oceanographic data, very few atlases cover the world ocean, and none provide monthly mean distributions for a particular year.

Since about ten years ago, substantial advances in remote and *in situ* techniques to record temperature, sea level, horizontal current, and surface wind have helped define annual cycles and interannual variations. Innovative ideas of how the ocean and atmosphere are coupled together occurred in parallel with new instrumentation. Analyses of monthly mean global distributions of surface oceanographic variables are becoming *de rigueur*.

Although both satellite- and ground-based recording systems provide essential information for global climate studies, satellite-borne instrumentation yields unprecedented spatial and temporal coverage of the global ocean. This report contains annual and monthly mean distributions for 1993 of satellite measurements of surface wind speed, surface wind velocity, sea surface temperature, and sea surface height. Very little averaging or interpolation of the data was made in order to retain the sampling characteristics of each data set. The report also displays surface wind velocity computed by a numerical forecast-analysis system.

2 DATA PROCESSING

2.1 SSMI Surface Wind Speed

The Special Sensor Microwave Imager (SSMI) is a 7-channel, 4-frequency, linearly polarized, passive microwave radiometer flown on U.S. Air Force Defense Meteorological Satellite Program (DMSP) spacecraft in a circular sun-synchronous near-polar orbit at an altitude of approximately 860 km and orbit period of 102.0 min. The first SSMI was mounted on the F8 DMSP spacecraft and was no longer used for wind speed data after December 1991. The second SSMI was launched on the F10 DMSP spacecraft on 1 December 1990. Caution is advised in creating a combined F8 and F10 SSMI wind speed data set (Halpern and Wentz, 1994) because the orientation of the SSMI on each spacecraft differed by 180° relative to the surface wind direction and, also, the spacecraft orbits were not identical. The nearly 1400-km swath of SSMI produces complete coverage between 87°36'S to 87°36'N every 3 days (Halpern *et al.*, 1992a). Each of the 7 separate passive radiometers measures naturally occurring microwave emissions from land, water and ice surfaces and from the intervening atmosphere. The SSMI receives both vertical and horizontal linearly polarized radiation at 19.3, 37.0 and 85.5 GHz and vertical only at 22.2 GHz.

The emitted microwave radiation at the ocean surface is affected by roughness of the sea surface, which is correlated with the near-surface wind speed. Attenuation of 37-GHz radiation propagating from the sea surface to the satellite is small, except when an appreciable amount of rain in the atmosphere scatters the 37-GHz radiation. The Wentz (1992) algorithm relates wind speed (m s^{-1}) at 19.5-m height to the 37-GHz brightness temperatures, which are computed from the SSMI 37-GHz horizontal and vertical polarized radiance measurements, and to the radiative transfer and absorption between the sea surface and SSMI. The wind speed is determined by the

Newton iteration method. A "first-guess" value of 8 m s^{-1}, which represents the typical wind speed over the ocean, is independent of the estimated wind speed. Convergence is defined when the difference between successive iterations of wind speed becomes less than 0.05 m s^{-1}. Convergence is usually found after 3 to 5 iterations. If convergence is not reached after 10 iterations, then the measured brightness temperatures are considered erroneous or caused by heavy rain. SSMI wind speeds referenced to 10-m height, which are equal to 94.3% of wind speed (Wentz, 1989), are used in the report.

2.1.1 Cross-Calibration of F8 and F10 SSMI Brightness Temperatures

Simultaneous F8 and F10 SSMI data were recorded during an approximate 1-year period from December 1990 to December 1991. Measurements associated with F8 and F10 orbit crossovers were used to minimize the error caused by space and time mismatches. A crossover is the region where the F8 and F10 data overlap with about a maximum time difference of 30 min, which is believed small enough that the effect on the results of the comparison is negligible.

The incidence angles of the F8 and F10 SSMI measurements differed by 0.2°, which corresponds to a brightness temperature difference of 0.2 K for horizontal polarization and 0.4 K for vertical polarization. After normalizing to the same incidence angle, the F10 37-GHz horizontal and vertical brightness temperatures, $(T_{B37^h})_{F10}$ and $(T_{B37^v})_{F10}$, respectively, were regressed according to the following model:

$$(T_{B37^h})_{F10} - (T_{B37^h})_{F8} = A_{37^h} + B_{37^h} (((T_{B37^h})_{F10} + (T_{B37^h})_{F8})/2)$$

and

$$(T_{B37^v})_{F10} - (T_{B37^v})_{F8} = A_{37^v} + B_{37^v} (((T_{B37^v})_{F10} + (T_{B37^v})_{F8})/2),$$

where $(T_{B37^h})_{F8}$ and $(T_{B37^v})_{F8}$ are the F8 37-GHz horizontal and vertical brightness temperatures, respectively. The regression coefficients, A_{37^h}, B_{37^h}, A_{37^v}, and B_{37^v}, were 0.44 K, 0.00165, -0.01 K, and 0.00335, respectively. The revised F10 horizontal and vertical brightness temperatures, $[(T_{B37^h})_{F10}]_{revised}$ and $[(T_{B37^v})_{F10}]_{revised}$, respectively, were

$$[(T_{B37^h})_{F10}]_{revised} = (1 - B_{37^h}) (T_{B37^h})_{F10} - A_{37^h}$$

and

$$[(T_{B37^v})_{F10}]_{revised} = (1 - B_{37^v}) (T_{B37^v})_{F10} - A_{37^v}.$$

The $[(T_{B37^h})_{F10}]_{revised}$ and $[(T_{B37^v})_{F10}]_{revised}$ are used in the wind speed retrieval algorithm so that the F8 and F10 wind speeds are independent of sensor differences, but they are not independent of the orientation of the SSMI relative to the surface wind direction (Halpern and Wentz, 1994).

2.1.2 Environmental Corrections

Environmental conditions reduce the amount of emitted radiation measured at the satellite. At 37 GHz, microwave emission from the ocean surface is masked by the emission and attenuation characteristics of rain. If the integrated liquid water content throughout the atmosphere is greater than 0.25 kg m^{-2}, then the Wentz (1989) algorithm is considered invalid because there would be too much radiative scattering from water droplets. Brightness temperatures measured within about 100 km of land, which is defined with a geographical data base, are not used to estimate surface wind speed because the emissivity of land is very different from that of water. For the same reason, surface wind speed within 200 km of the climatological-mean monthly position of the ice edge was not used in the report.

2.1.3 1/3° x 1/3° Monthly Mean Wind Speed

The Wentz (1989) data set contains wind speeds in nonoverlapping areas of 25 km x 25 km, which are arrayed across the 1394-km SSMI swath width. Geographical coordinates are provided at the center of each 25-km x 25-km region. SSMI wind speeds within nonoverlapping 1/3° x 1/3° squares were arithmetically averaged to form the basic data set for the report. Most of the 1/3° x 1/3° areas contained at least 50 wind speed values per month, or about 1 - 2 values per day.

The total number of 1/3° x 1/3° monthly averaged SSMI wind speeds displayed an annual cycle (Figure 1A). A maximum occurred each year during Southern Hemisphere summer when the ice cover around Antarctica was at a minimum. Beginning in 1992, the coverage of SSMI wind speed retrievals near the Antarctica ice zone was reduced because a different ice mask was used. Each 1/3° x 1/3° SSMI wind speed represented the arithmetic mean of several values. The total number of individual SSMI values was low in July 1987 and January 1988 (Figure 1B) because the instrument was not operated the whole of both months. The December 1987 data ended on 4 December because of a 40-day off-period to avoid possible damage to the SSMI by increased solar heating of the bearing and power transfer assembly (Hollinger *et al.*, 1990). During subsequent winters, the DMSP spacecraft solar arrays were repositioned and the SSMI was not turned off. The F8 SSMI data set terminated on 18 December 1991 and, consequently, there are a smaller number of SSMI retrievals in December 1991 compared to those of previous months (Figure 1B) because F10 measurements were first used in January 1992.

2.1.4 Accuracy

The SSMI accuracy specification for wind speed retrievals under rain-free conditions is ± 2 m s^{-1} root-mean-square (rms) over the range 3 - 25 m s^{-1}. Wentz (1992) compared SSMI wind speeds with a National Oceanic and Atmospheric Administration (NOAA) National Data Buoy Center moored buoy wind data set prepared by Goodberlet *et al.* (1990), and found differences of zero bias and 1.6 m s^{-1} rms. Halpern (1993) reported that the bias and rms difference between monthly mean Wentz (1989) SSMI wind speeds and moored buoy wind observations were 0.25 m s^{-1} and 1.2 m s^{-1}, respectively. Different orientations of the SSMI on the F8 and F10 spacecraft relative to the surface wind direction caused differences between F8 and F10 SSMI wind speeds (Halpern and Wentz, 1994). Model functions different than Wentz' (1989) physically based algorithm exist. The Environmental Research and Technology (ERT) algorithm for SSMI surface wind speed did not meet the accuracy specification (Goodberlet *et al.*, 1990). Bates' (1991) statistical algorithm with brightness temperatures from five SSMI channels had a 1.1 m s^{-1} bias and a 1.8 m s^{-1} rms difference with moored buoy wind measurements.

2.2 AVHRR/2 Sea Surface Temperature

The NOAA satellite platforms (called NOAA-j where j is an integer) are in sun-synchronous orbits at altitudes of 833 or 870 km with ascending equatorial crossings at 0730 or 1400 local time. Odd-numbered NOAA satellites have a five-channel advanced very high resolution radiometer called AVHRR/2. Even-numbered satellites have a four-channel advanced very high resolution radiometer called AVHRR. The NOAA-11 AVHRR/2 was operational in 1993.

The AVHRR/2 scan rate is 360 swaths per min with a total field of view of ± 55.4° from nadir and with an effective ground resolution of 1.1 km at nadir in five co-registered bands. Two spectral channels are in the visible range (0.58 - 0.68 and 0.725 - 1.1 μm) and three in the infrared range (3.55 - 3.93 (*i. e.*, 3.7) μm, 10.3 - 11.3 (*i. e.*, 11) μm, 11.5 - 12.5 (*i. e.*, 12) μm).

Infrared radiation received by a satellite radiometer is determined primarily by the sea surface emissivity and temperature and by atmospheric transmittance. Infrared radiation emitted from the ocean surface at wavelengths of about 3.5 - 4.0 μm propagates through a dry atmosphere with little attenuation, while under similar conditions the radiation in the 10 - 12 μm window can have approximately 10 - 15% attenuation (Maul, 1985). Only about 30% of the emitted radiation at 10 - 12 μm is transmitted through a wet atmosphere with 5.5-cm precipitable water. The oceanic emissivity in both spectral bands is approximately constant and close to unity for small satellite zenith angles (sza) or nadir viewing. Emissivity changes with sza, but the change from near-unity is small for zenith angles less than 40° (Bramson, 1968). The NOAA AVHRR/2 algorithms assume unit emissivity for all bands and angles. Thus the amount of radiation emitted at the surface can be assumed to be proportional to the sea surface temperature (SST).

(A) Number of 1/3° x 1/3° SSMI 10-m Height Wind Speed Pixels per Monthly Global Distribution

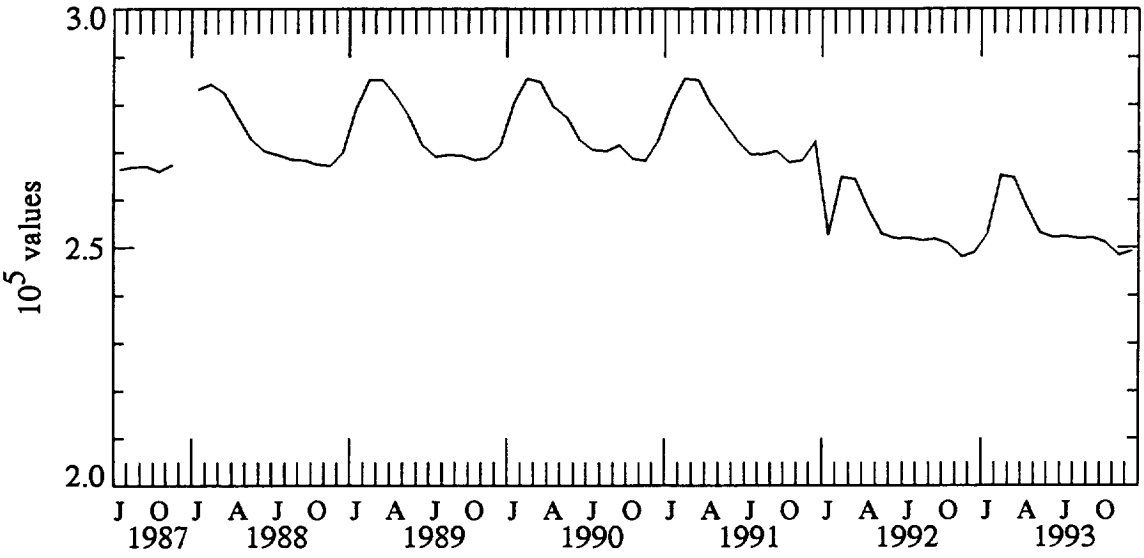

(B) Number of 25 km x 25 km SSMI 10-m Height Wind Speed Values per Monthly Global Distribution

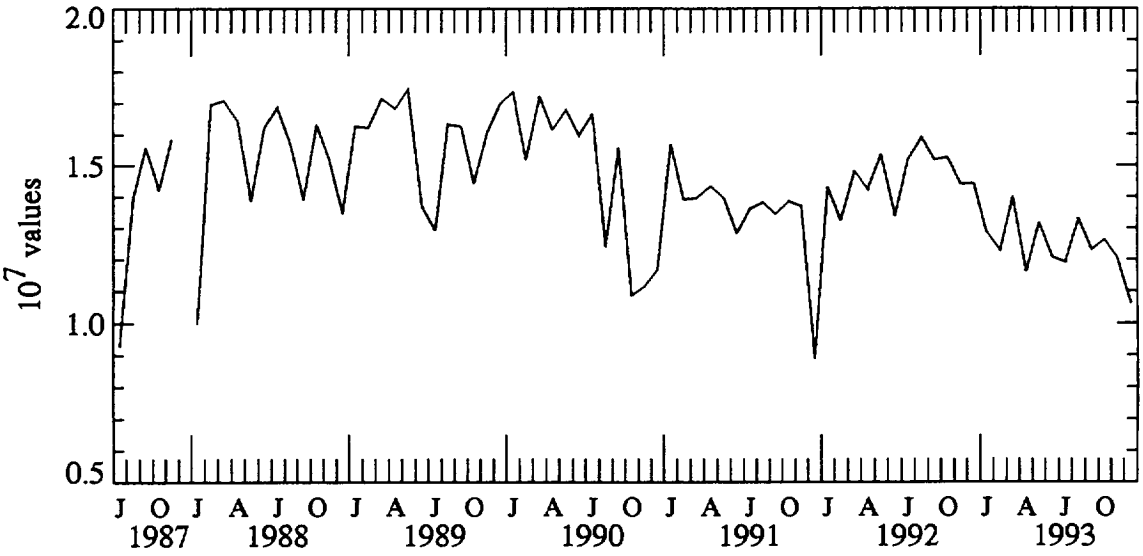

Figure 1. Time series of monthly totals of (A) number of pixels or picture elements and (B) number of 10-m height wind speeds.

Atmospheric absorption of emitted radiation at the AVHRR/2 infrared wavelengths is primarily by water vapor, which occurs in the lower levels of the atmosphere so that the atmosphere is perceived to be optically thin. The transmission of emitted radiation through the atmosphere differs for each AVHRR/2 wavelength so that the difference of satellite-measured radiances at two or more wavelengths is dependent on atmospheric absorber concentration. For small cumulative amounts of water vapor in the atmosphere, a linear combination of AVHRR/2 infrared radiation measurements recorded at the satellite yields an estimate of SST, originally known as multi-channel sea surface temperature (MCSST) (Maul, 1985; McClain *et al.*, 1985).

This report contains daytime SST data produced operationally by NOAA's National Environmental Satellite and Data Information Service (NESDIS). The procedure to compute the SST was described by McClain *et al.* (1985) and Kidwell (1991). Two SST algorithms were used in 1993. From 1 January - 31 May the daytime algorithm was (C. Walton, personal communication, 1994)

$$SST = 0.96219T_{11} + 0.083398T_{FLD}\,(T_{11} - T_{12}) + 0.65\,(T_{11} - T_{12})\,(SEC\ sza - 1) - 261.1$$

where SST is the sea surface temperature in °C, T_{11} and T_{12} are the brightness temperatures in K computed from radiance measurements at 11 μm (AVHRR/2 Channel 4) and 12 μm (AVHRR/2 Channel 5), respectively, SEC sza is secant of the satellite zenith angle, and T_{FLD} is the prior day's satellite field analysis temperature in °C. From 1 June - 31 December the daytime SST algorithm was (C. Walton, personal communication, 1994)

$$SST = 0.92323T_{11} + 0.082523T_{FLD}\,(T_{11} - T_{12}) + 0.46\,(T_{11} - T_{12})\,(SEC\ sza - 1) - 250.1.$$

2.2.1 Environmental Corrections

Major sources of error are water vapor absorption in the lower atmosphere and aerosol extinction. Radiance measurements from only cloud-free areas are processed by NOAA into SST. Very conservative cloud tests, which involve various combinations of the visible and infrared AVHRR/2 data, detect clouds so that cloud-free SSTs are computed (McClain *et al.*, 1985); on a typical day, less than 2% of the maximum possible number of SSTs are retained.

2.2.2 1/3° x 1/3° 28-Day Sea Surface Temperature

The 1.1-km AVHRR/2 observations are available only within areas containing a downlink ground station to receive high-resolution data transmission or from limited onboard local area coverage (LAC) recordings (≈ 12 minutes per orbit). Global AVHRR/2 measurements have an effective ground resolution of ≈ 4 km. A processor on board the NOAA spacecraft generates an average radiance for each channel from four 1.1-km elements within each nonoverlapping group of five consecutive 1.1-km measurements along a scan. Each daytime SST archived on the NESDIS global area coverage (GAC) data tapes represents the average SST within an 8-km x 8-km area, which occurs in a cloud-free environment at a variable spacing ranging from 8 km in the U.S. coastal waters to 25 km in the open ocean. The 8-km x 8-km SSTs are mapped at the University of Miami's Rosenstiel School of Marine and Atmospheric Sciences (RSMAS) onto a cylindrical equi-rectangular grid of 2048 (longitude) x 1024 (latitude) space elements (Olson *et al.*, 1988). At the equator the dimensions of each space-element are approximately 18 km x 18 km, and geographical coordinates are assigned to the center of the element. The origin of the grid is 90°N, 180°W. RSMAS produces SSTs averaged over 7 days. For this report, four consecutive 7-day values are arithmetically averaged to form 28-day mean SST values, except on one occasion (4 August - 1 September) when data from four weeks were employed but no data existed for the week of 18 August. A 1024 x 512 grid was created by computing the arithmetic mean of four 18-km x 18-km SSTs adjacent to each other in a 2-dimensional array. The average SSTs of 4-element groups, which were independent of each other, represent an approximate 1/3° x 1/3° SST data set.

A February-to-June decrease in the number of 1/3° x 1/3° monthly SST pixels occurred yearly (Figure 2A). The RSMAS SST data set contains the number of 8-km x 8-km values averaged to yield the 2048 x 1024 grid. The small number of 8-km x 8-km SST retrievals per month for about a year from July 1991 (Figure 2B) was caused by the extensive amount of

(A) Number of 36 km x 36 km AVHRR/2 Sea Surface Temperature Pixels per Monthly Global Distribution

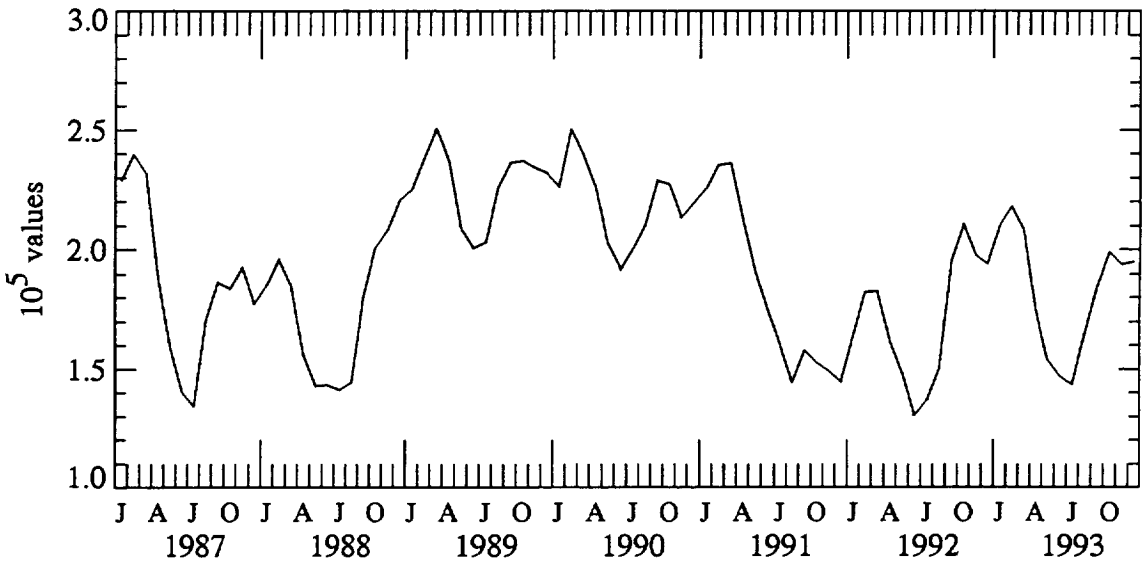

(B) Number of 36 km x 36 km AVHRR/2 Sea Surface Temperature Values per Monthly Global Distribution

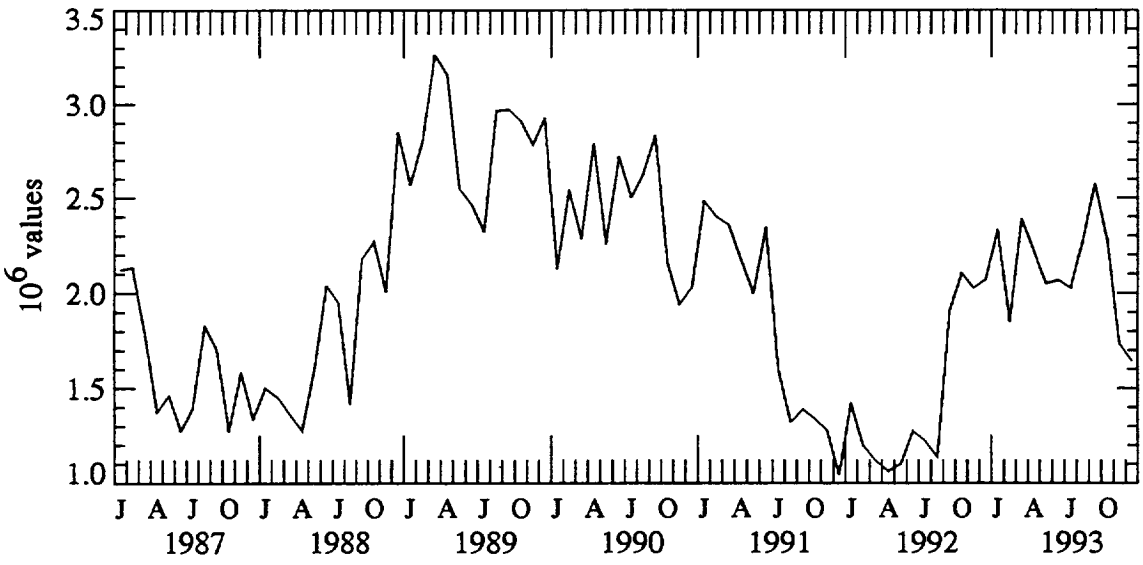

Figure 2. Time series of monthly totals of (A) number of pixels or picture elements and (B) number of sea surface temperature retrievals.

aerosols injected into the atmosphere by Mount Pinatubo on 15 June 1991 (Reynolds, 1993).

2.2.3 Accuracy

Coefficients used in the SST algorithm change as the operational satellite is replaced and on rare occasions when the validation procedure indicates a need for a change. NOAA continuously monitors the performance of the SST data product with satellite-tracked drifting buoy SST measurements, which are recorded within 25 km and 4 h of the location of the SST. During 1993, the average SST retrieval was 0.18°C smaller than the *in situ* measurement and the rms difference was 0.54°C for an average of 621 matchups per month throughout the global ocean (Table 1).

Table 1

Monthly mean bias and root-mean-square (rms) difference between daytime SST and drifting buoy sea surface temperature (DRIBU SST) global matchups during 1993. Bias = DRIBU SST - SST. (Courtesy of C. Walton, NOAA NESDIS)

Month	Number of Matchups	Bias °C	RMS Difference °C
Jan	582	0.29	0.55
Feb	512	0.26	0.61
Mar	671	0.24	0.59
Apr	562	0.26	0.57
May	628	0.31	0.54
Jun	607	0.04	0.57
Jul	642	0.11	0.52
Aug	749	0.13	0.50
Sep	818	0.13	0.51
Oct	860	0.07	0.52
Nov	460	0.11	0.55
Dec	359	0.21	0.49

2.3 AMI Surface Wind Velocity

The European Space Agency (ESA) first European Remote Sensing (ERS-1) satellite, launched 17 July 1991, carries an Active Microwave Instrument (AMI) that operates in synthetic aperture radar (SAR), Wind, and Wind-Wave modes. In Wind and Wind-Wave modes, the AMI functions as a scatterometer, acquiring sea surface backscatter normalized radar cross-section measurements (σ_o) from three azimuth angles for calculation of near surface wind velocity (speed and direction).

The ERS-1 AMI instrument is described by Francis *et al.* (1991). Measurements of σ_o at 5.3 GHz (C-band) are obtained from three antennas oriented at 45°, 90°, and 135° with respect to the satellite motion vector, yielding a measurement swath approximately 500 km wide and offset about 225 km from the nadir track. The ERS-1 AMI cannot operate simultaneously as a scatterometer and SAR, and backscatter measurements required to calculate wind velocity are available only when the instrument is operating in Wind or Wind-Wave modes.

2.3.1 Wind Velocity Calculation

At moderate incidence angles typical of the ERS-1 measurement swath, σ_o varies with wind speed and relative azimuth angle between the incident radiation and wind direction. Calculation of velocity for a given radar viewing geometry, a "wind retrieval" algorithm that yields a set of

possible vector winds from collocated σ_o measurements requires a "model function" relating σ_o to wind velocity solutions consistent with the σ_o measurements, and an "ambiguity removal" algorithm that allows selection of a unique wind velocity from among the (up to four) possible solutions determined at each location by the wind retrieval algorithm (Naderi *et al.*, 1991). Freilich and Dunbar (1993a) calculated 10-m neutral stability wind velocities, named CMODFD, from ERS-1 σ_o data using an empirical C-band model function (see Freilich and Dunbar (1993b) for a general description of the technique), a maximum likelihood wind retrieval algorithm (Naderi *et al.*, 1991 and references therein), and a variant of the circular median filter ambiguity removal algorithm (Schultz, 1990; Shaffer *et al.*, 1991). As the ERS-1 C-band system had very little upwind downwind discrimination skill, a limited initialization was performed by choosing the most likely ambiguity closest to the direction interpolated from contemporary operational NOAA National Meteorological Center (NMC) surface analyses. It should be noted that the NMC products were used only to initialize the circular median filter algorithm; in many cases, the final selected vectors obtained after application of the algorithm had significantly different directions from (and were not the closest ambiguities to) the NMC directions used to initialize the field.

2.3.2 1/3° x 1/3° Monthly Mean Wind Speed and 2.5° x 2.5° Monthly Mean Wind Direction

Although the spatial resolution of the ERS-1 σ_o measurements is about 50 km, σ_o values are reported on a 25-km grid within the measurement swath. Therefore, adjacent σ_o and, consequently, wind velocity measurements are not independent. Geographical coordinates are provided at the center of each 25-km x 25-km region. The 1-day average wind speed and the 1-day average east-west and north-south wind components were computed in nonoverlapping 1/3° x 1/3° areas. Then a monthly mean 1/3° x 1/3° wind speed data set was created, the daily east-west and north-south wind components were averaged within nonoverlapping 2.5° x 2.5° areas and monthly mean 2.5° x 2.5° wind components were computed from the daily data, and monthly mean wind speed and direction were calculated from the monthly mean wind components. Appendix A8 displays all monthly mean 1/3° x 1/3° average wind speeds and, for clarity, every alternate 2.5° x 2.5° average wind direction. The AMI 1/3° x 1/3° wind speeds are shown for possible comparison with the SSMI 1/3° x 1/3° wind speeds (Appendix A2). Direction arrows have two different lengths and colors: a black arrow is associated with wind speeds greater than 7 m s^{-1}, and a smaller white arrow corresponds to wind speeds less than 7 m s^{-1}.

The global coverage of 1/3° x 1/3° wind vectors (Figure 3A) displayed an abrupt increase in April 1992 because of a change in the ERS-1 orbit. From 1 January to 1 April 1992 the basic spacecraft sampling repeated at 3 day intervals. From approximately 2 April 1992 the orbit repeat was 35 days. No data were recorded 2-14 April 1992 during the Roll-Tilt Phase. Throughout 1993, the ERS-1 spacecraft was kept in a 35-day repeat orbit, yielding high consistent coverage each month (Figure 3A).

2.3.3 Accuracy

Fully calibrated σ_o measurements were first produced in March 1992, and no further changes were made by ESA afterwards. The Freilich-Dunbar CMODFD data set presented here is based on a consistent reprocessing of the ERS-1 data using a single model function and stable algorithms.

Initial intercomparisons between CMODFD and moored-buoy wind measurements have been made. During 1992 the rms difference between monthly mean collocated 2/3° x 2/3° CMODFD and moored-buoy wind components was about 1.25 m s^{-1}, correlation coefficient was about 0.9, and bias was 0.5 m s^{-1} (Halpern *et al.*, 1994).

2.4 TOPEX/POSEIDON Sea Surface Height

The joint United States and France TOPEX/POSEIDON satellite was launched on 10 August

(A) Number of 1/3° x 1/3° ERS-1 AMI Wind Vector Pixels per Monthly Global Distribution

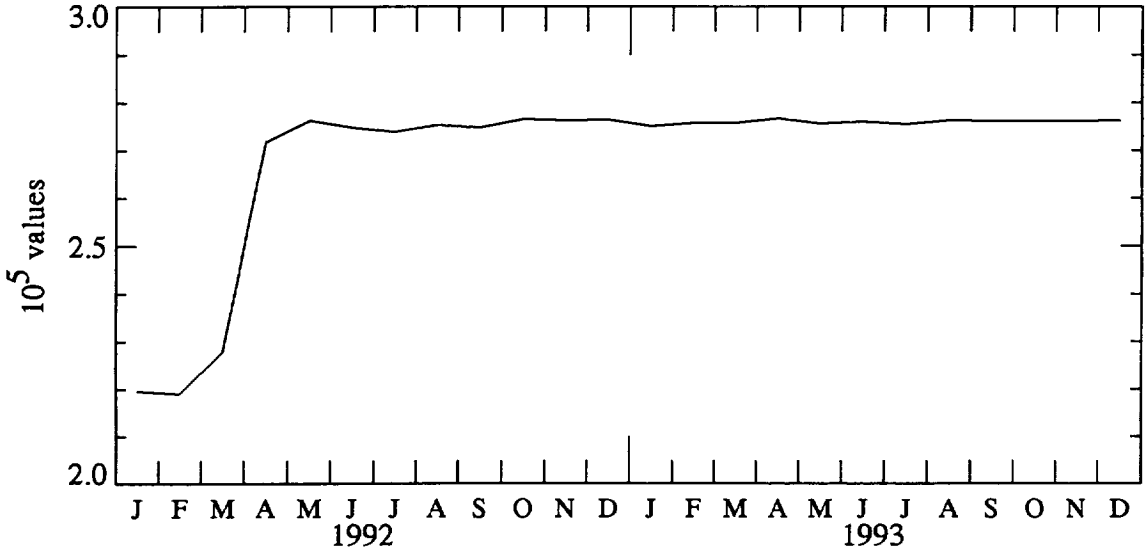

(B) Number of 25 km x 25 km ERS-1 AMI Wind Vector Values per Monthly Global Distribution

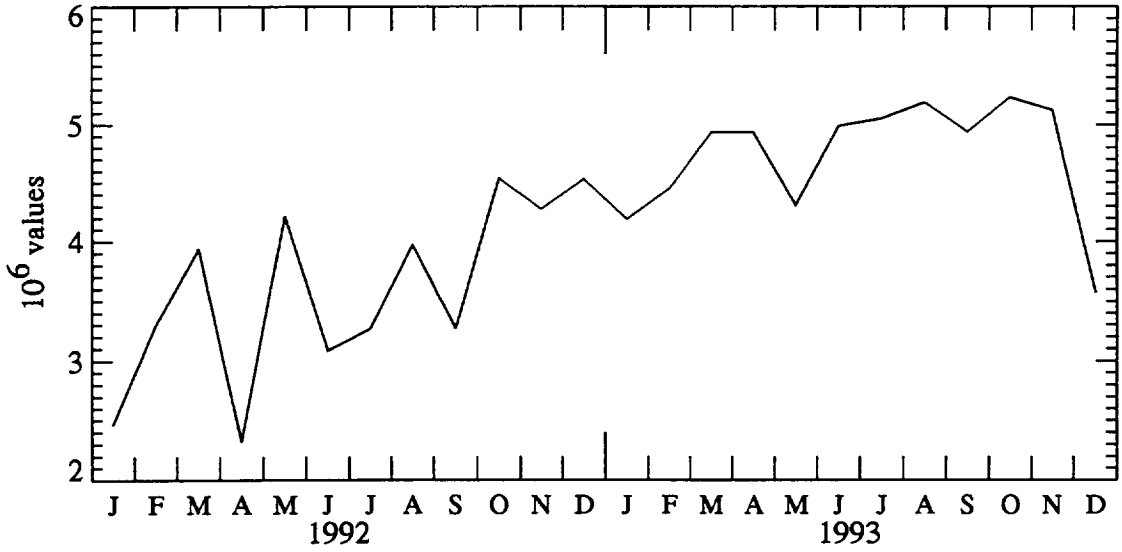

Figure 3. Time series of monthly totals of (A) number of pixels or picture elements and (B) number of 10-m height wind vectors.

1992 to make altimetric observations of the sea surface. Each orbit repeats within 1 km every 9.91564 days, which is a nominal 10-day repeat interval. Two altimeters operate alternately. The NASA altimeter, named ALT, operates approximately 90% of the time and has two frequencies (5.3 and 13.6 GHz) in order to directly measure the radar range delay caused by free electrons in the ionosphere. The Centre National d'Etudes Spatiale (CNES) 13.6-GHz solid-state altimeter, named SSALT, operates approximately 10% of the time. Since April 1993 the SSALT was operated for a 10-day repeat cycle approximately every 10 repeat cycles. The ALT and SSALT data returns have been greater than 98% without systematic data losses over any geographgic area.

The TOPEX/POSEIDON sea surface data set used in this report is based on the Geophysical Data Record (GDR) that was described by Callahan (1994). The technique is complex to convert a radar altimeter's travel time measurement between the satellite and the sea surface into an accurate estimate of the elevation of the sea surface relative to a reference ellipsoid, which becomes the oceanographic signal of interest. Numerous algorithms are involved. Data processing procedures, including application of environmental corrections, were the same for both TOPEX and POSEIDON measurements, unless otherwise noted.

2.4.1 Altimeter Measurement

Measurement noise associated with the altimeter measurement varies with significant wave height (SWH) because the electromagnetic radiation recorded at the spacecraft becomes more scattered when the SWH is larger. An altimeter directly measures SWH from the slope of the leading edge of the electromagnetic waveform, and these data are listed on the Callahan (1994) GDR. The ALT noise varies from 1.7 cm at 2-m SWH to 2-2.5 cm for SWH larger than 3 m (Fu *et al.*, 1994). The SSALT has a 20% higher noise level before 24 October 1993; afterwards, SSALT noise varies from 2 cm at 2-m SWH to 2.8 cm at 5-m SWH (Fu *et al.*, 1994).

The GDR contained 10 altimeter height measurements per s and a 1-s arithmetic mean altimeter height value was computed from the 10 per s values; very few of the 10 per s altimeter height measurements were rejected. The 1-s averaged altimeter height measurement is called H_{alt}, which is representative of circular areas with diameters between 3 and 12 km. H_{alt} forms the basic data set for subsequent data processing.

2.4.2 Orbit Height

Uncertainty in the radial component of the satellite orbit has long been the largest error source in satellite altimetry. Improvements in our knowledge of the earth's gravity field and an improved satellite tracking system, which included satellite laser ranging and ground-based Doppler orbitography and radiopositioning integrated by satellite (DORIS), created unprecented accuracy for orbit determination. The rms accuracy of the satellite height above the reference ellipsoid, H_{orbit}, is 3.5 cm (Tapley *et al.*, 1994). Most of the error is random and can be reduced by time-averaging. The systematic component, which is correlated geographically and cannot be reduced by time-averaging, is less than 2 cm.

2.4.3 Environmental Corrections

TOPEX/POSEIDON's altitude was approximately 1336 km above the sea surface and the round-trip travel time of the radar altimeter electromagnetic pulse between the sea surface and the satellite is affected by atmospheric and ionospheric conditions. Also, ocean surface waves complicate the interpretation of the returned radar pulse. In addition, the sea surface height relative to the reference ellipsoid,

$$SSH = H_{orbit} - H_{alt},$$

is influenced by vertical displacements caused by earth tides, ocean tides, and the static response of the sea surface to atmospheric pressure load (*i. e.*, the inverse barometer effect). Atmospheric and ionospheric effects on travel time produce an apparent lowering of the sea surface height, and the corrections are added to the altimeter range to yield the correct range.

The largest environmental corrections affecting the altimeter pulse are the travel-time delays or path lengthening caused by air molecules within the troposphere (*i. e.*, dry troposphere correction, H_{dry}) and by water vapor within the troposphere (*i. e.*, wet troposphere correction, H_{wet}). The global average of H_{dry} is about 225 cm (Chelton, 1988); H_{wet} is about 15 cm (Monaldo, 1990). Of all environmental corrections, H_{wet} is the most troublesome because the magnitude changes by about 10 - 15 cm over spatial scales which closely match mesoscale oceanographic phenomena (Emery *et al.*, 1990).

H_{dry} was computed from the surface atmospheric pressure, p_o, which was a data product of the European Center for Medium-Range Weather Forecasts (ECMWF) 12-hour, 2.5°-latitude x 2.5°-longitude global forecast-analysis system. This report uses the GDR values of H_{dry}. A rms 3 mb uncertainty in p_o produces an error in H_{dry} of about 0.7 cm.

H_{wet}, which is related to the total columnar water vapor content in the altimeter nadir path, was determined from brightness temperatures measured with the 3-frequency TOPEX Microwave Radiometer (TMR). This report uses H_{wet} values provided on the GDR. H_{wet} is smoothed over approximately 50 km during processing (Callahan, 1994). Comparison of TMR, ground-based water vapor radiometer, and radiosonde observations indicated that the H_{wet} rms accuracy was about 1.1 cm (Ruf *et al.*, 1994).

Ocean waves complicate the interpretation of the measurement of the two-way travel time of the radar altimeter pulse because the radar backscatter cross section is larger at wave troughs than at wave crests. Because an ocean wave signature is generally skewed with a flat trough and peaked crest, the returned power of the radar pulse is biased towards wave troughs. This correction is called electromagnetic (em) bias, H_{em}, and is related to wind speed and SWH for Gaussian wave heights. The $(H_{em})_{ALT}$ or $(H_{em})_{SSALT}$ rms accuracy is about 0.01 SWH (Rodriguez and Martin, 1994a; Gaspar *et al.*, 1994). A second correction caused by ocean waves is related to the non-Gaussian nature of the skewed sea surface height distribution, $H_{skewness}$, which is less than 2 cm rms and which is associated with horizontal dimensions larger than about 600 km (Rodriguez and Martin, 1994b; E. Rodriguez and O. Zanife, personal communication, 1994). $H_{skewness}$ is not considered in the data processing.

Free electrons in the ionosphere reduce the speed of the altimeter signal compared to the speed of light in a vacuum; the range correction caused by refraction from ionospheric electrons is denoted H_{ion}. This report uses H_{ion} values provided on the GDR and retrieved by the dual-frequency ALT or, when the SSALT is in operation, by the DORIS dual frequency measurements. For a typical 2-m SWH, the $(H_{ion})_{ALT}$ rms accuracy is about 0.7 cm, which could be reduced to 0.53 cm had spatial averages over distances smaller than 100 km been made because of the small variation of ionospheric free electrons associated with distances less than 100 km (Imel, 1994). The $(H_{ion})_{SSALT}$ rms accuracy is about 1.7 cm (Picot and Escudier, unpublished manuscript).

Ocean tide corrections, $H_{ocean\ tide}$, provided on the GDR were not used in this report, and a more accurate representation of $H_{ocean\ tide}$ was computed by Fu *et al.* (unpublished manuscript). This report used the solid-earth tide correction, $H_{solid\ tide}$, contained in the GDR, which was computed from the tide generating potential and its gradient over a 30-s interval along the groundtrack according to the method developed by Cartwright and Tayler (1971) and Cartwright and Edden (1973). For $H_{solid\ tide}$ the first-degree Love number was equal to 0.52 to account for resonance. Tide corrections, $H_{ocean\ tide} + H_{solid\ tide}$, are about 3 cm rms.

The weight of the atmosphere influences the height of the sea surface, and surface atmospheric pressure is used to compute an inverted barometer correction, $H_{barom\ pressure}$, which is defined by (Callahan, 1994)

$$H_{barom\ pressure}\ [mm] = -10.1\ [mm\ mb^{-1}]\ (p_o^* - 1013.3)\ [mb].$$

p_o^* is the surface atmospheric pressure computed from ECMWF analysis.

2.4.4 Corrected Sea Surface Height

The environmentally corrected TOPEX/POSEIDON sea surface height relative to the reference ellipsoid is defined by

$$SSH_{corrected} = H_{orbit} - H_{alt} - H_{solid\ tide} - H_{ocean\ tide} - H_{barom\ pressure} - H_{dry} - H_{wet} - H_{ion} - H_{em}$$

2.4.5 2/3° x 2/3° Monthly Mean Sea Surface Height

All ALT and SSALT data were used to compute monthly mean sea surface height variations from the annual mean. A 15.3-cm bias (Christensen *et al.*, 1994; Menard *et al.*, 1994), which was determined at two specialized verification sites, was defined to make the ALT and SSALT altimeter data sets consistent. Along each groundtrack, the $SSH_{corrected}$ values were resampled at 6 km intervals using a cubic spline. No interpolation was made over a data gap larger than 3 s (≈ 20 km). The groundtrack was repeated at nominal 10-day intervals. A time series of $SSH_{corrected}$ was associated with each fixed point, and the 1-year mean for 1993 was computed at each fixed point. Differences between the 10-day $SSH_{corrected}$ and the annual mean $SSH_{corrected}$ are called residuals, SSH'. All SSH' values with positions within nonoverlapping 2/3° x 2/3° squares were arithmetically averaged in calendar month intervals to form the monthly data set for the report.

The total number of 2/3° x 2/3° monthly averaged SSH' values was almost the same each month (Figure 4A). Each 2/3° x 2/3° monthly mean SSH' value represented the arithmetic mean of one to about 100 individual 10-day measurements. The total number of individual 10-day measurements used to compute the monthly mean SSH' varied by about 15% throughout 1993 (Figure 4B).

2.4.6 Accuracy

Over the global ocean the rms accuracy of individual SSH' measurements is about 4.5 cm (Fu *et al.*, 1994). The accuracy of monthly mean sea surface height variations depends on the number of values averaged because the error is proportional to the square root of the number of individual SSH' measurements employed in the calculation of the monthly mean. The error of the monthly mean SSH' varied from 0.75 cm for 36 individual 10-day SSH' values, which was typical, to 4.5 cm if only a single SSH' value occurred during the month, which rarely happened.

2.5 ECMWF Surface Wind Velocity

The 1987 to 1992 annual atlases contained 10-m height wind components that were produced at the European Center for Medium-Range Weather Forecasting (ECMWF) because no satellite surface wind vector data product was available until 1992. For continuity the ECMWF data product is included in this atlas. The ECMWF forecast-analysis system, like all operational atmospheric general circulation models, is continually being modified.

ECMWF analyses, instead of other model-generated results, were initially employed because Trenberth and Olson (1988) considered them to be the best operational global analyses available for 1988 for general use. Kalnay *et al.* (1990) showed that ECMWF northern hemisphere daily 1000- and 500-hPa rms height errors of 1-, 3-, and 5-day forecasts during August 1989 were smaller than that of NMC.

The area of each element of the ECMWF 144 x 73 grid is approximately 2.5° x 2.5°. ECMWF forecast-analyses of surface wind components at 10-m height were issued twice a day, at 0000 and 1200 GMT. Values of 1-day mean 2.5° x 2.5° wind speed and east-west and north-south components were used to compute the monthly mean wind speed and monthly mean wind components, respectively. Monthly mean wind direction was computed from the monthly mean wind components. Appendix A13 displays all 2.5° x 2.5° monthly mean wind speeds and, for clarity, every alternate 2.5° x 2.5° monthly mean wind direction. Direction arrows have two different lengths and colors: a black arrow is associated with wind speeds greater than 7 m s^{-1}, and a smaller white arrow corresponds to wind speeds less than 7 m s^{-1}.

(A) Number of 2/3° x 2/3° TOPEX/POSEIDON Sea Surface Height Pixels per Monthly Global Distribution

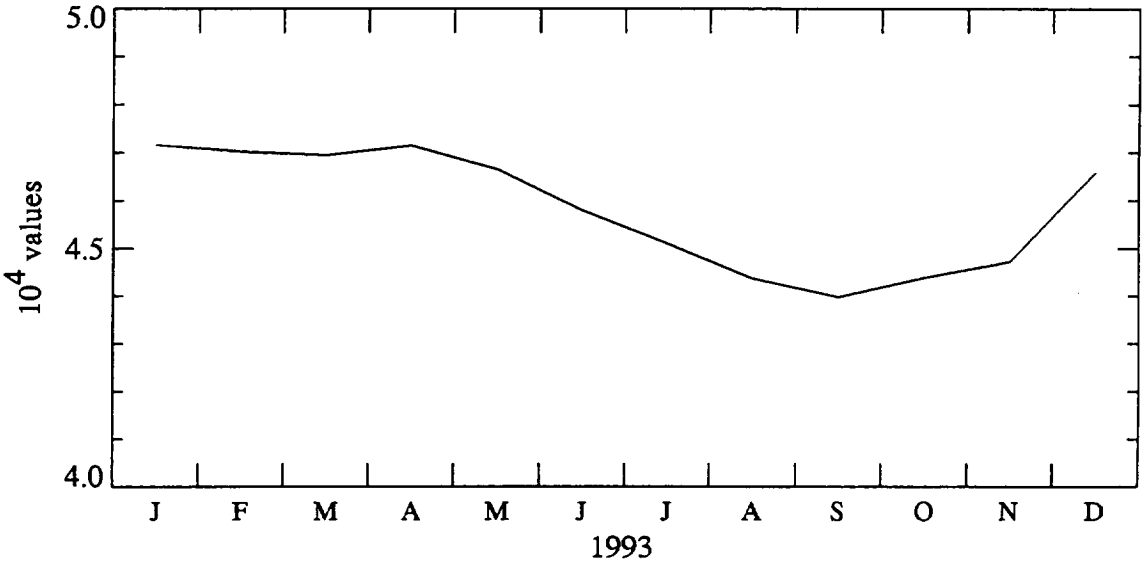

(B) Number of TOPEX/POSEIDON Sea Surface Height Values per Monthly Global Distribution

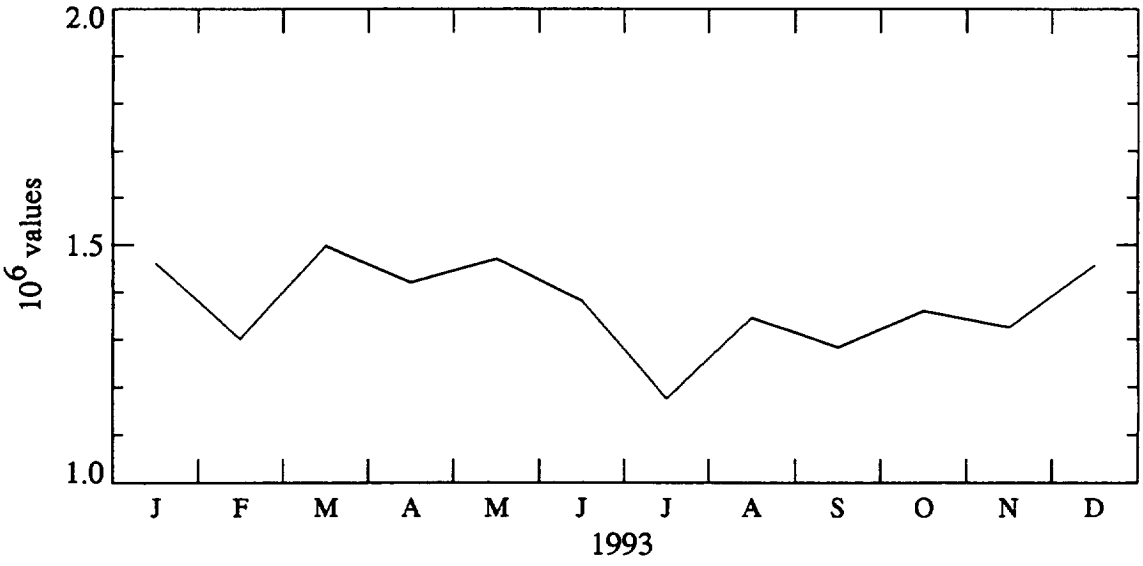

Figure 4. Time series of monthly totals of (A) number of pixels or picture element and (B) number of sea surface height measurements.

3 DATA PRESENTATION

All data are presented in the form of color-coded maps. To ease interpretation of features among different parameters, a common color code is used: blues represent low values, reds are high values, yellow and green are in the middle range, white means no data, and black represents land. Data are linearly scaled for color and an incremental color scale represents a contour interval. A single geographical scale is used for all maps. The land mask, which was prepared by O. Brown from the U.S. Central Intelligence Agency (CIA) World Data Base II, is the same throughout the report.

The color maps were generated on a Sun™ SPARCstation 10 computer using IDL®, which prepared the PostScript® files, and printed on a Tektronix™ Phaser CP Color Printer. All data values are retained in the PostScript image files. The SSMI images contain 1080 x 540 pixels (picture elements) and the AVHRR images contain 1024 x 512 pixels. All images are plotted on a 5.75-in. x 2.875-in. map. The PostScript interpreter linearly transforms the size of each pixel within the user image file into a source-image coordinate system, which is compatible with the 300 dot-per-in. resolution of the Tektronix, to achieve the maximum rendition of the image within the specified dimensions (Adobe Systems, 1985).

4 DATA AVAILABILITY

Data presented in Appendices A2, A5, A8 and A10 are available from the Physical Oceanography Distributed Active Archive Center (PODAAC), M/S 300-320, Jet Propulsion Laboratory, 4800 Oak Grove Drive, Pasadena, CA 91109. Data presented in all previous atlases are available from PODAAC.

5 REFERENCES

Adobe Systems, Inc. (1985) *PostScript® Language Reference Manual.* Addison-Wesley, 321 pp.

Bates, J.J. (1991) High frequency variability of SSMI-derived wind speed and moisture during an intraseasonal oscillation. *Journal of Geophysical Research, 96*, 3411-3424.

Bramson, M.A. (1968) *Infrared Radiation: A Handbook for Applications.* Plenum Press, New York, 623 pp.

Callahan, P.S. (1994) TOPEX/POSEIDON Project GDR users handbook. JPL Internal Document D-8944, Revision A, Jet Propulsion Laboratory, Pasadena, 84 pp.

Cartwright, D.E. and A.C. Edden (1973) Corrected tables of tidal harmonics. *Geophysical Journal of the Royal Astronomical Society, 33*, 253-264.

Cartwright, D.E., and R.J. Tayler (1971) New computations of the tide generating potential. *Geophysical Journal of the Royal Society, 23*, 45-74.

Chelton, D.B. (1988) WOCE/NASA altimeter algorithm workshop. U.S. WOCE Technical Report No. 2, U.S. Planning Office for WOCE, Texas A&M University, College Station, 70 pp.

Christensen, E.J., B.J. Haines, S.J. Keihm, C.S. Morris, R.A. Norman, G.H. Purcell, B.G. Williams, B.D. Wilson, G.H. Born, M.E. Parke, S.K. Gill, C.K. Shum, B.D. Tapley, R. Kolenkiewicz and R.S. Nerem (1994) Calibration of TOPEX/POSEIDON at platform Harvest. *Journal of Geophysical Research, 99*, 24465-24486.

Emery, W.J., G.H. Born, D.G. Baldwin and C.L. Norris (1990) Satellite-derived water vapor corrections for GEOSAT altimetry. *Journal of Geophysical Research, 95*, 2953-2964.

Francis, R., G. Graf, P. G. Edwards, M. McCaig, C. McCarthy, P. Dubock, A. Lefebvre, B. Pieper, P.-Y. Pouvreau, R. Wall, F. Wechsler, J. Louet and R. Zobl (1991) The ERS-1 spacecraft and its payload. ESA Bulletin, No. 65, European Space Agency, Paris, 27-48.

Freilich, M. H. and R. S. Dunbar (1993a) A preliminary C-band scatterometer model function for the ERS-1 AMI instrument. Proceedings of First ERS-1 Symposium, ESA SP-359, European Space Agency, Paris, 79-84.

Freilich, M. H. and R. S. Dunbar (1993b) Derivation of satellite wind model functions using operational surface wind analyses: An altimeter example. *Journal of Geophysical Research, 98*, 14633-14649.

Fu, L.-L., E. J. Christensen, C.A. Yamarone, M. Lefebvre, Y. Menard, M. Dorrer and P. Escudier (1994) TOPEX/POSEIDON mission overview. *Journal of Geophysical Research, 99*, 24369-24383.

Gaspar, P., F. Ogor, P.Y. Le Traon and O.Z. Zanife (1994) Estimating the sea-state bias of the TOPEX and POSEIDON altimeters from crossover differences. *Journal of Geophysical Research, 99,* 24981-24994.

Goodberlet, M.A., C.T. Swift and J.C. Wilkerson (1990) Ocean surface wind speed measurements of the special sensor microwave imager (SSMI). *IEEE Transactions on Geoscience and Remote Sensing, 28*, 823-828.

Halpern, D. (1993) Validation of the Remote Sensing System algorithm of Special Sensor Microwave Imager 10-m height monthly-mean wind speed from July 1987 to December 1989. *IEEE Transactions on Geoscience and Remote Sensing, 31*, 692-699.

Halpern, D. and F. Wentz (1994) On the problem of measuring interannual surface wind speed variations from satellites. *Geophysical Research Letters, 21*, 193-196.

Halpern, D., M. H. Freilich and R. S. Dunbar (1994) ERS-1 scatterometer estimates of annual variations of Atlantic ITCZ and Pacific NECC. In: *Proceedings of Second ERS-1 Symposium, Hamburg, 11-14 October 1993*, European Space Agency, Paris, 1003-1008.

Halpern, D., W. Knauss, O. Brown, M. Freilich and F. Wentz (1994) An atlas of monthly mean distributions of SSMI surface wind speed, ARGOS buoy drift, AVHRR/2 sea surface temperature, AMI surface wind components, and ECMWF surface wind components during 1992. JPL Publication 94-4, Jet Propulsion Laboratory, Pasadena, 143 pp.

Halpern, D., W. Knauss, O. Brown and F. Wentz (1993a) An atlas of monthly mean distributions of SSMI surface wind speed, ARGOS buoy drift, AVHRR/2 sea surface temperature, and ECMWF surface wind components during 1990. JPL Publication 93-1, Jet Propulsion Laboratory, Pasadena, 111 pp.

Halpern, D., W. Knauss, O. Brown and F. Wentz (1993b) An atlas of monthly mean distributions of SSMI surface wind speed, ARGOS buoy drift, AVHRR/2 sea surface temperature, and ECMWF surface wind components during 1991. JPL Publication 93-10, Jet Propulsion Laboratory, Pasadena, 111 pp.

Halpern, D., V. Zlotnicki, J. Newman, D. Dixon, O. Brown and F. Wentz (1992a) An atlas of monthly mean distributions of GEOSAT sea surface height, SSMI surface wind speed, AVHRR/2 sea surface temperature, and ECMWF surface wind components during 1987. JPL Publication 92-3, Jet Propulsion Laboratory, Pasadena, 111 pp.

Halpern, D., W. Knauss, O. Brown and F. Wentz (1992b) An atlas of monthly mean distributions of SSMI surface wind speed, ARGOS buoy drift, AVHRR/2 sea surface temperature, and ECMWF surface wind components during 1989. JPL Publication 92-17, Jet Propulsion Laboratory, Pasadena, 112 pp.

Halpern, D., V. Zlotnicki, J. Newman, O. Brown and F. Wentz (1991) An atlas of monthly mean distributions of GEOSAT sea surface height, SSMI surface wind speed, AVHRR/2 sea surface temperature, and ECMWF surface wind components during 1988. JPL Publication 91-8, Jet Propulsion Laboratory, Pasadena, 110 pp.

Hollinger, J.P., J.L. Pierce and G.A. Poe (1990) SSMI instrument evaluation. *IEEE Transactions on Geoscience and Remote Sensing, 28*, 781-790.

Imel, D.A. (1994) Evaluation of the TOPEX dual-frequency ionospheric correction. *Journal of Geophysical Research, 99,* 24895-24906.

Kalnay, E., M. Kanamitsu and W.E. Baker (1990) Global numerical weather prediction at the National Meteorological Center. *Bulletin of the American Meteorological Society, 71*, 1410-1428.

Kidwell, K.B. (1991) NOAA polar orbiter data users guide. National Environmental Satellite, Data, and Information Service, National Oceanic and Atmospheric Administration, Washington, DC 20233.

Maul, G.A. (1985) *Introduction to Satellite Oceanography*. Matinus Nijhoff, Dordrecht, 606 pp.

McClain, E.P., W.G. Pichel and C.C. Walton (1985) Comparative performance of AVHRR-based multichannel sea surface temperatures. *Journal of Geophysical Research, 90*, 11587-11601.

Menard, Y., E. Jeansou and P. Vincent (1994) Calibration of the TOPEX/POSEIDON altimeters over Lampedusa with additional results over Harvest. *Journal of Geophysical Research, 99*, 24487-24504.

Monaldo, F. (1990) Path length variations caused by atmospheric water vapor and their effects on the measurement of mesoscale ocean circulation features by a radar altimeter. *Journal of Geophysical Research, 95*, 2923-2932.

Naderi, F. M., M. H. Freilich, and D. G. Long (1991) Spaceborne radar measurement of wind velocity over the ocean -- An overview of the NSCAT scatterometer system. *Proceedings of IEEE, 79*, 850-866.

Olson, D.B., G.P. Podesta, R.H. Evans and O.B. Brown (1988) Temporal variations in the separation of Brazil and Malvinas Currents. *Deep-Sea Research, 35*, 1971-1990.

Reynolds, R.W. (1993) Impact of Mount Pinatubo aerosols on satellite-derived sea surface temperatures. *Journal of Climate, 6*, 768-774.

Rodriguez, E. and J. Martin (1994a) Determination and modeling of the EM bias from retracked data. *Journal of Geophysical Research, 99*, 24972-24980.

Rodriguez, E. and J. Martin (1994b) Assessment of TOPEX/POSEIDON altimeter performance from wave form retracking. *Journal of Geophysical Research, 99*, 24957-24970.

Ruf, C., S. Keihm, B. Subramanya and M. Jassen (1994) TOPEX microwave radiometer performance and in-flight calibration. *Journal of Geophysical Research, 99*, 24915-24926.

Schultz, H. (1990) A circular median filter approach for resolving ambiguities in wind fields retrieved from spaceborne scatterometer data. *Journal of Geophysical Research, 95*, 5291-5303.

Shaffer, S. J., R. S. Dunbar, S. V. Hsiao and D. G. Long (1991) A median-filter-based ambiguity removal algorithm for NSCAT. *IEEE Transactions on Geoscience and Remote Sensing, 29*, 167-174.

Stommel, H., and M. Fieux (1978) *Oceanographic Atlases*. Woods Hole Press, Woods Hole, Massachusetts, 6 pp + 97 charts.

Tapley, B.D., J.C. Ries, G.W. Davis, R.J. Eanes, B.E. Schutz, C.K. Shum, M.M. Watkins, J.A. Marshall, R.S. Nerem, B.H. Putney, S.M. Klosko, S.B. Luthcke, D. Pavlis, R.G. Williamson and N.P. Zelensky (1994) Precision orbit determination for TOPEX/POSEIDON. *Journal of Geophysical Research, 99*, 24383-24405.

Trenberth, K.E., and J.G. Olson (1988) ECMWF global analysis 1979-1986: Circulation statistics and data evaluation. NCAR Technical Note NCAR/TN-300+STR, National Center for Atmospheric Research, Boulder, 94 pp.

Wentz, F.J. (1989) User's manual: SSMI geophysical tapes. RSS Technical Report 060989, Remote Sensing Systems, Santa Rosa, California, 16 pp.

Wentz, F. (1992) Measurement of oceanic wind vector using satellite microwave radiometers. *IEEE Transactions on Geoscience and Remote Sensing, 30*, 960-972.

APPENDIX

ATLAS OF MONTHLY MEAN DISTRIBUTIONS

A1

Annual Mean and Sampling Distribution of SSMI Surface Wind Speed

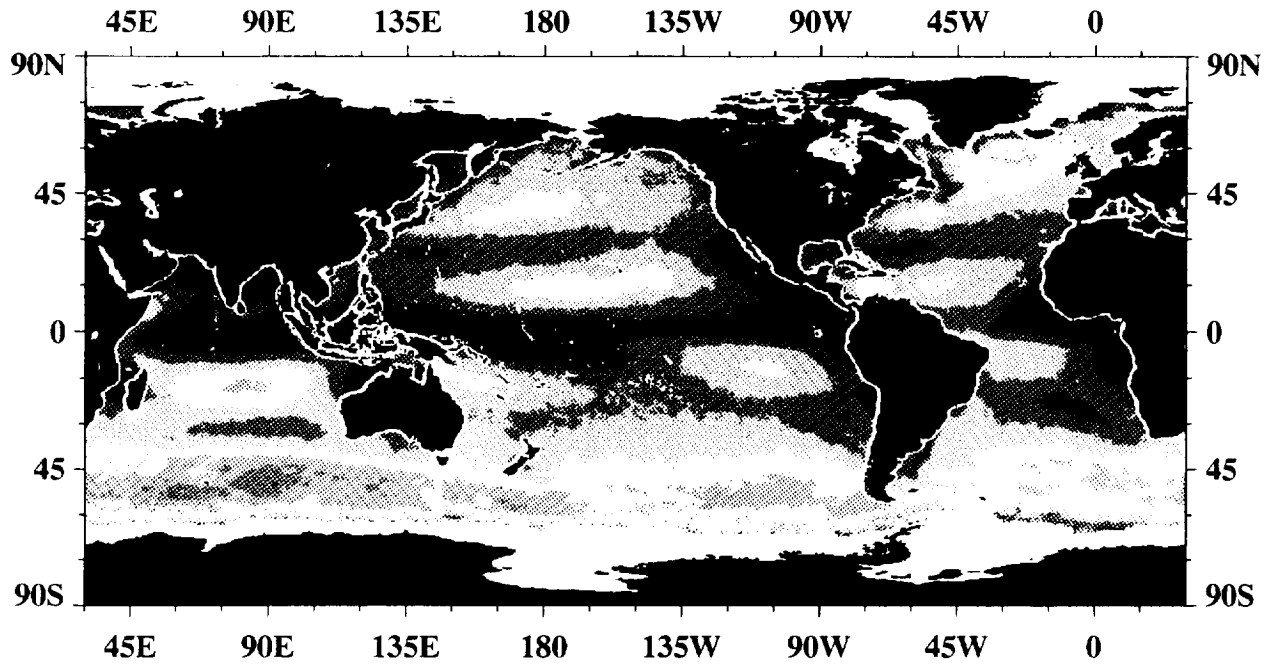

Annual Mean 1993

SSMI Wind Speed Referenced to 10 m, m s^{-1}

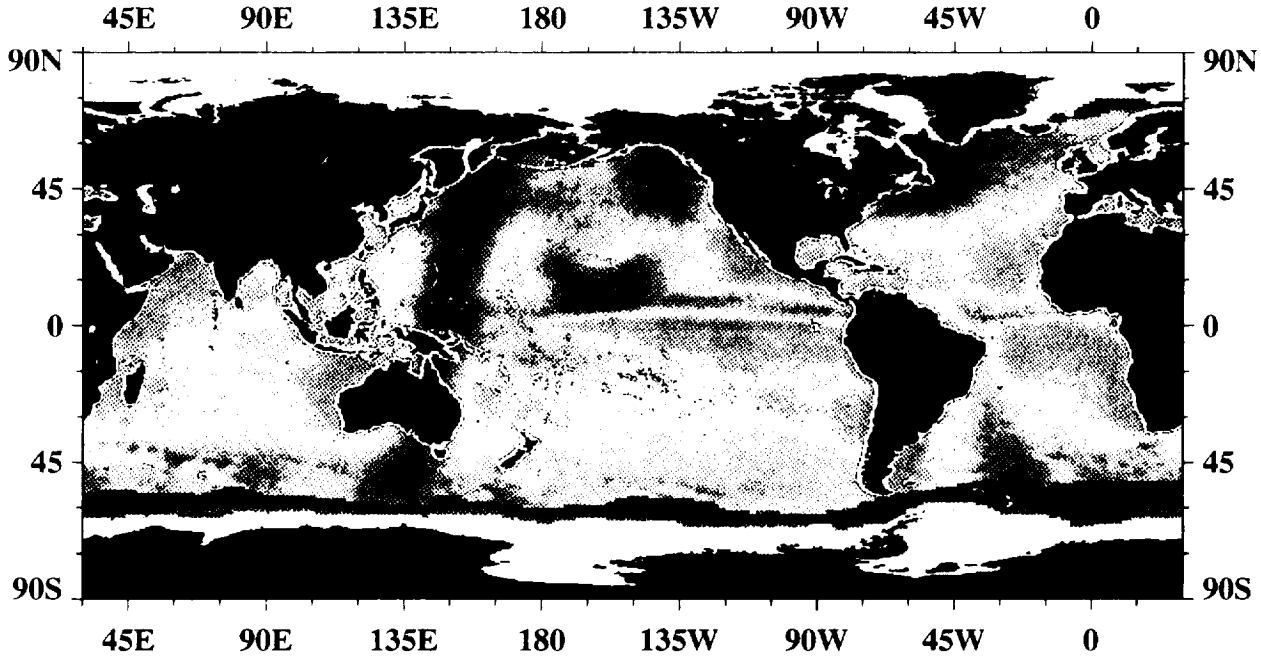

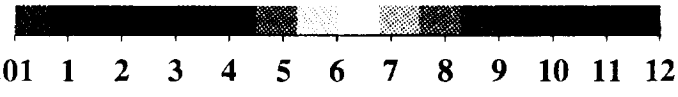

Number x 100 of SSMI Wind Speed Values per Pixel During 1993, max = 867

A2

Monthly Mean SSMI Surface Wind Speed

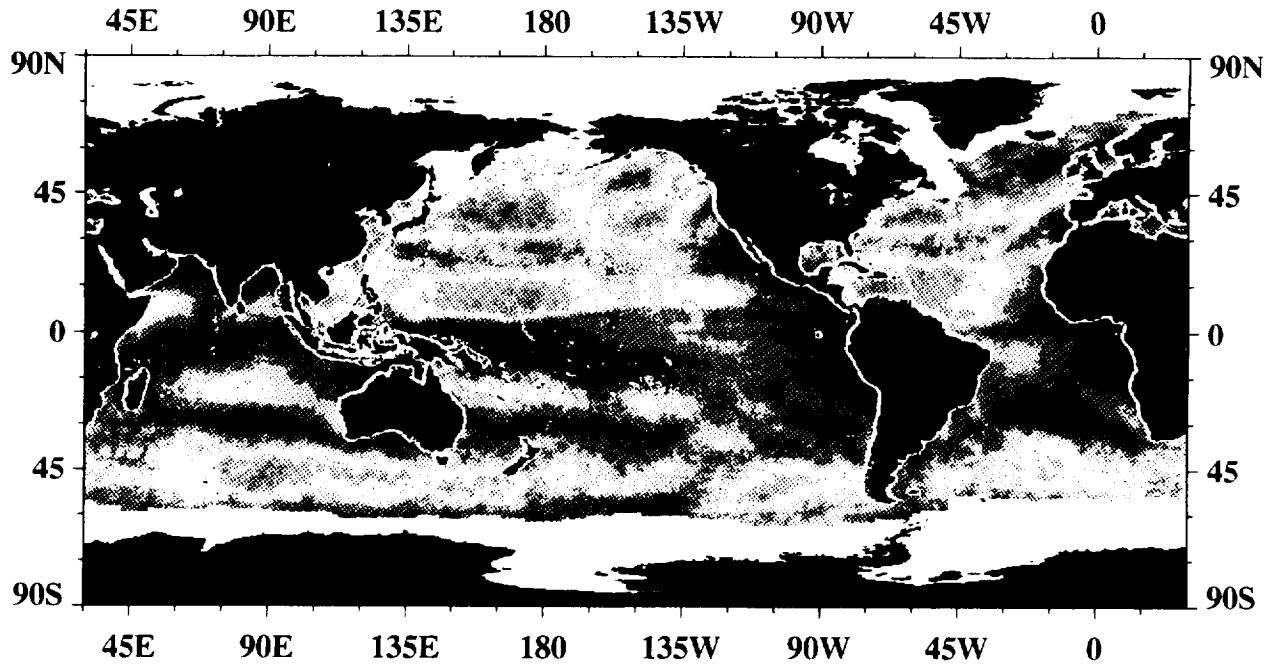

January 1993

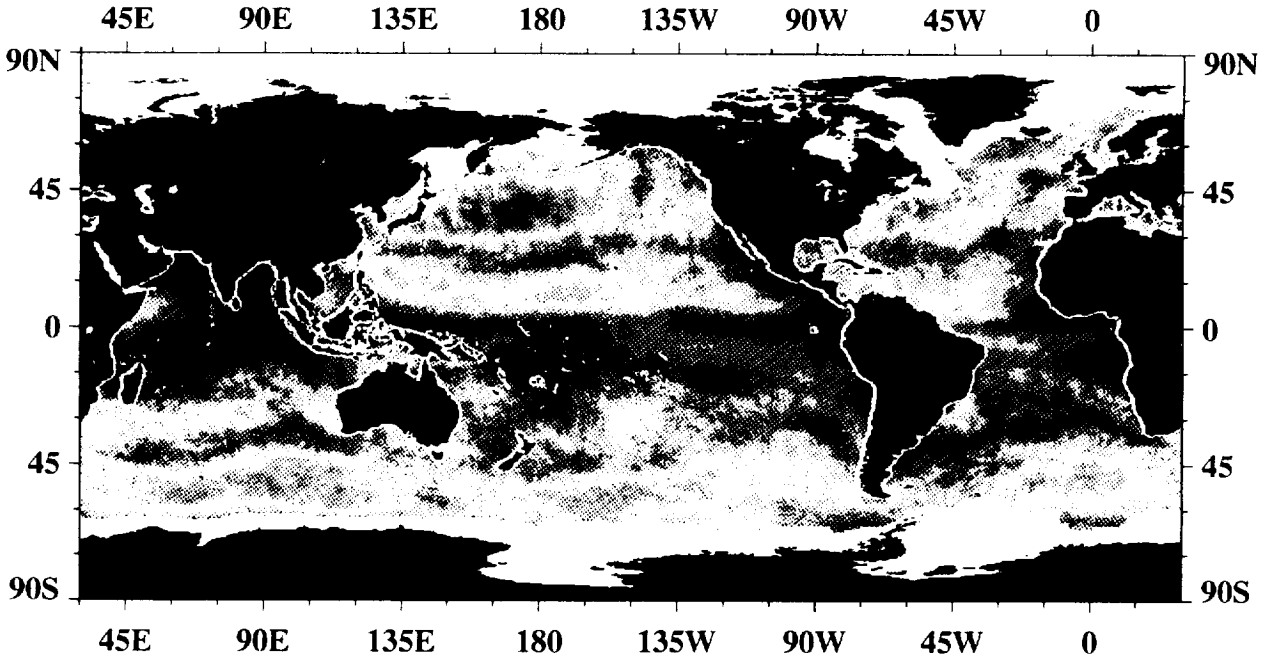

February 1993

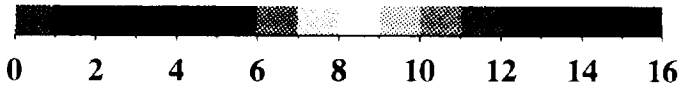

SSMI Wind Speed Referenced to 10 m, m s^{-1}

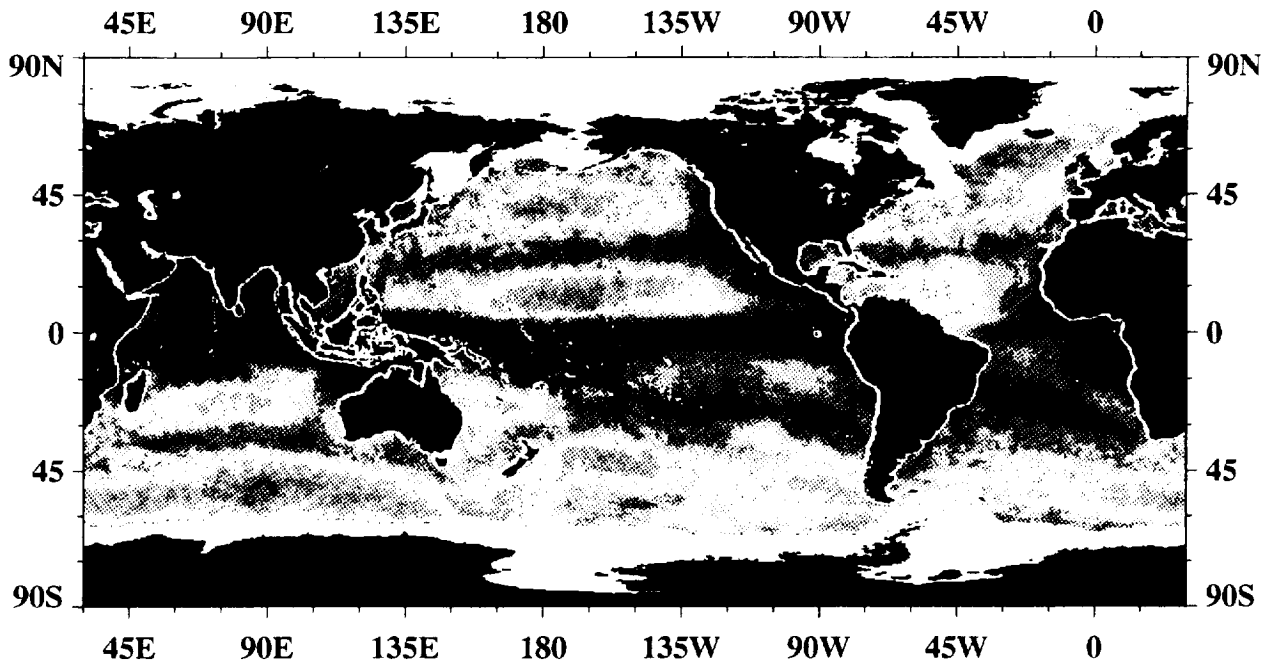

March 1993

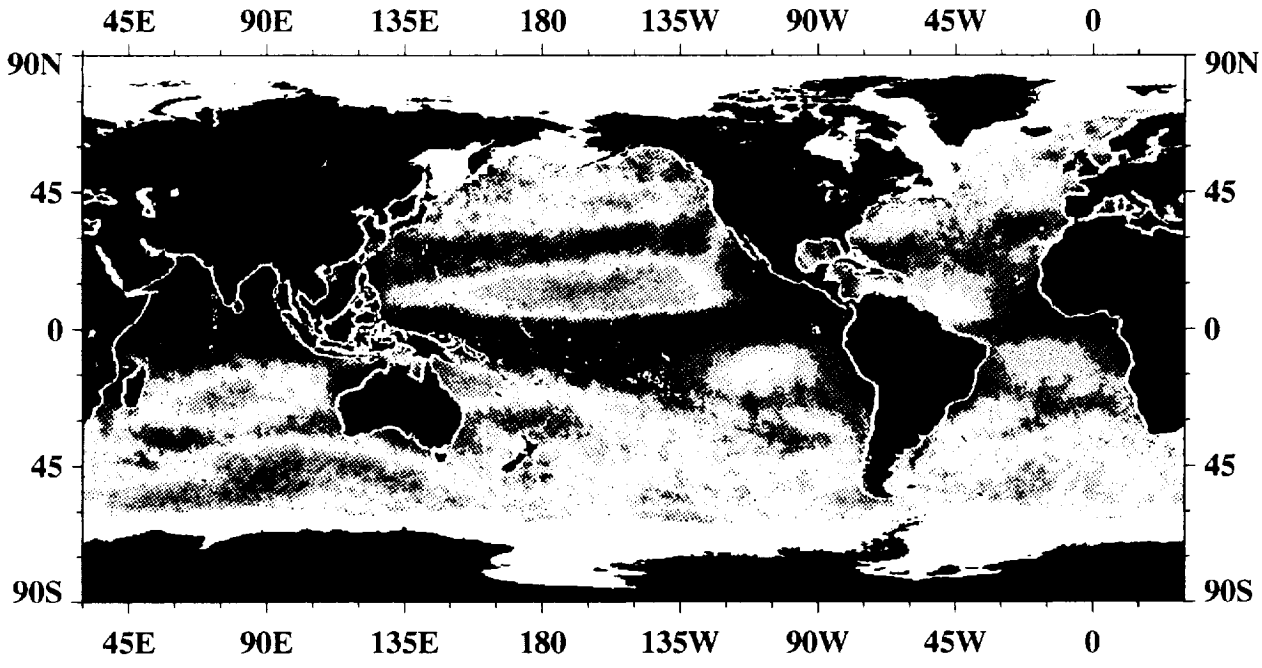

April 1993

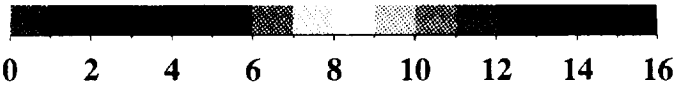

SSMI Wind Speed Referenced to 10 m, m s^{-1}

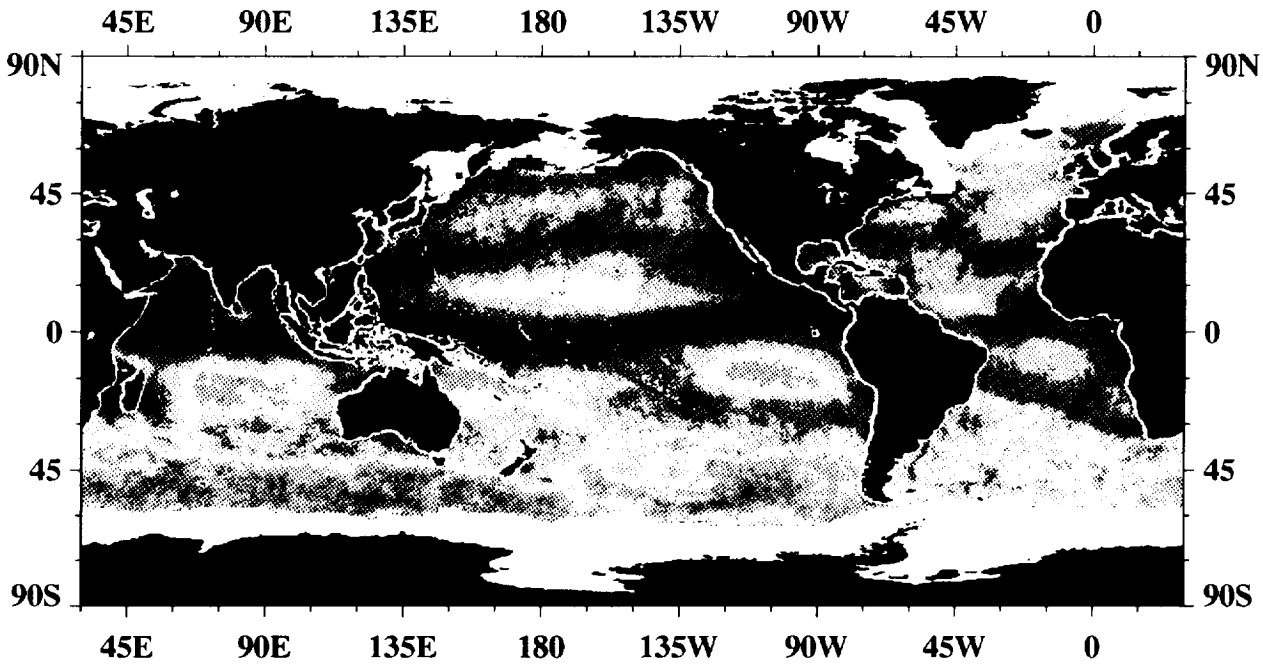

May 1993

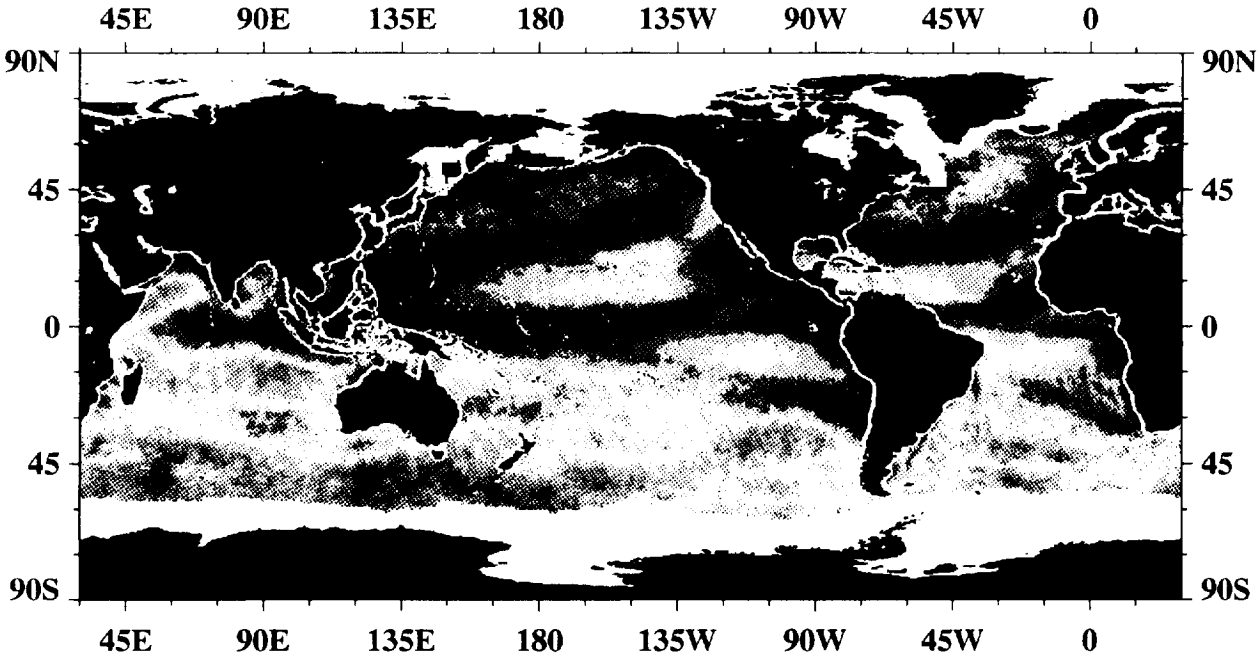

June 1993

SSMI Wind Speed Referenced to 10 m, m s^{-1}

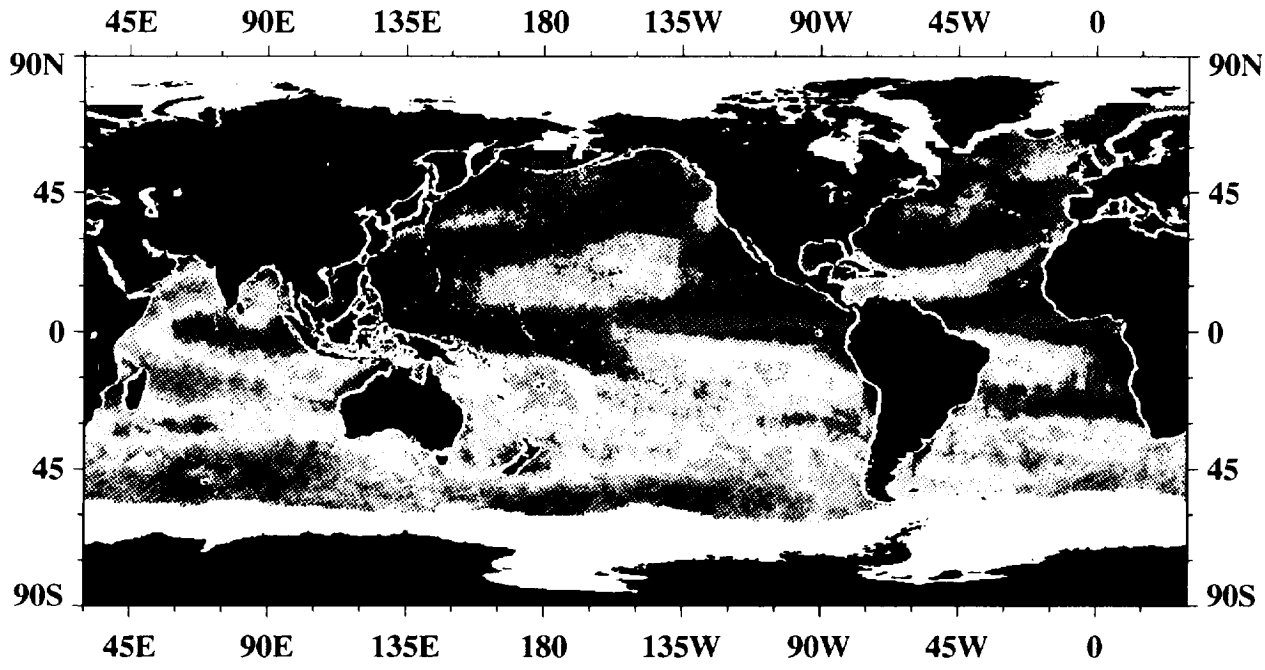

July 1993

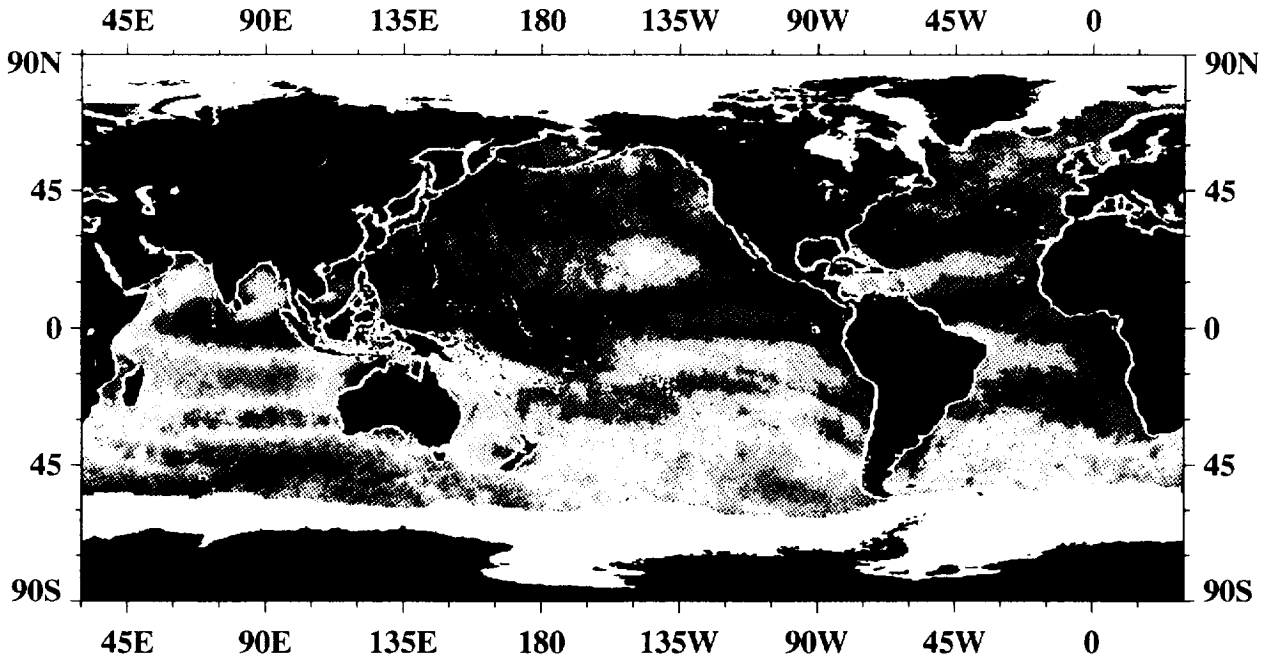

August 1993

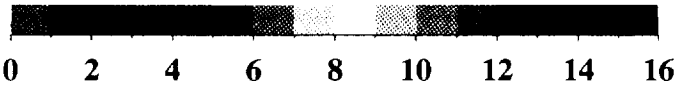

SSMI Wind Speed Referenced to 10 m, m s^{-1}

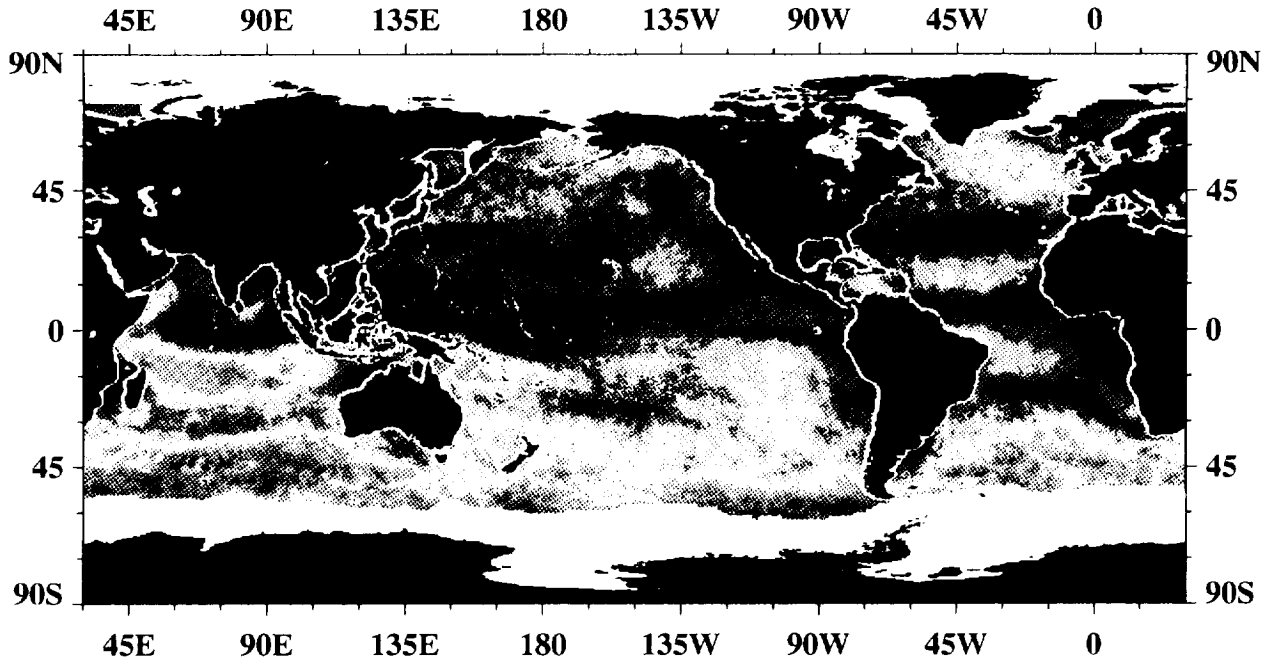

September 1993

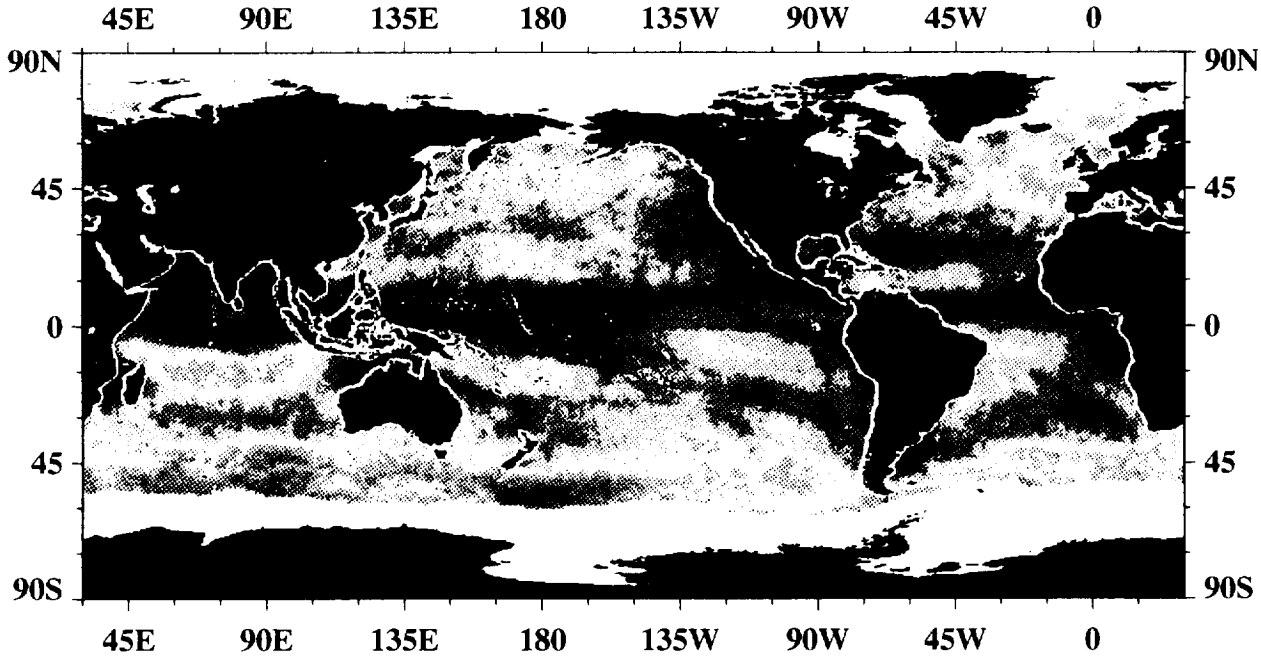

October 1993

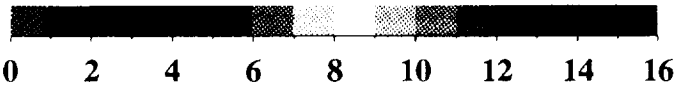

SSMI Wind Speed Referenced to 10 m, m s^{-1}

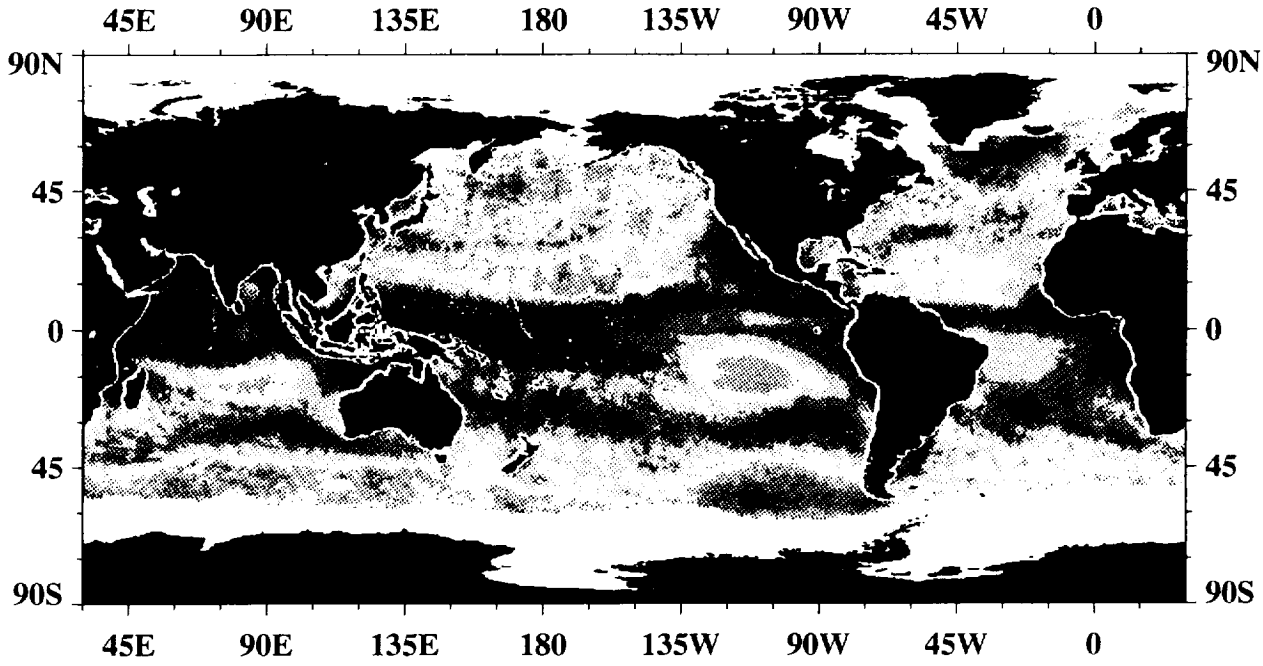

November 1993

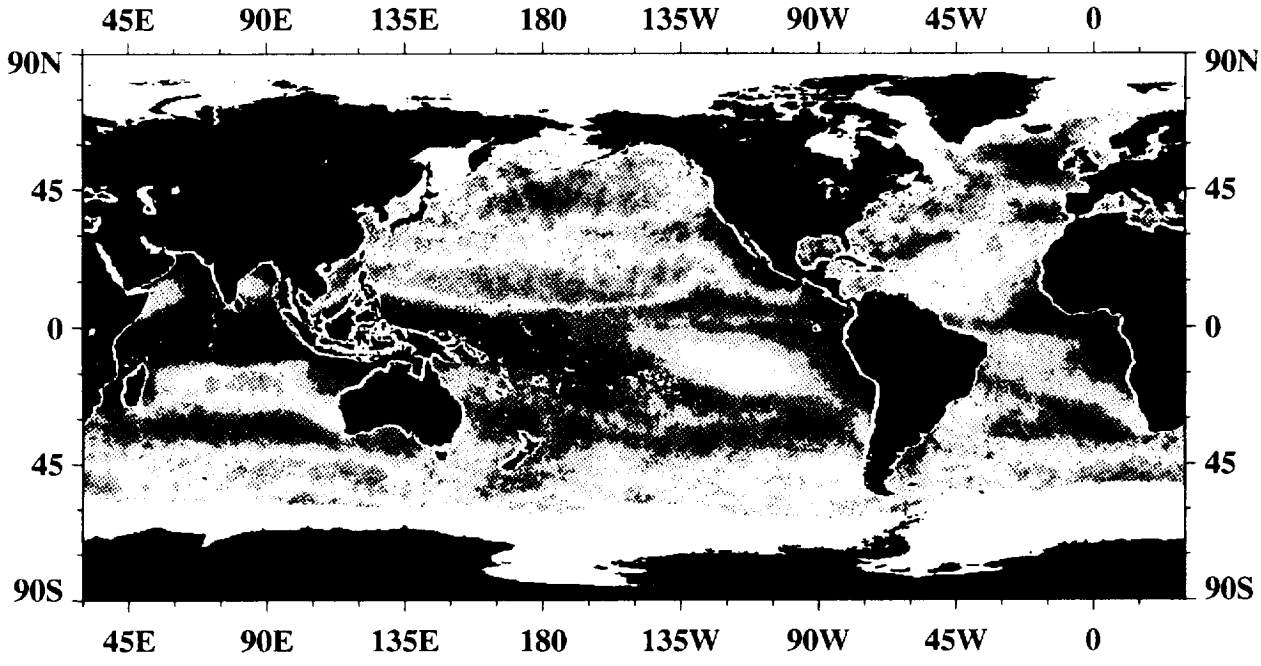

December 1993

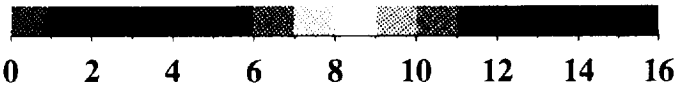

SSMI Wind Speed Referenced to 10 m, m s^{-1}

A3

Monthly SSMI Sampling Distribution

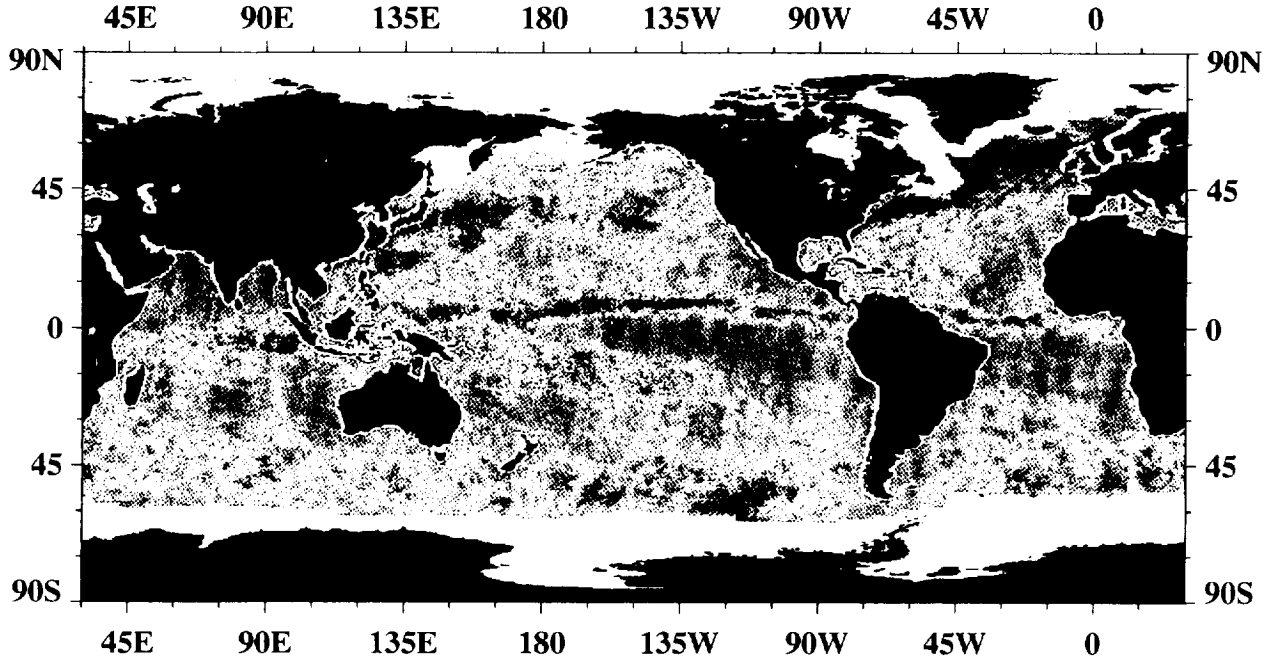

January 1993, max = 89

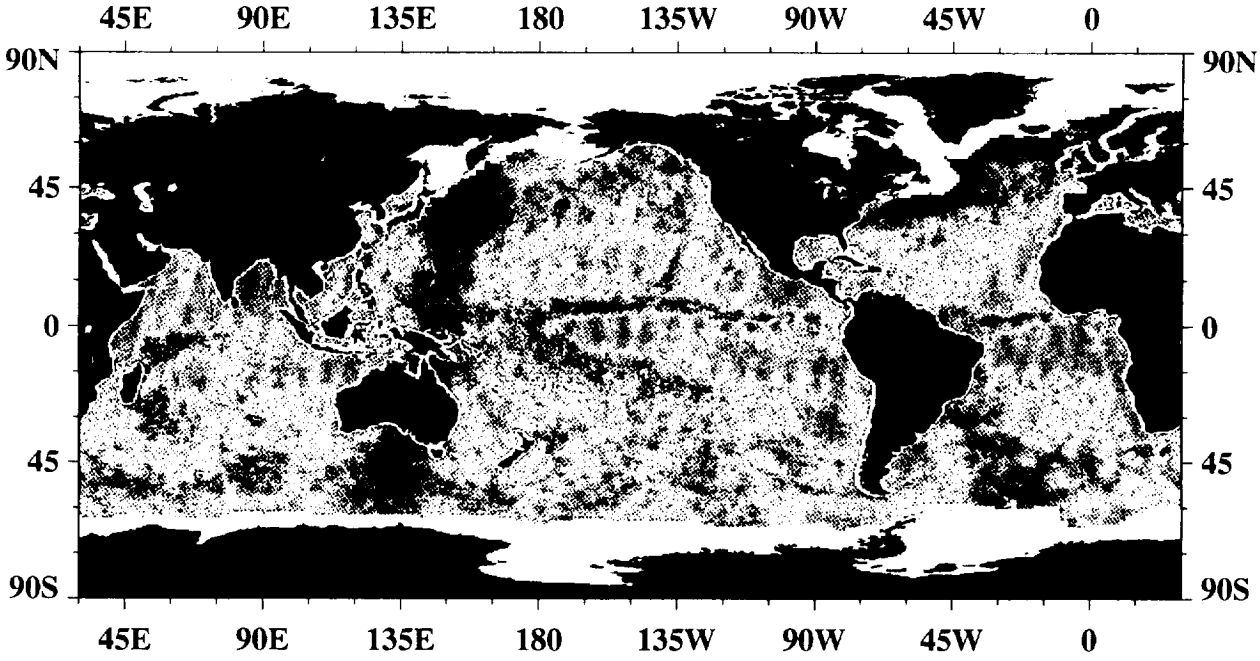

February 1993, max = 88

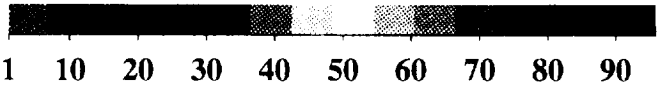

Number of SSMI Wind Speed Values per Pixel

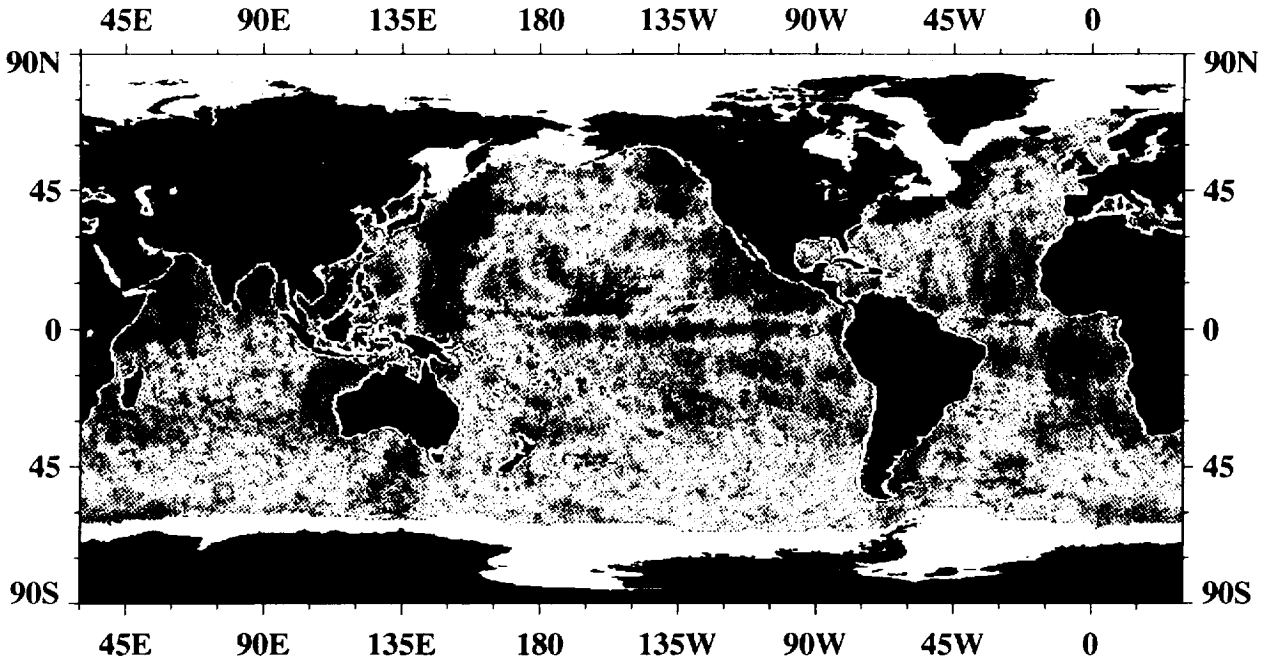

March 1993, max = 100

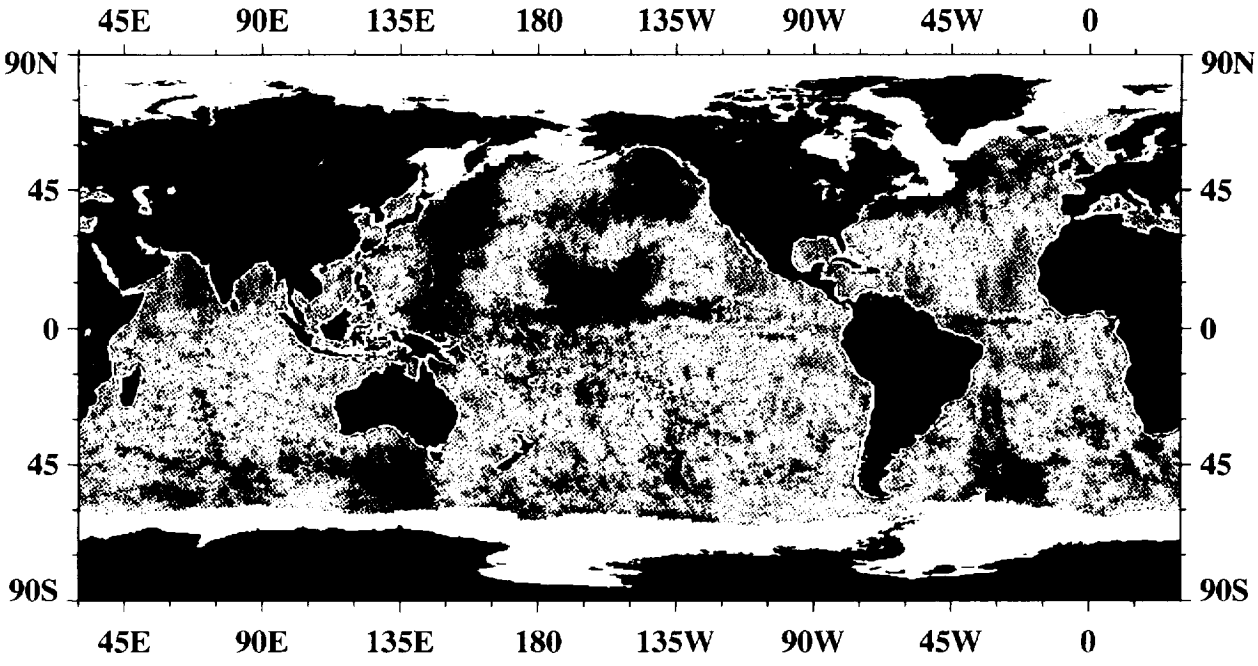

April 1993, max = 86

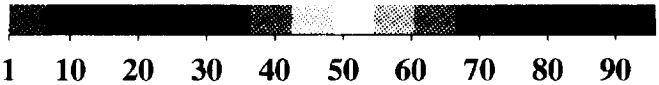

Number of SSMI Wind Speed Values per Pixel

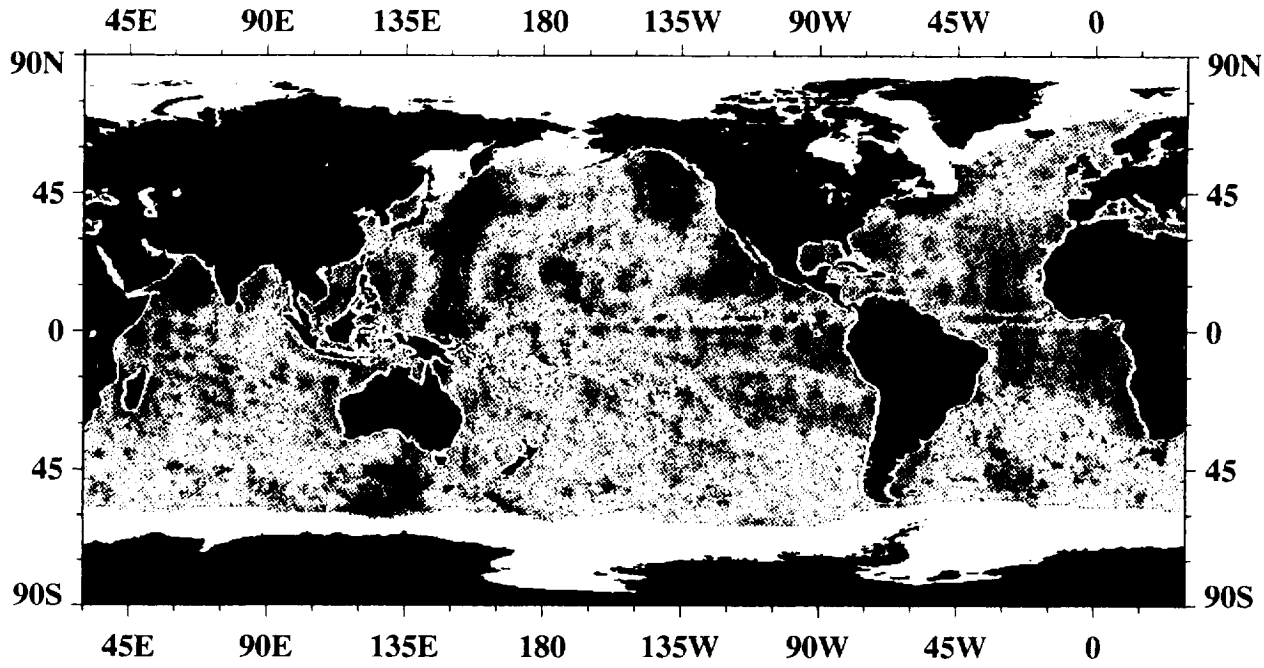

May 1993, max = 101

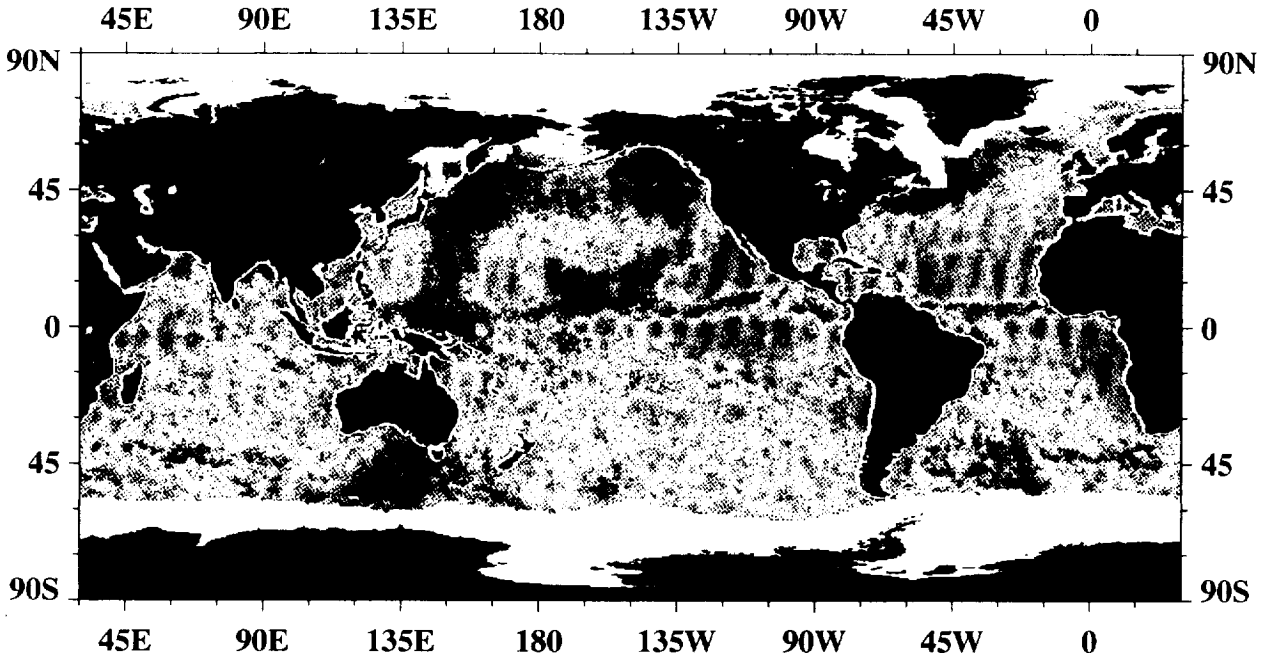

June 1993, max = 90

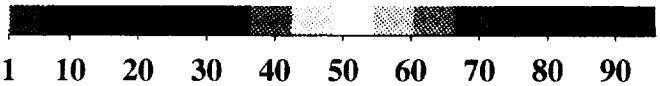

Number of SSMI Wind Speed Values per Pixel

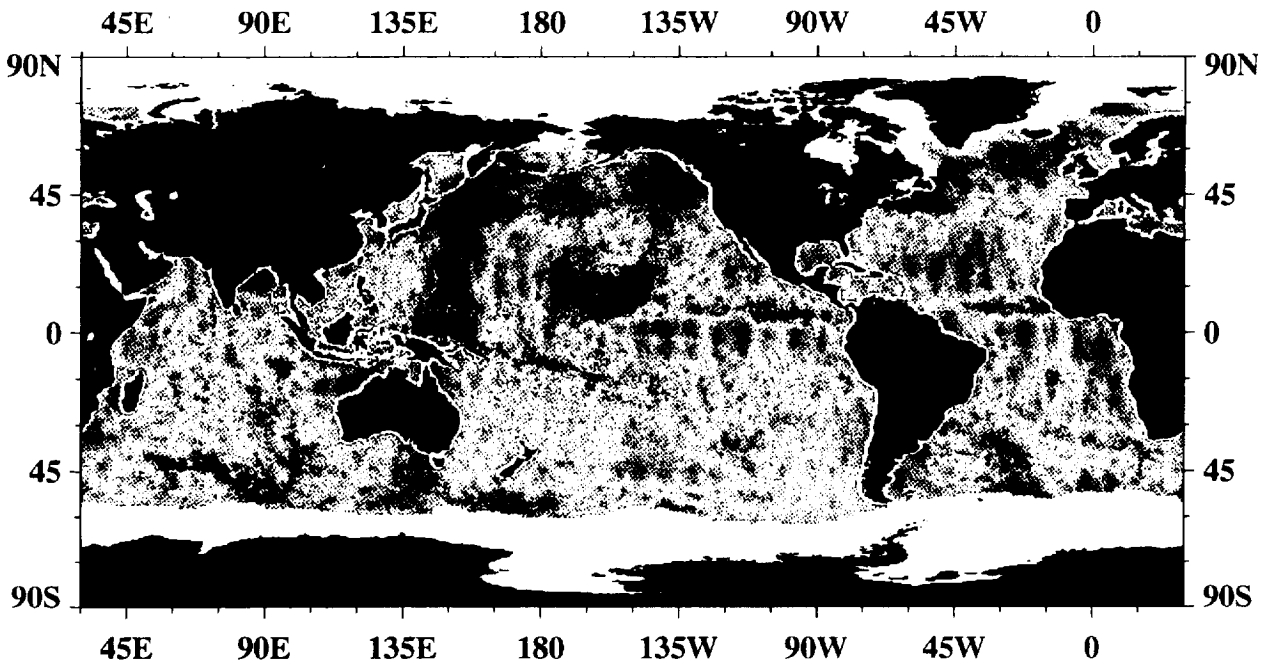

July 1993, max = 96

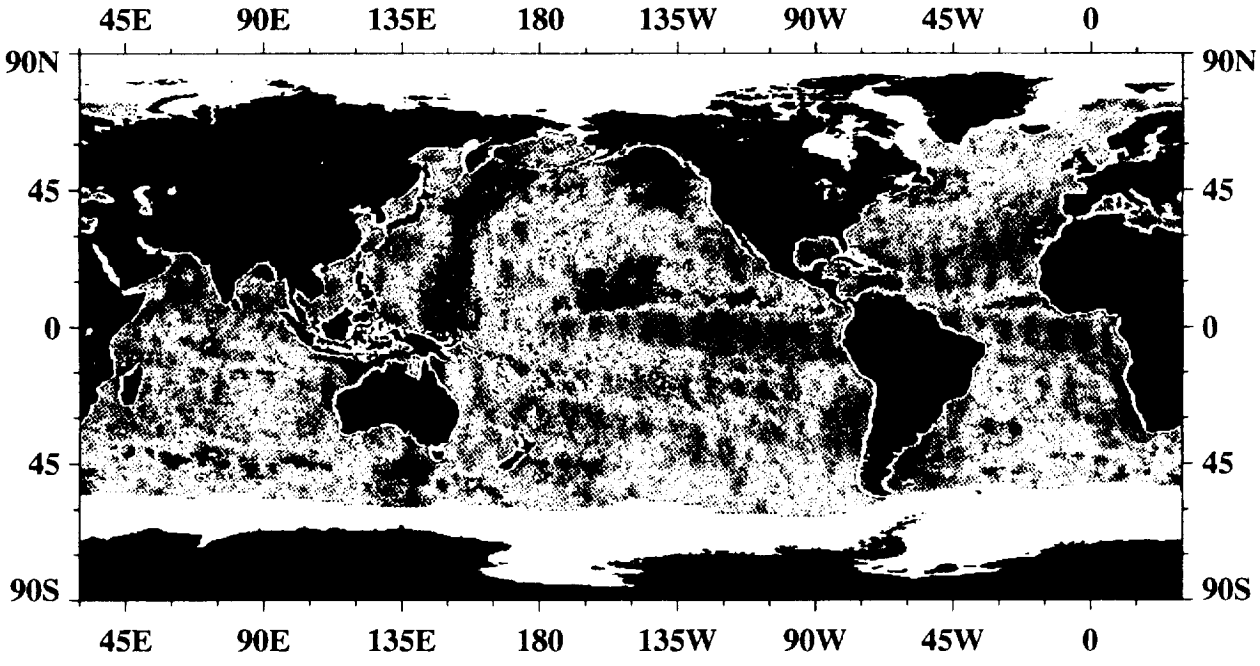

August 1993, max = 99

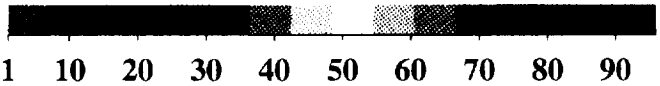

Number of SSMI Wind Speed Values per Pixel

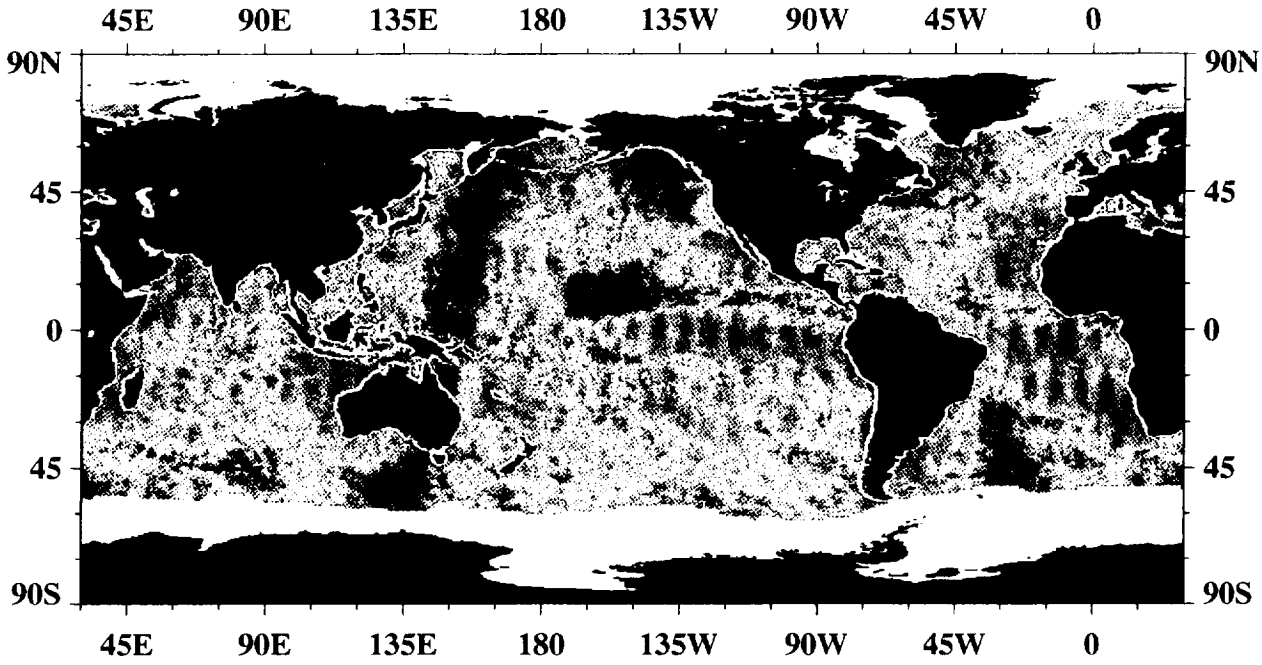

September 1993, max = 92

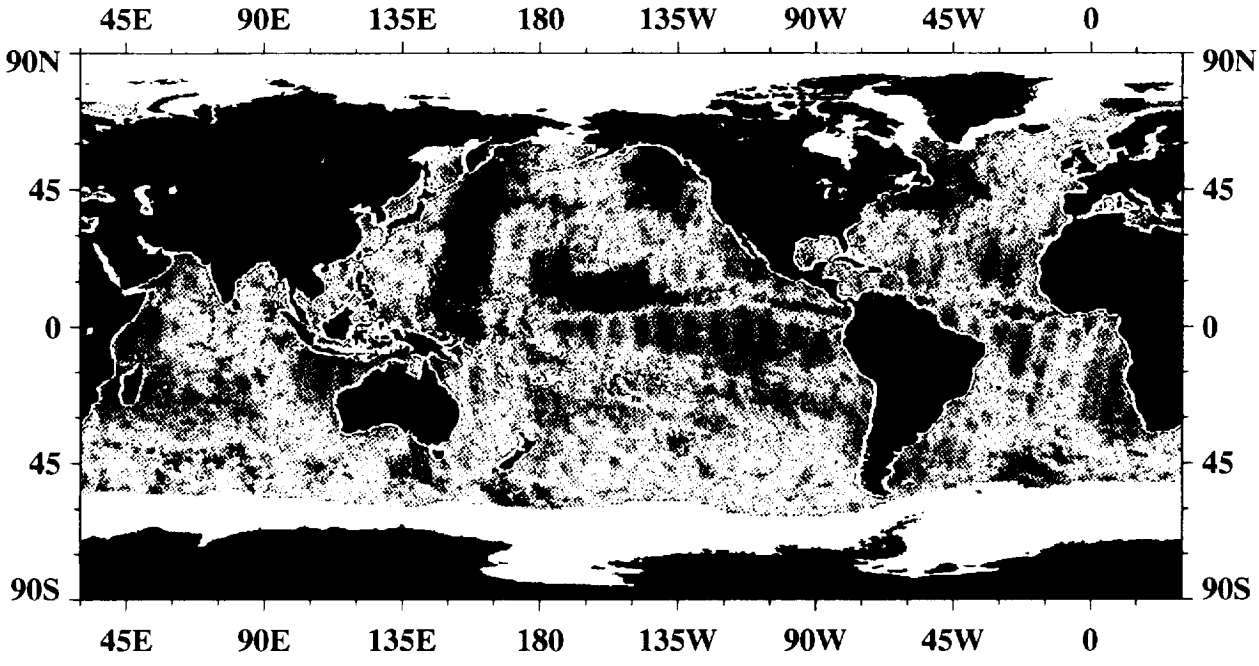

October 1993, max = 93

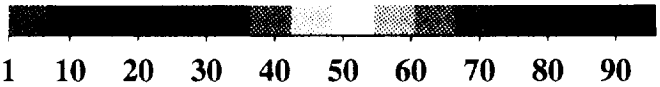

Number of SSMI Wind Speed Values per Pixel

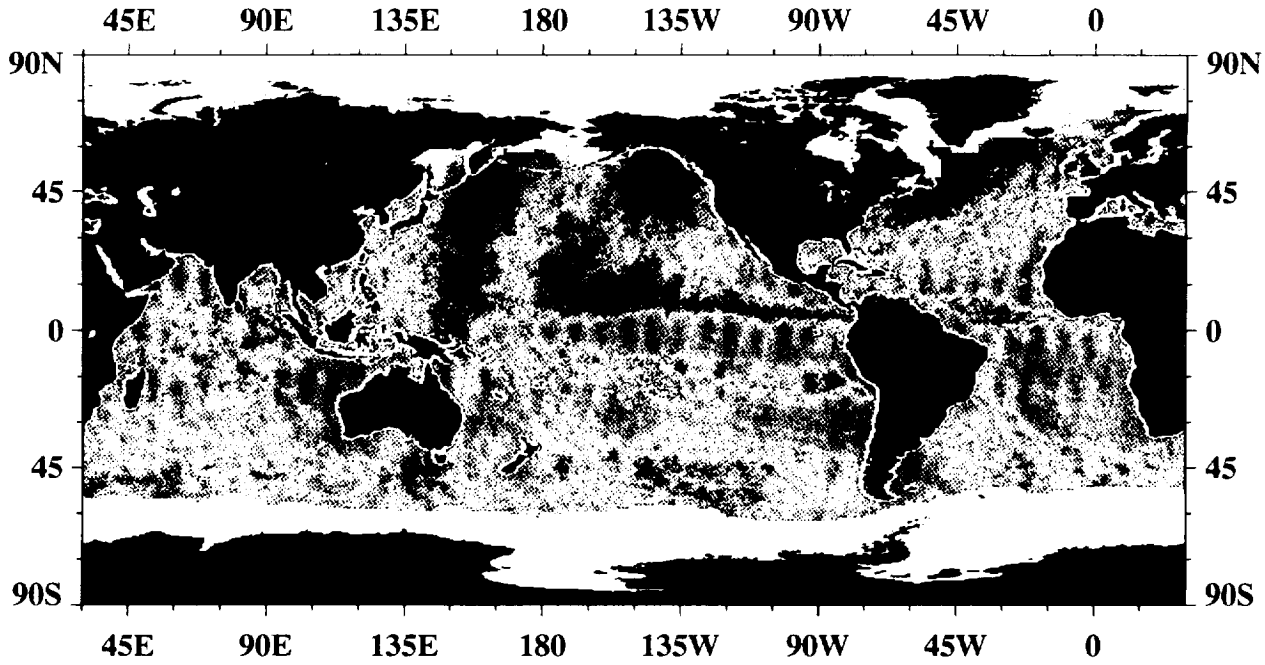

November 1993, max = 91

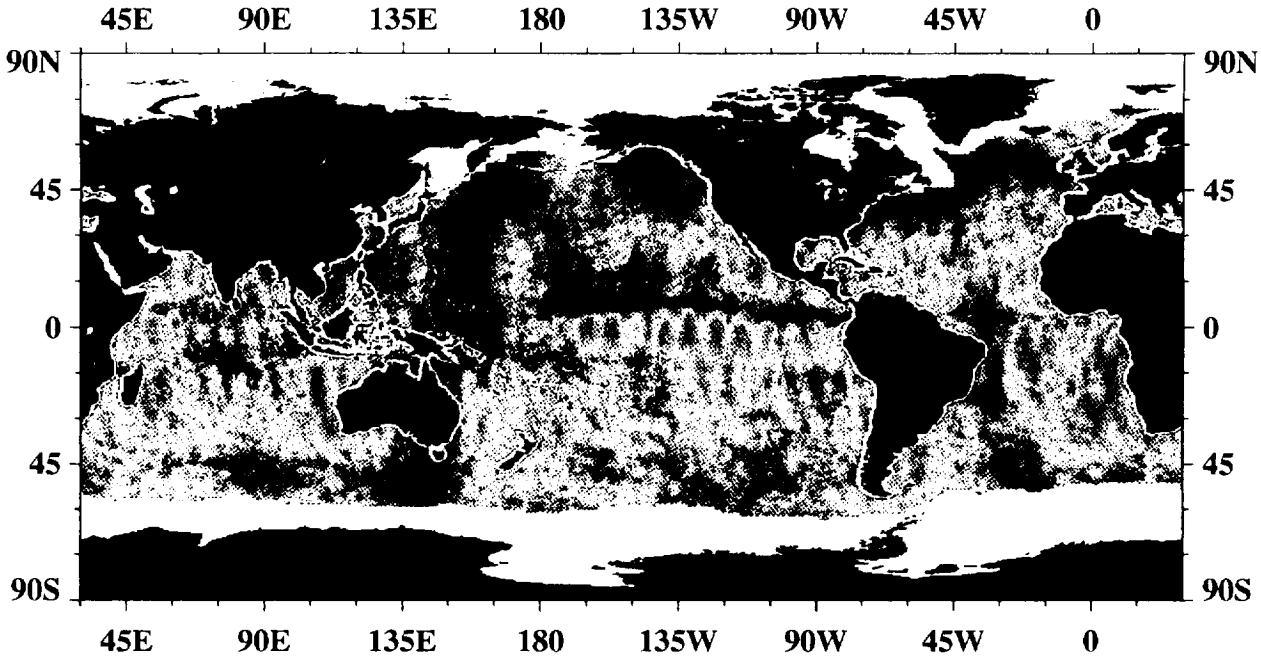

December 1993, max = 89

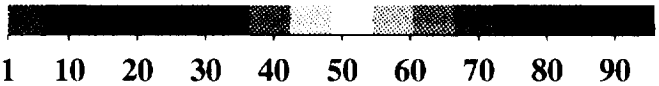

Number of SSMI Wind Speed Values per Pixel

A4

Annual Mean and Sampling Distribution of AVHRR/2 Sea Surface Temperature

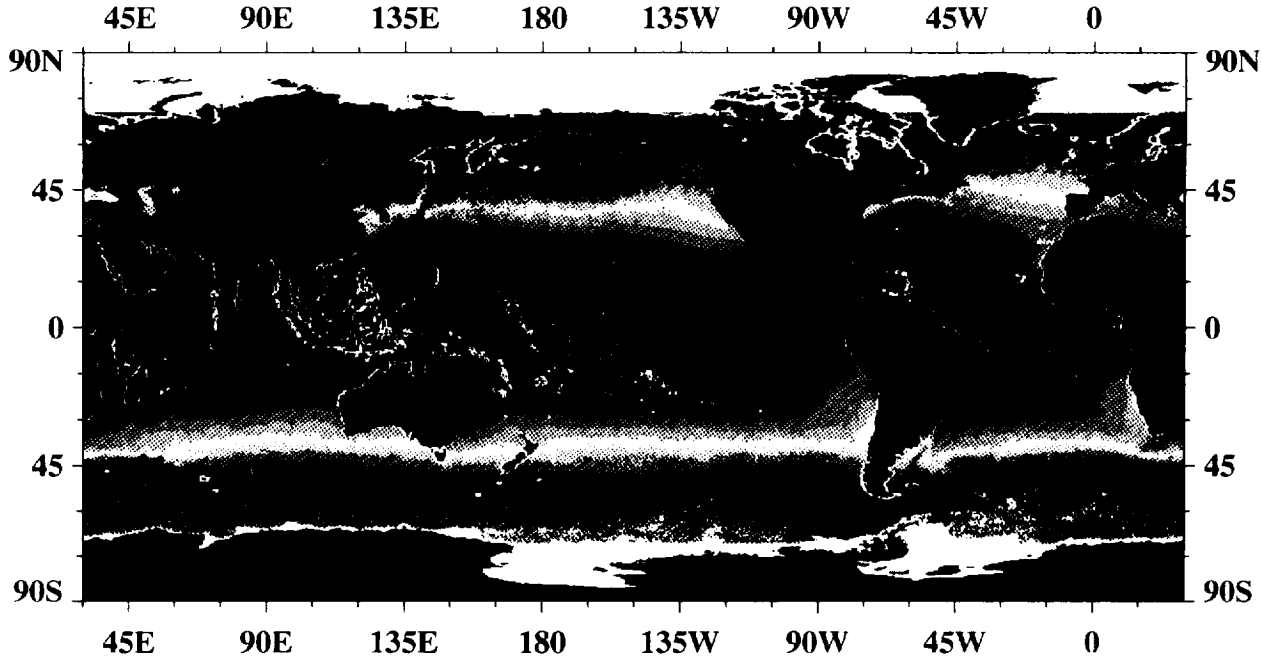

Annual Mean 1993

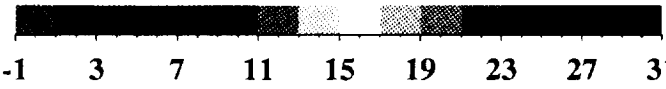

AVHRR Sea Surface Temperature, ^{o}C

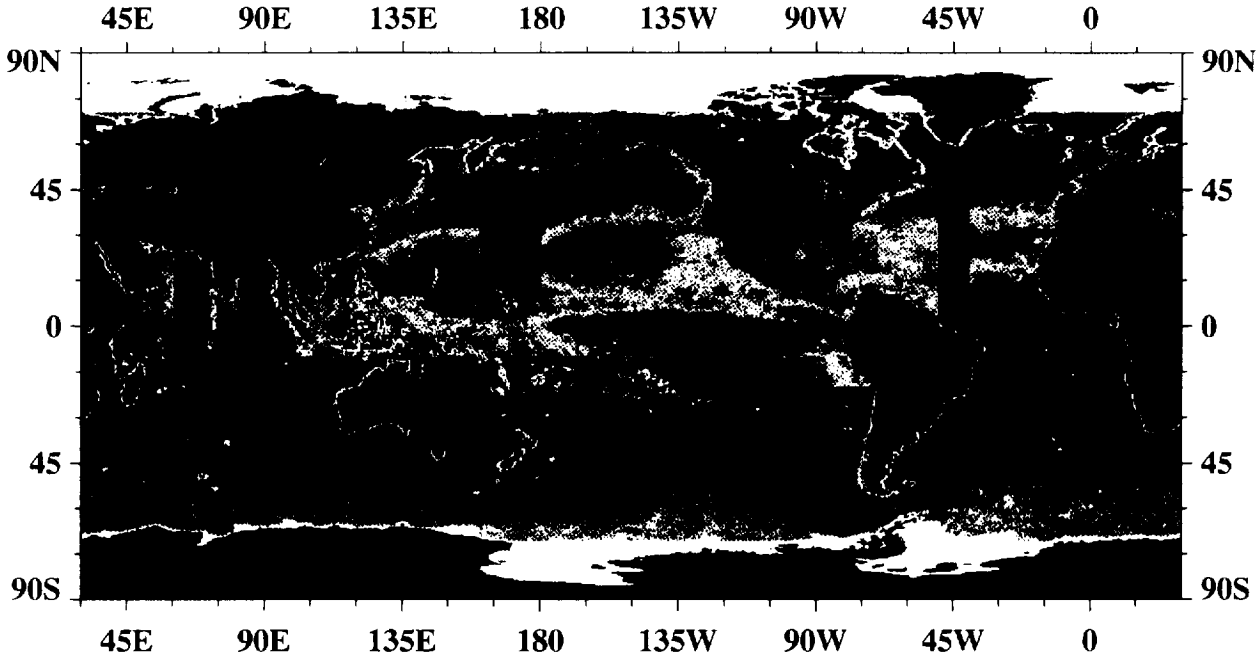

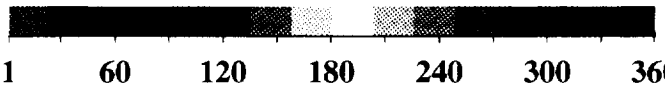

Number of Sea Surface Temperature Values per Pixel During 1993, max = 1252

A5

28-Day Mean AVHRR/2 Sea Surface Temperature

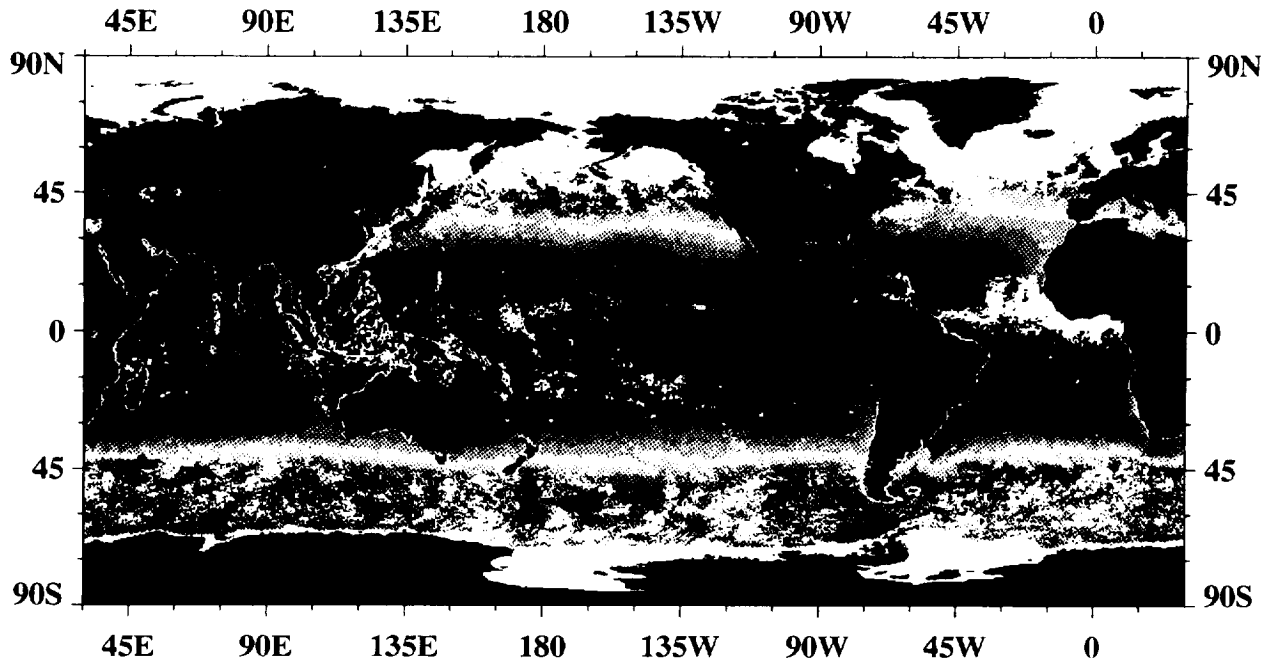

7 January to 3 February 1993

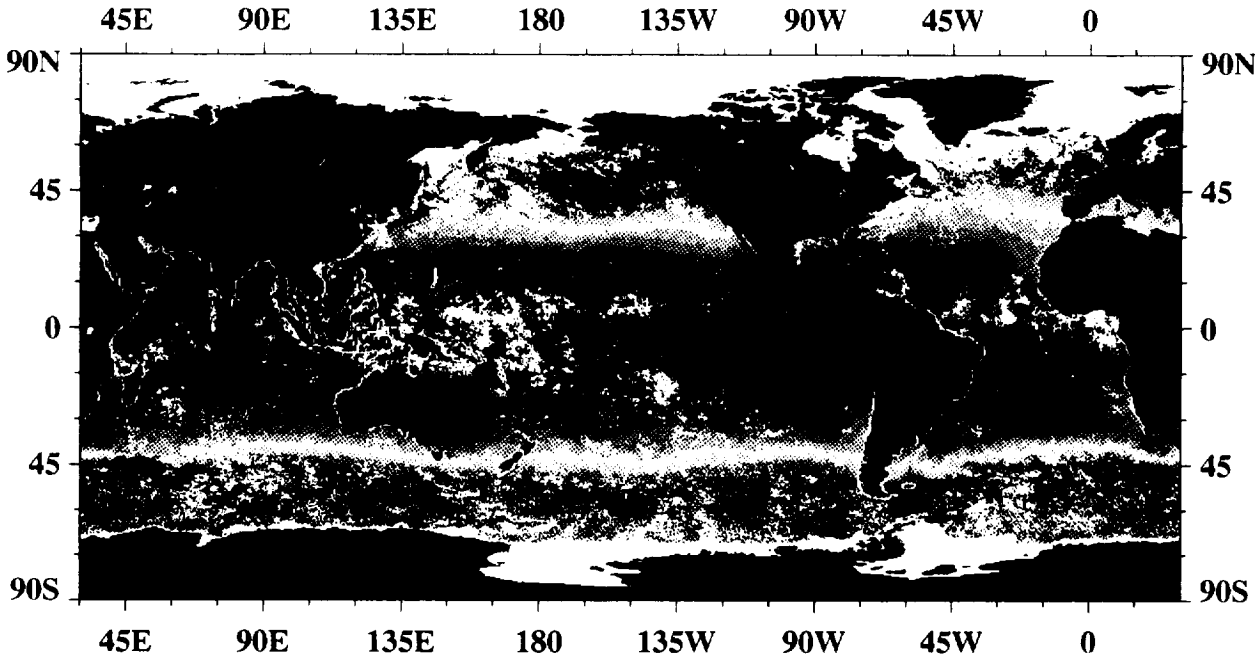

4 February to 3 March 1993

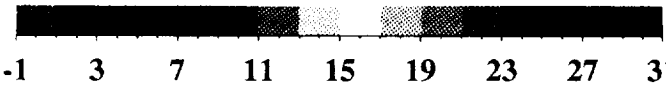

AVHRR Sea Surface Temperature, ^{o}C

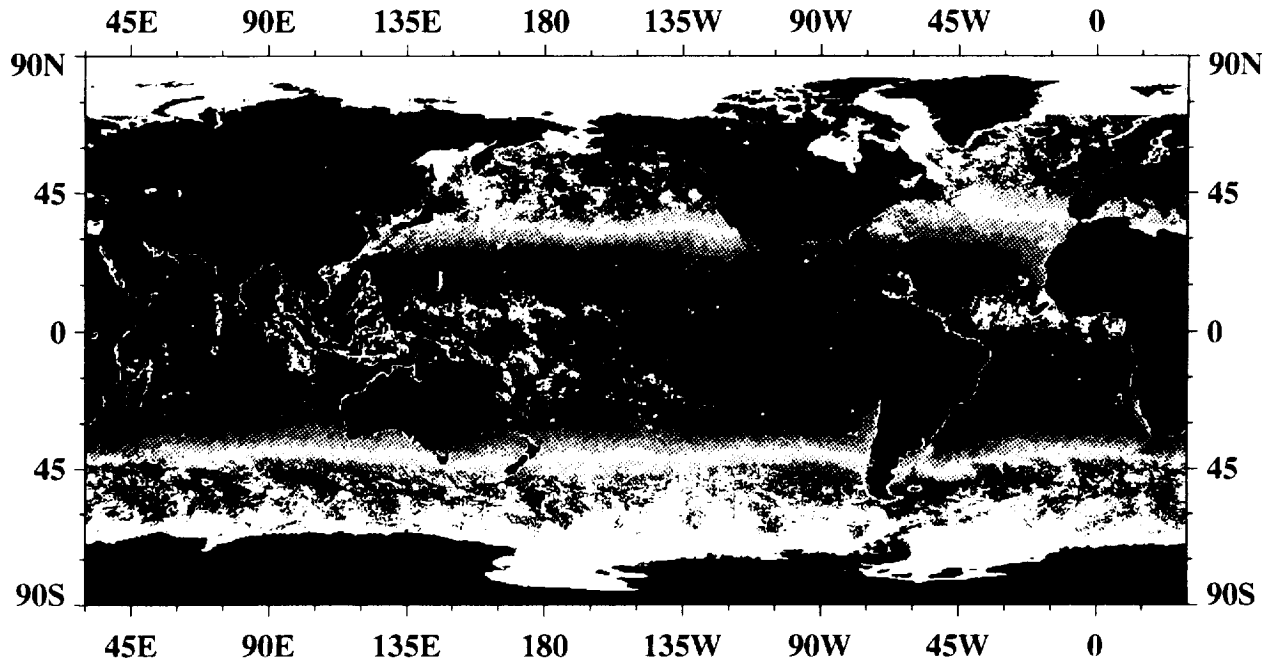

4 March to 30 March 1993

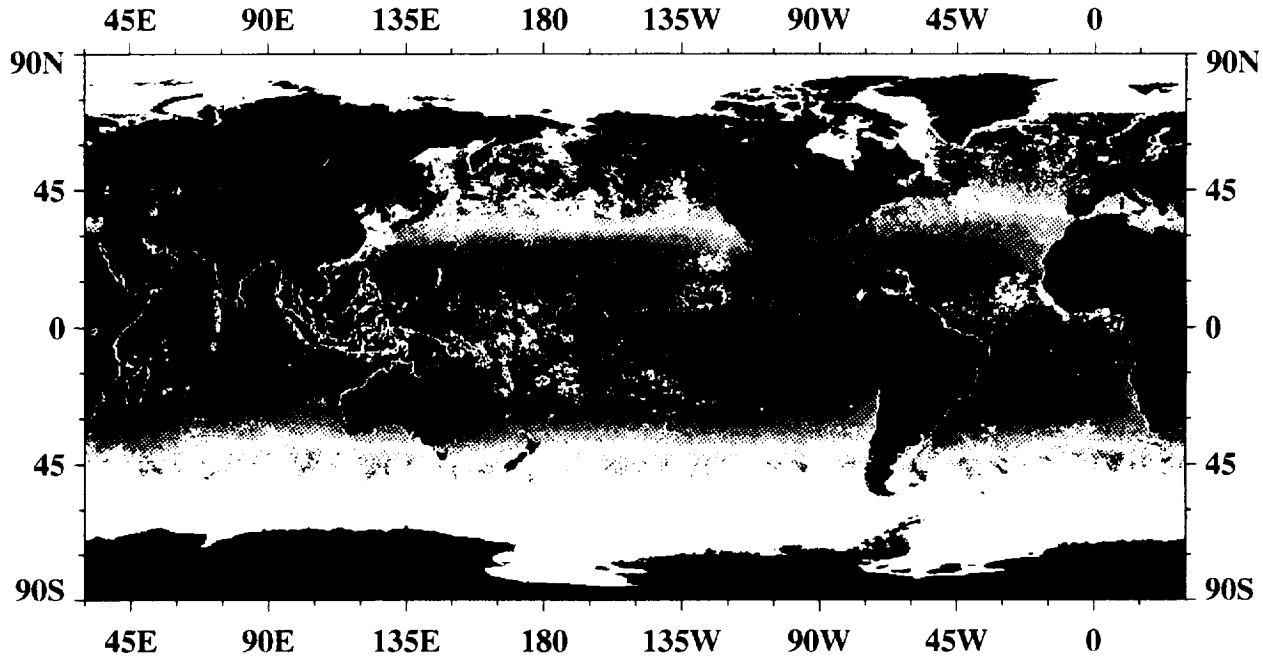

1 April to 28 April 1993

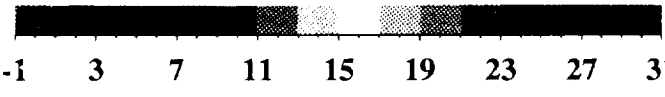

AVHRR Sea Surface Temperature, ^{O}C

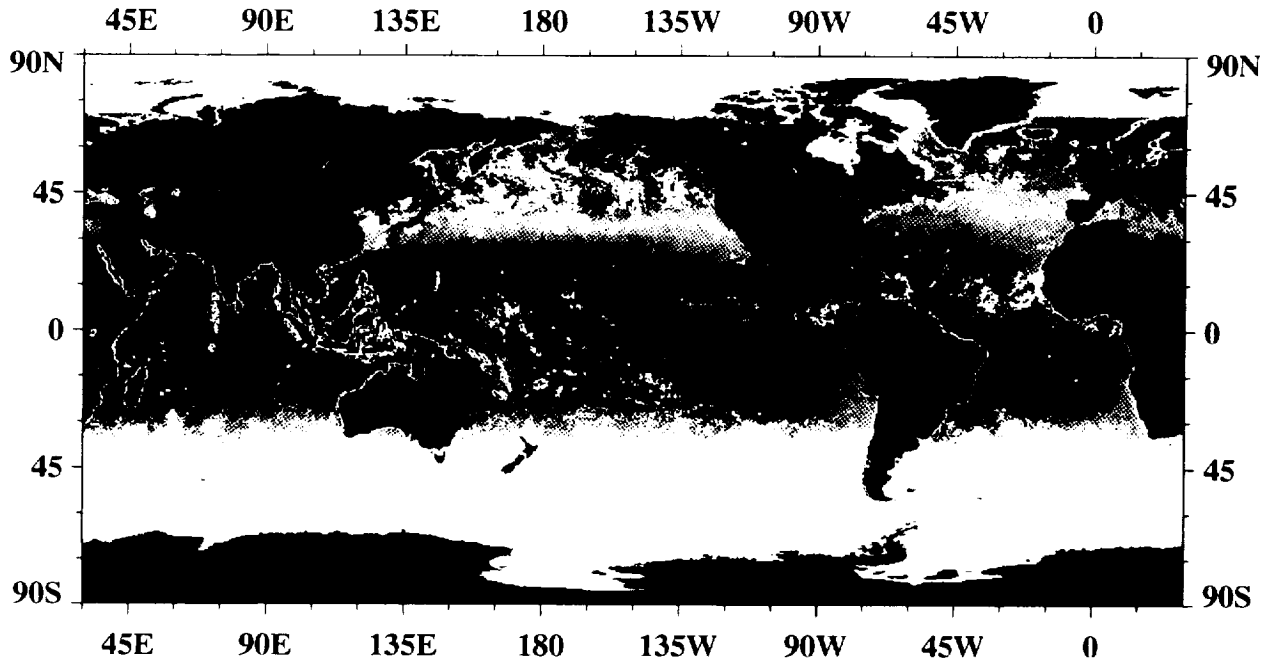

29 April to 26 May 1993

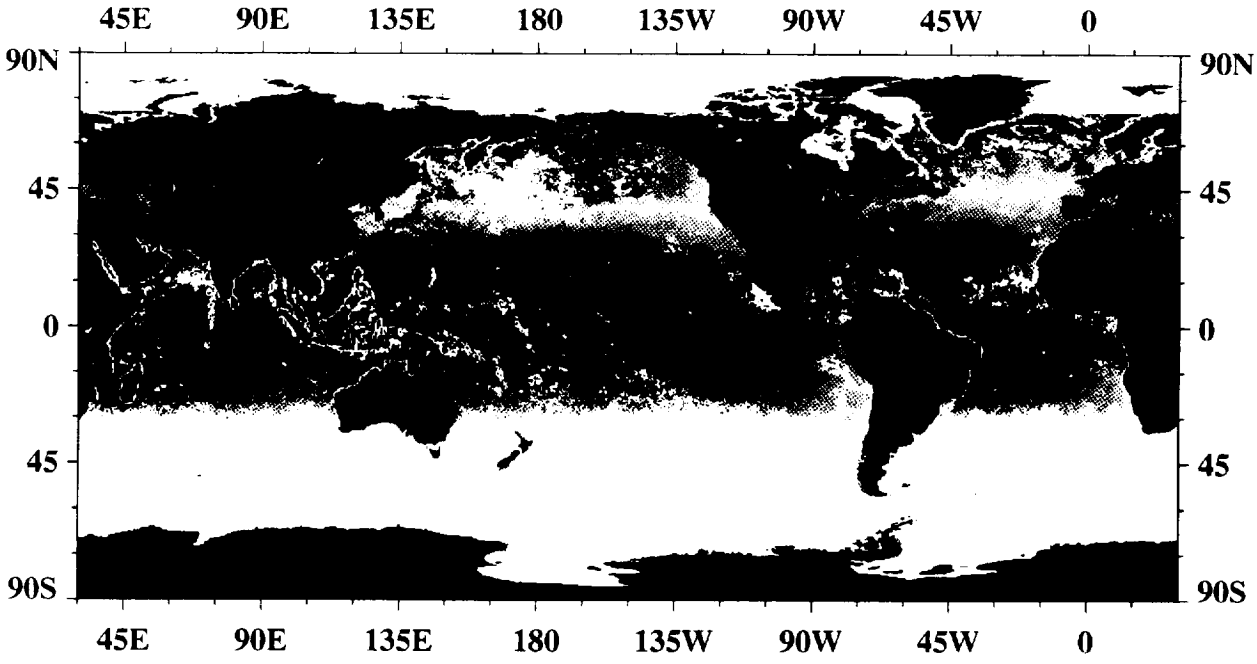

3 June to 30 June 1993

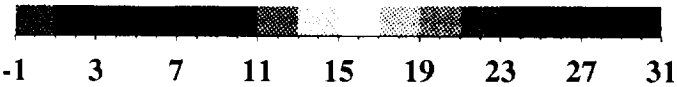

AVHRR Sea Surface Temperature, ^{O}C

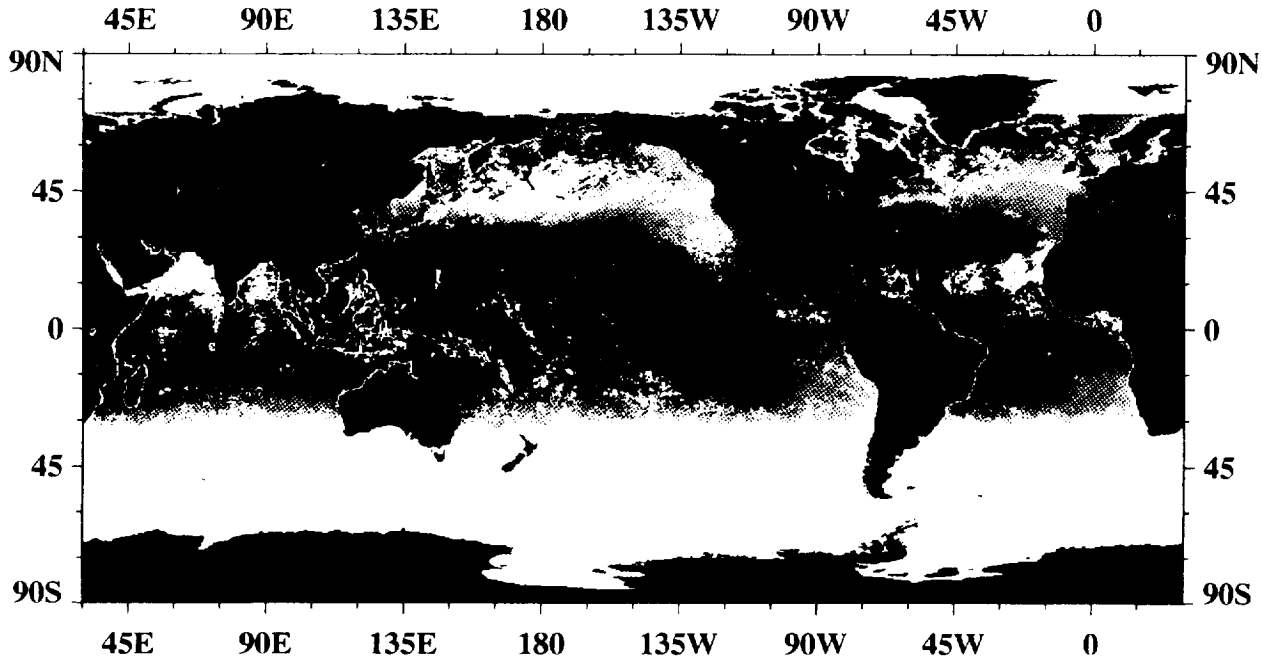

1 July to 28 July 1993

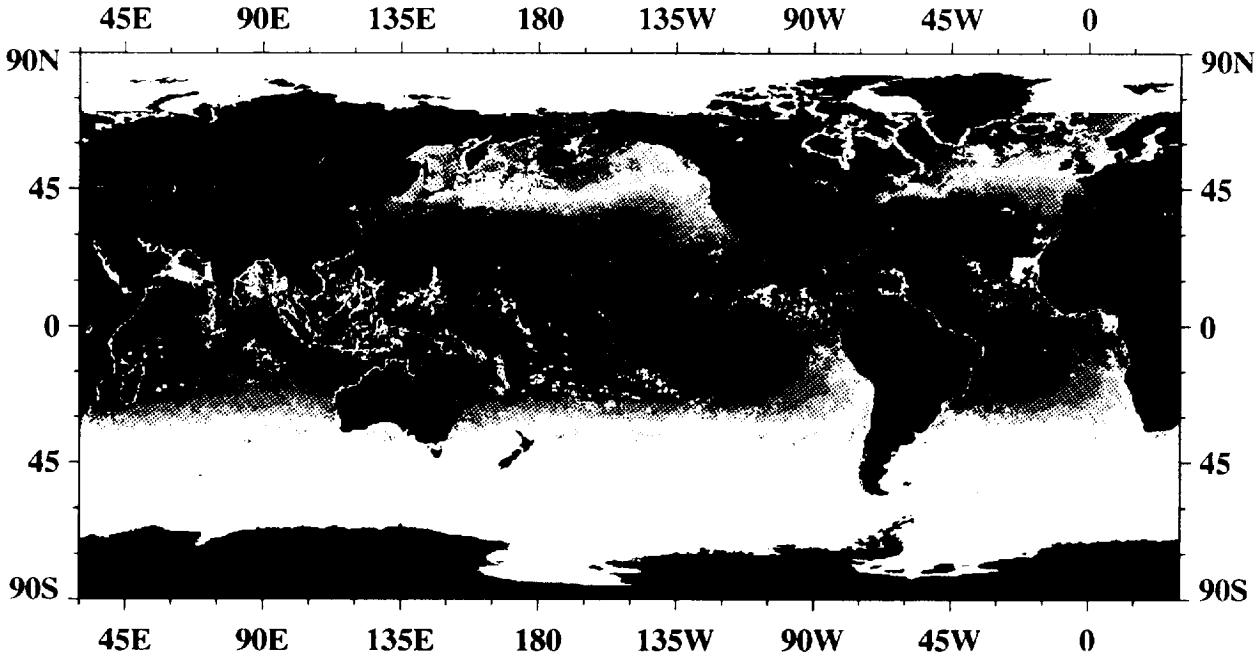

29 July to 1 September 1993

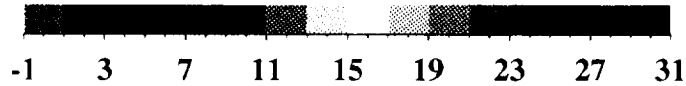

AVHRR Sea Surface Temperature, ^{O}C

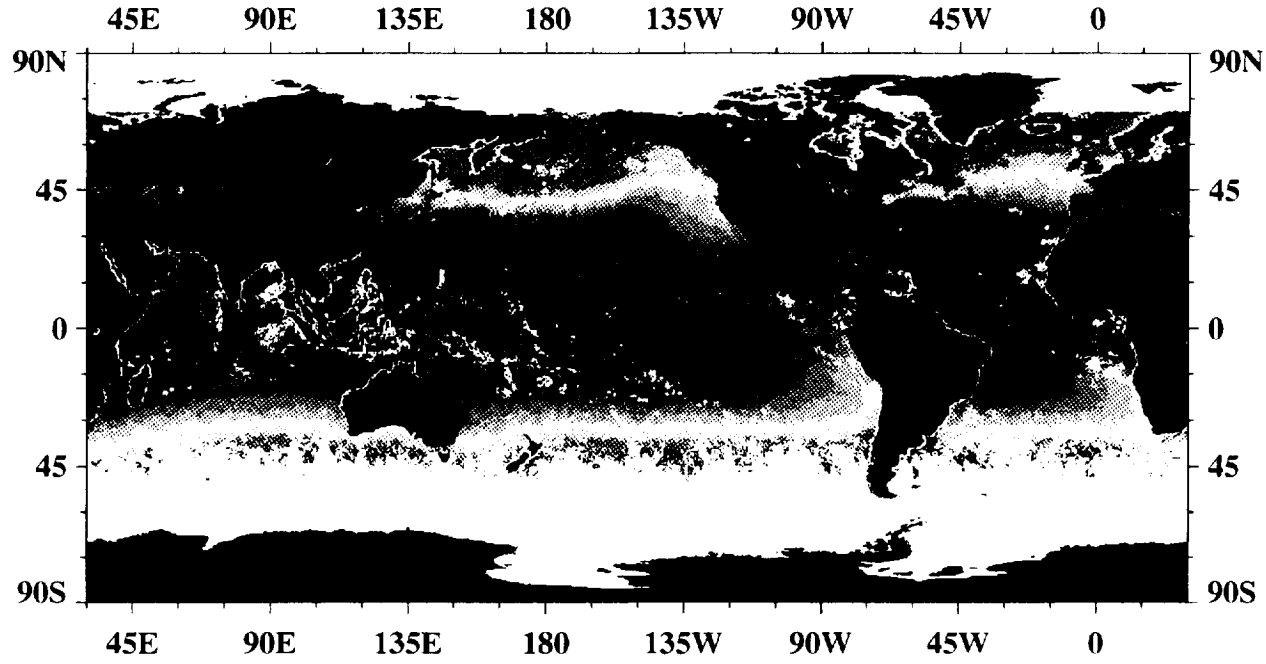

2 September to 29 September 1993

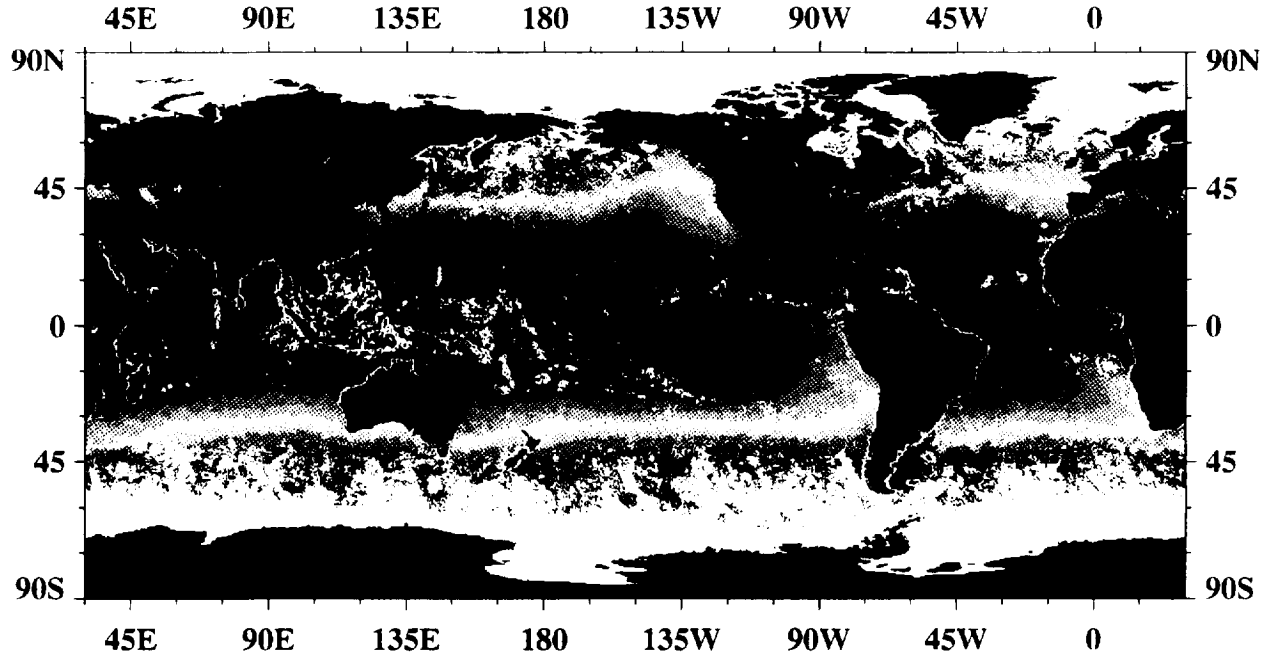

30 September to 27 October 1993

AVHRR Sea Surface Temperature, ^{o}C

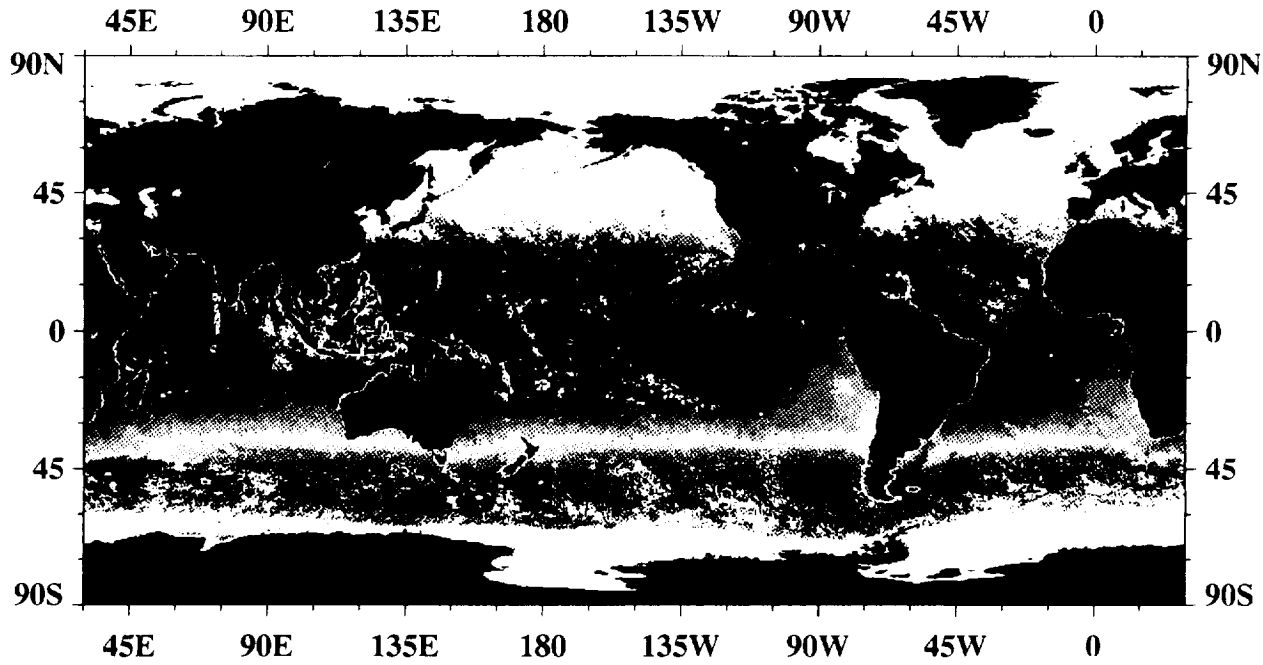

4 November to 1 December 1993

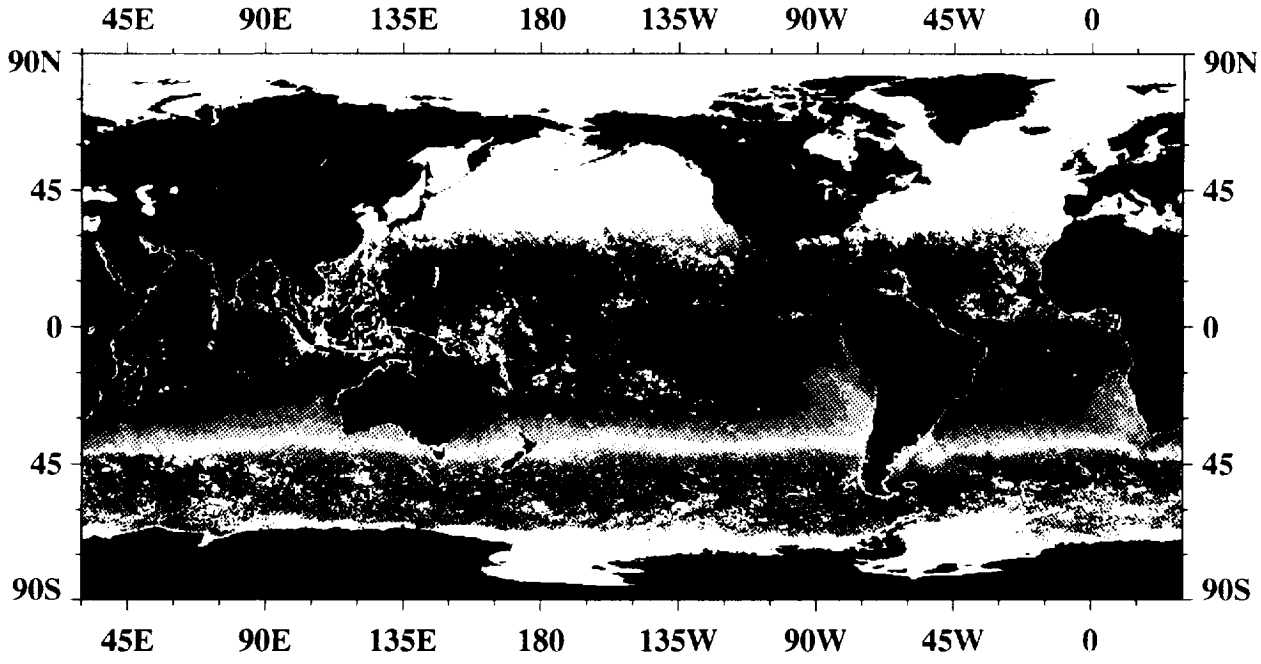

2 December to 29 December 1993

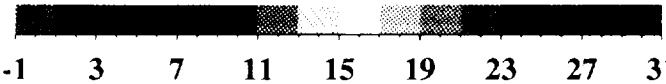

AVHRR Sea Surface Temperature, ^{o}C

A6

28-Day AVHRR/2 Sampling Distribution

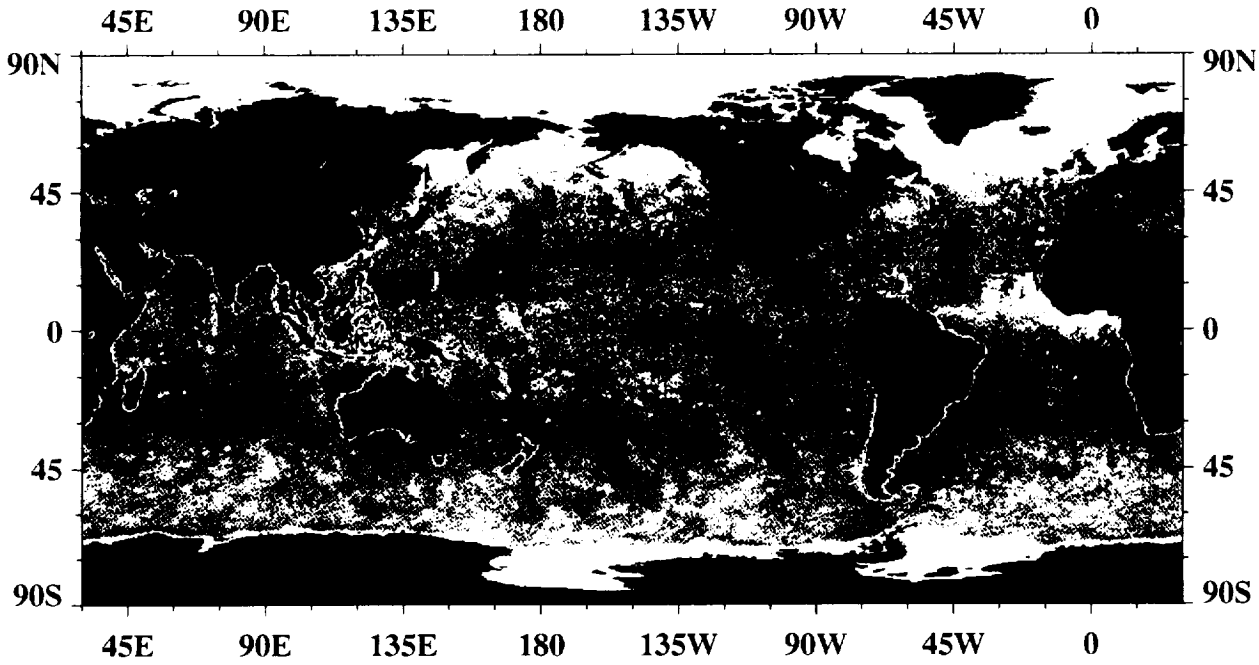

7 January to 3 February 1993, max = 161

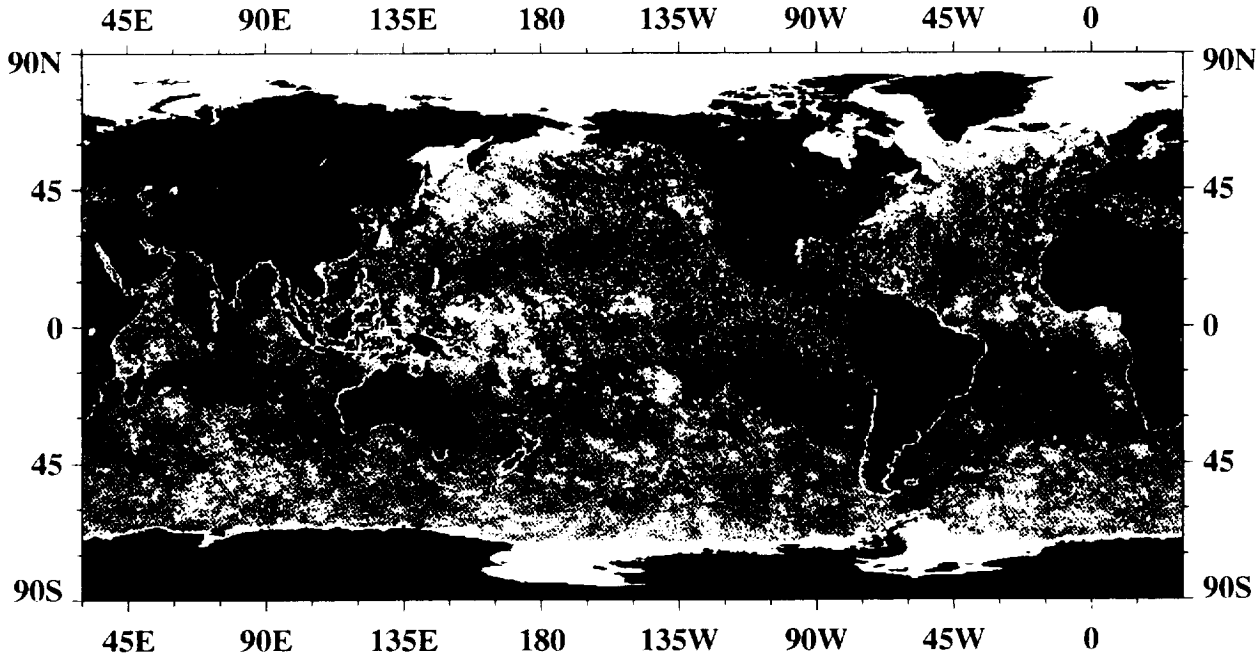

4 February to 3 March 1993, max = 199

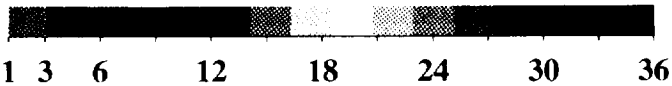

Number of AVHRR Sea Surface Temperature Values per Pixel

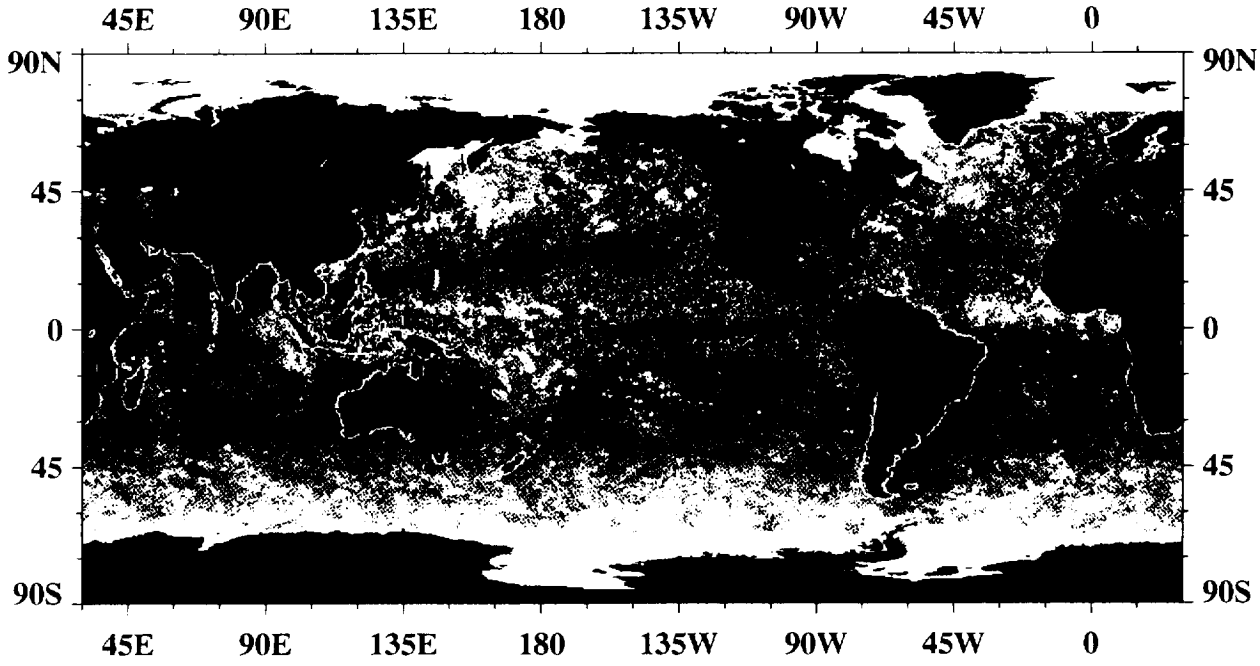

4 March to 30 March 1993, max = 195

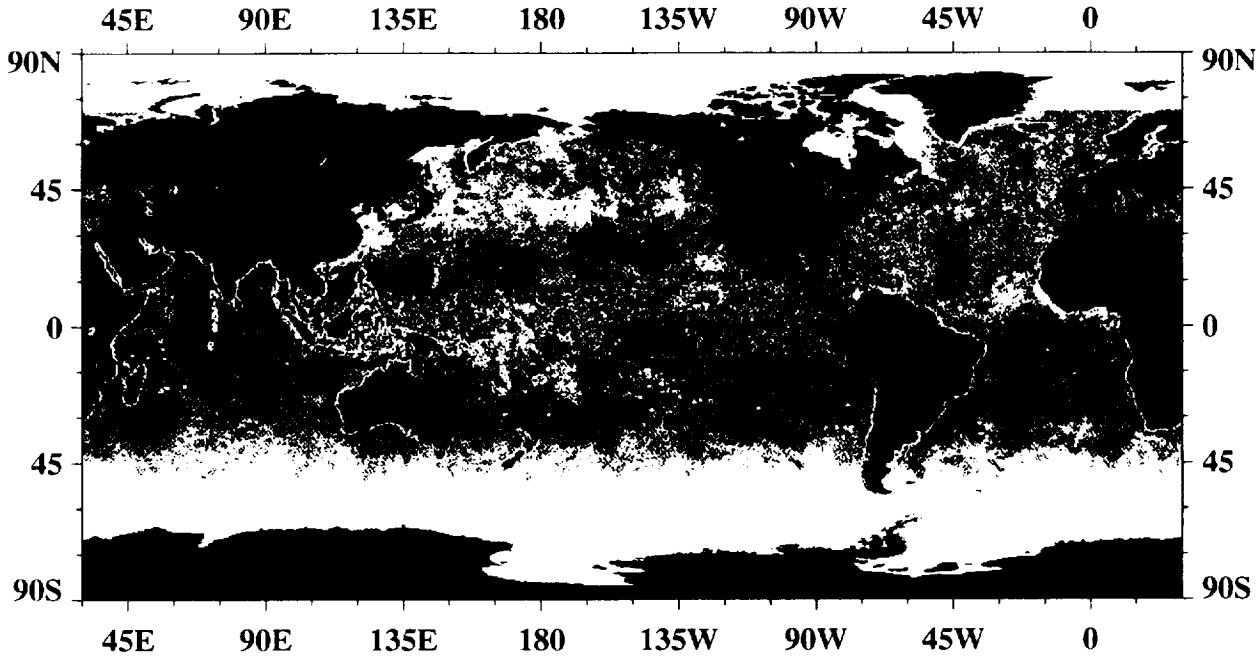

1 April to 28 April 1993, max = 206

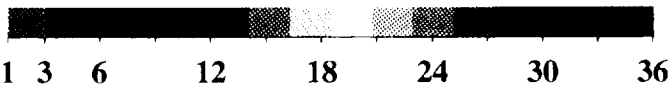

Number of AVHRR Sea Surface Temperature Values per Pixel

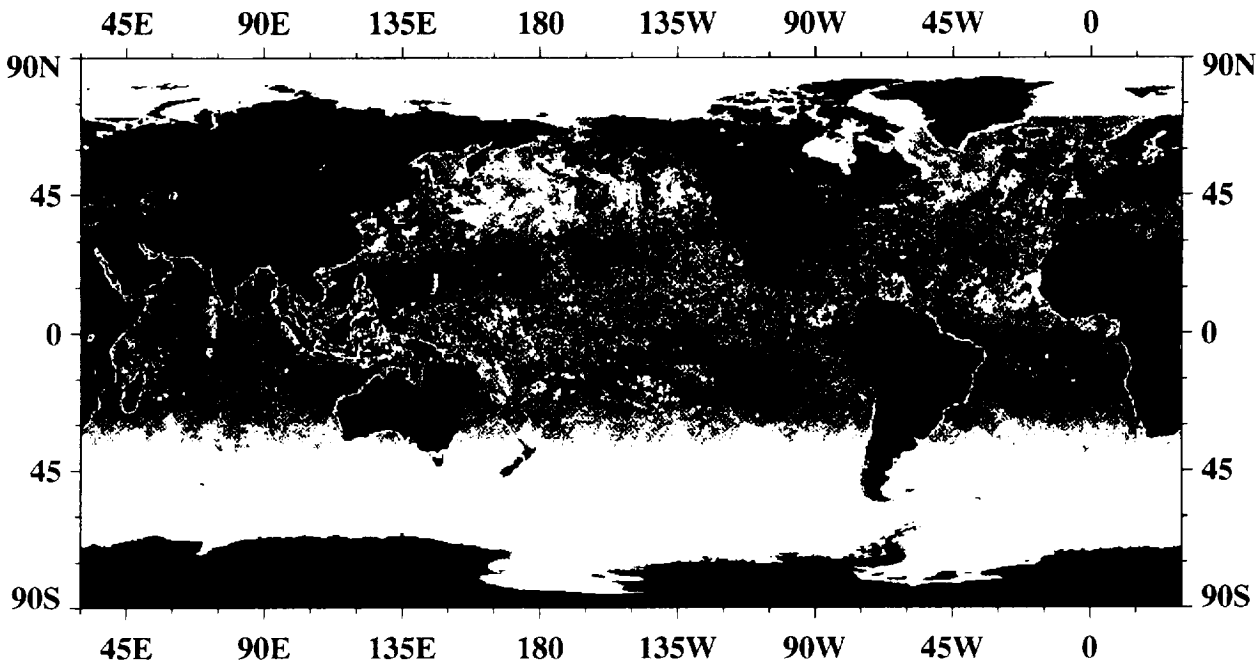

29 April to 26 May 1993, max = 155

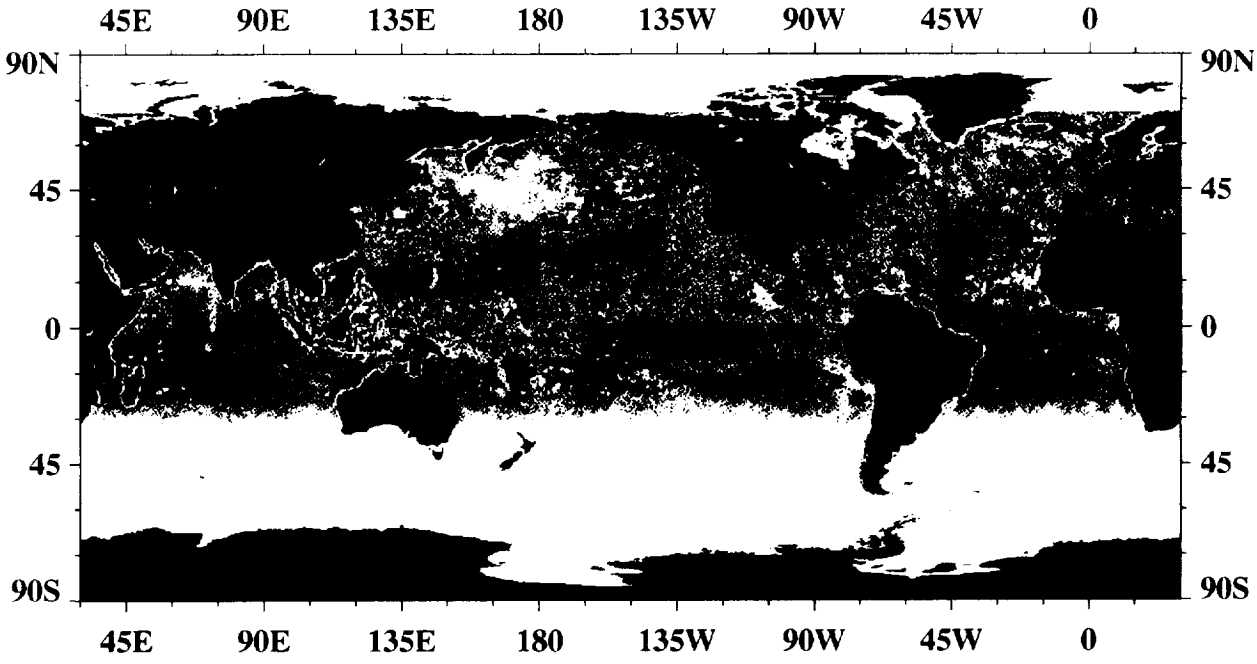

3 June to 30 June 1993, max = 135

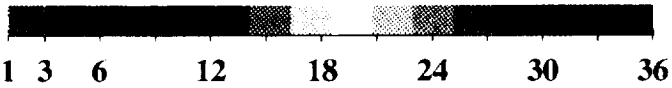

Number of AVHRR Sea Surface Temperature Values per Pixel

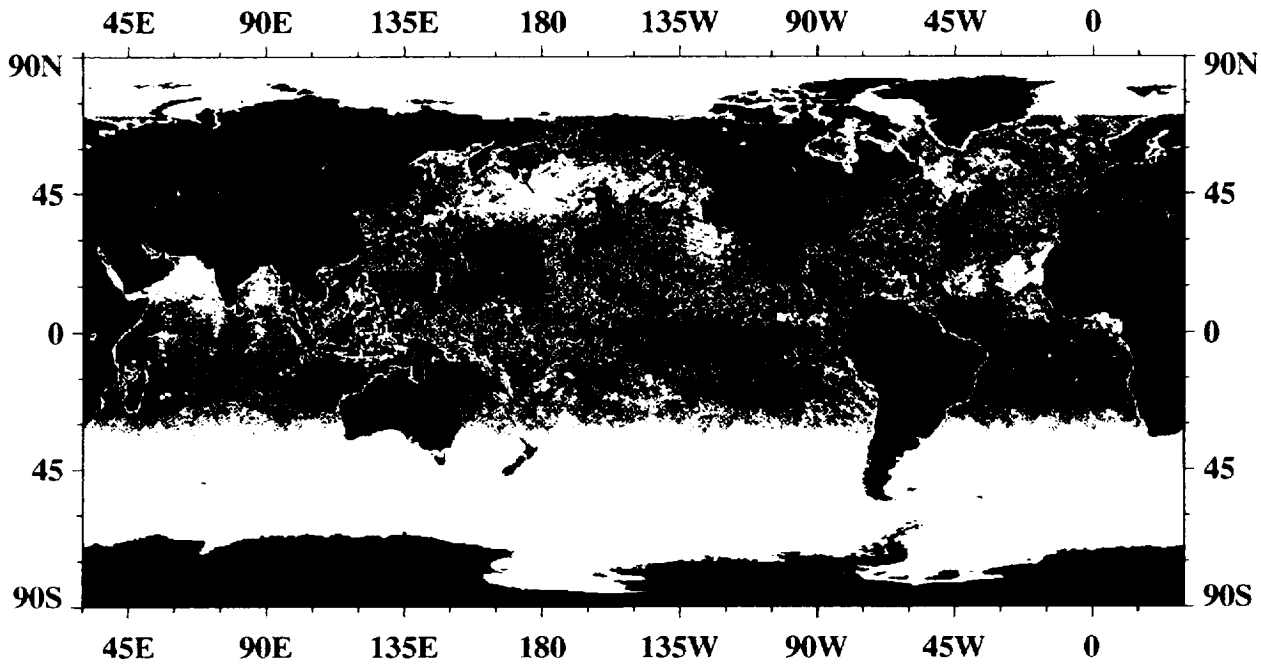

1 July to 28 July 1993, max = 155

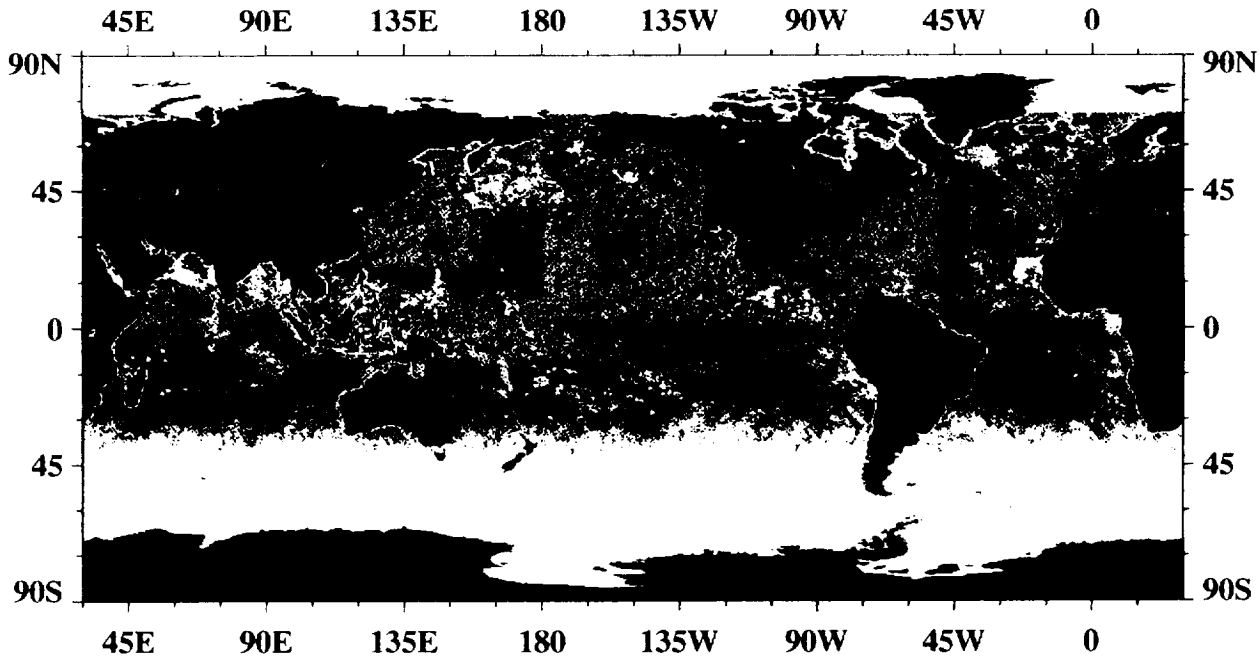

29 July to 1 September 1993, max = 129

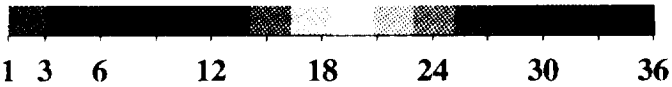

Number of AVHRR Sea Surface Temperature Values per Pixel

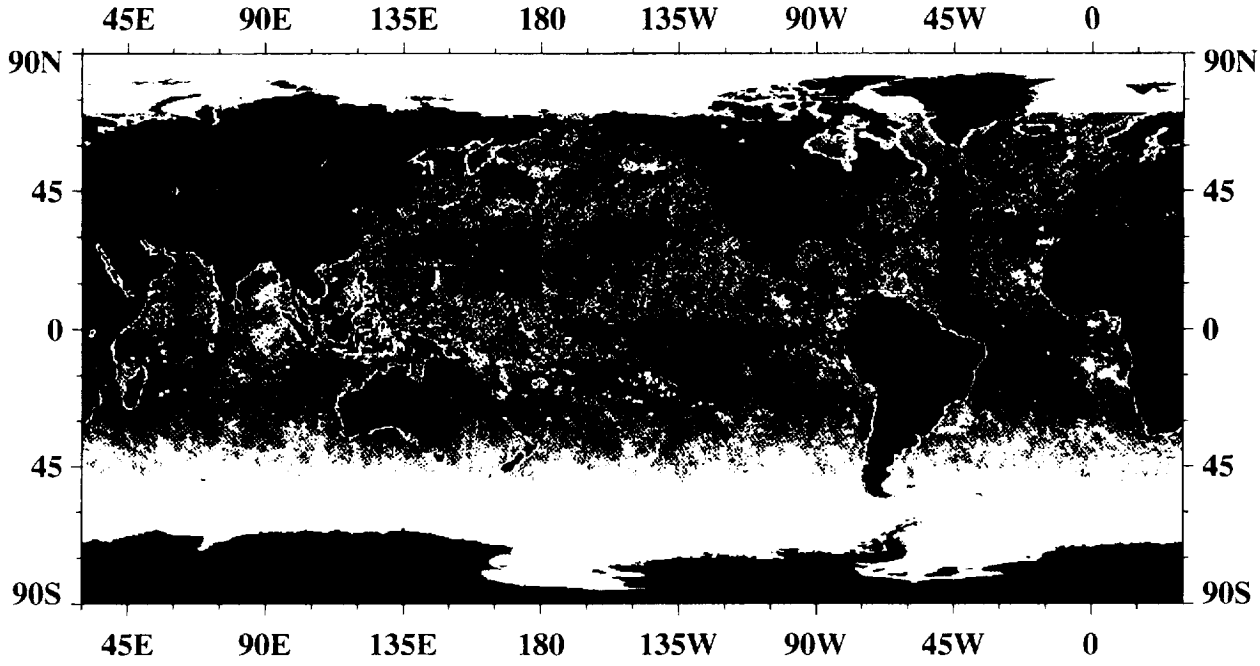

2 September to 29 September 1993, max = 132

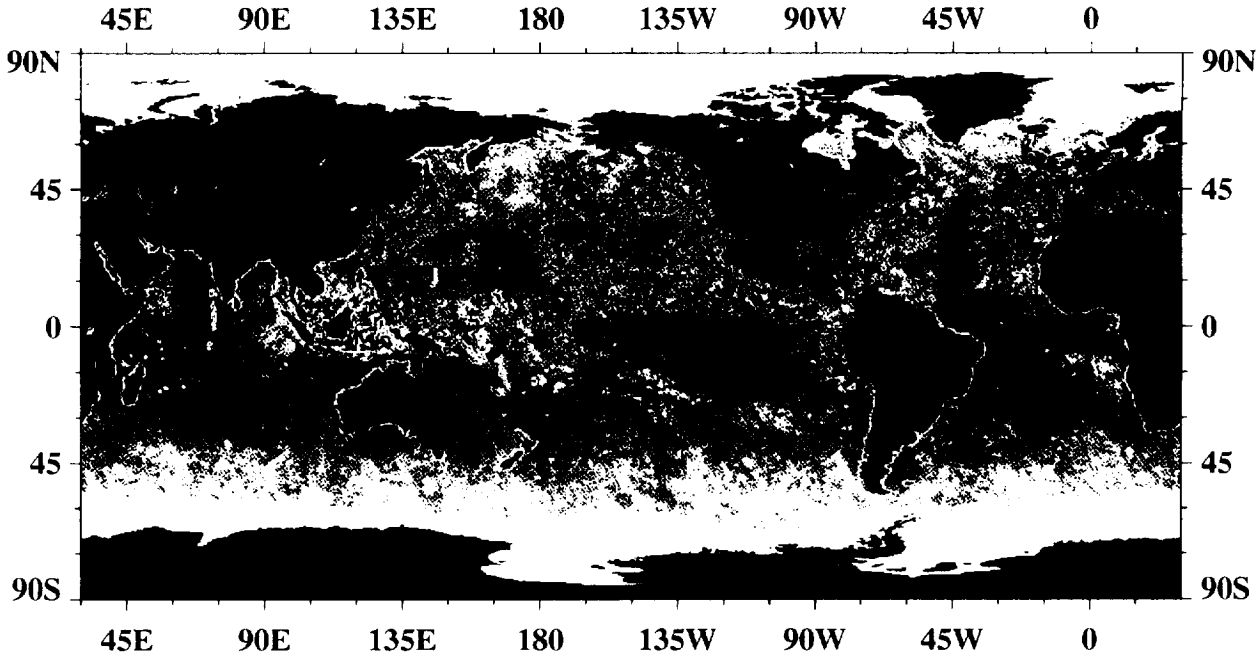

30 September to 27 October 1993, max = 115

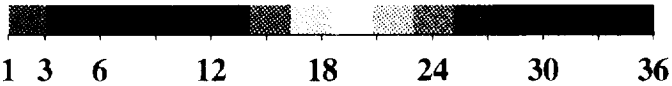

Number of AVHRR Sea Surface Temperature Values per Pixel

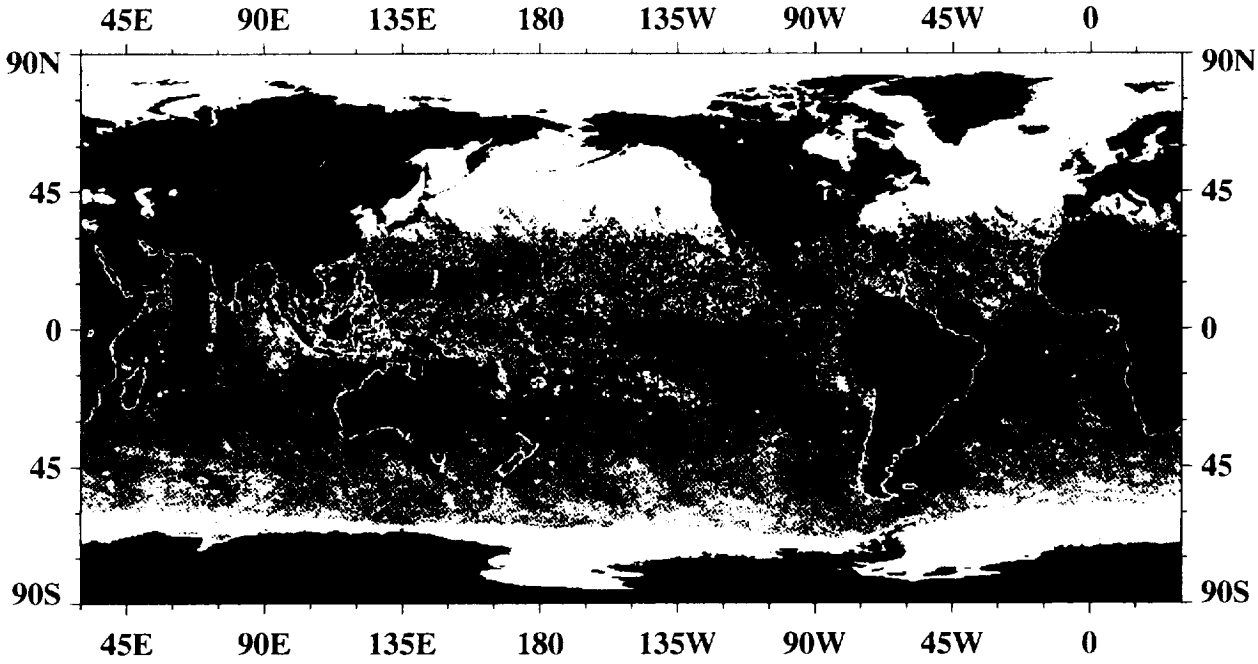

4 November to 1 December 1993, max = 117

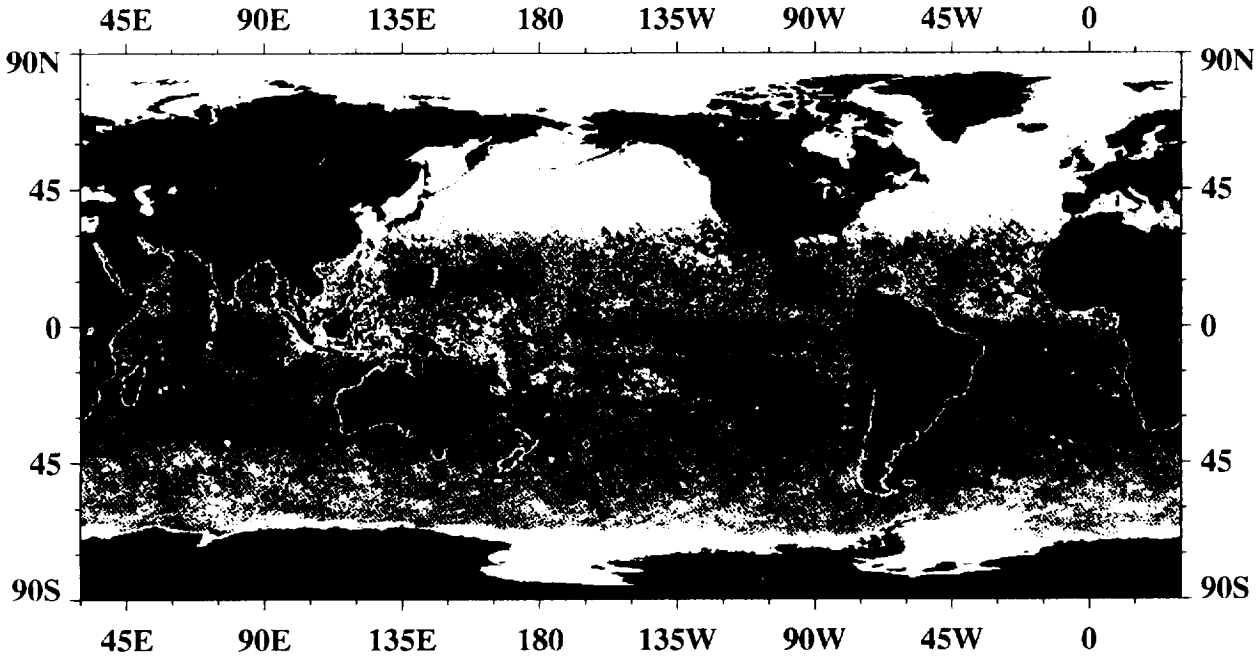

2 December to 29 December 1993, max = 130

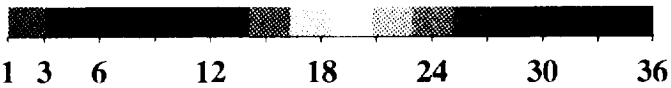

Number of AVHRR Sea Surface Temperature Values per Pixel

A7

Annual Mean AMI Surface Wind Velocity

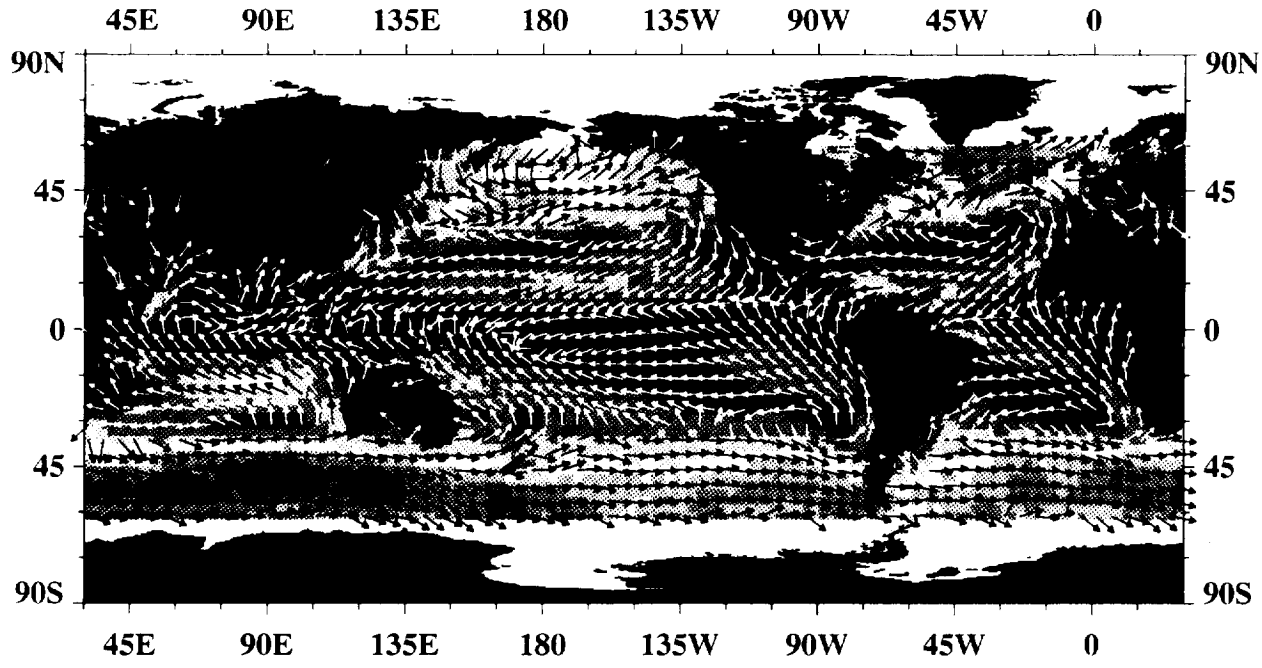

Annual Mean 1993

ERS-1 AMI 10 m Wind Speed, m s^{-1}

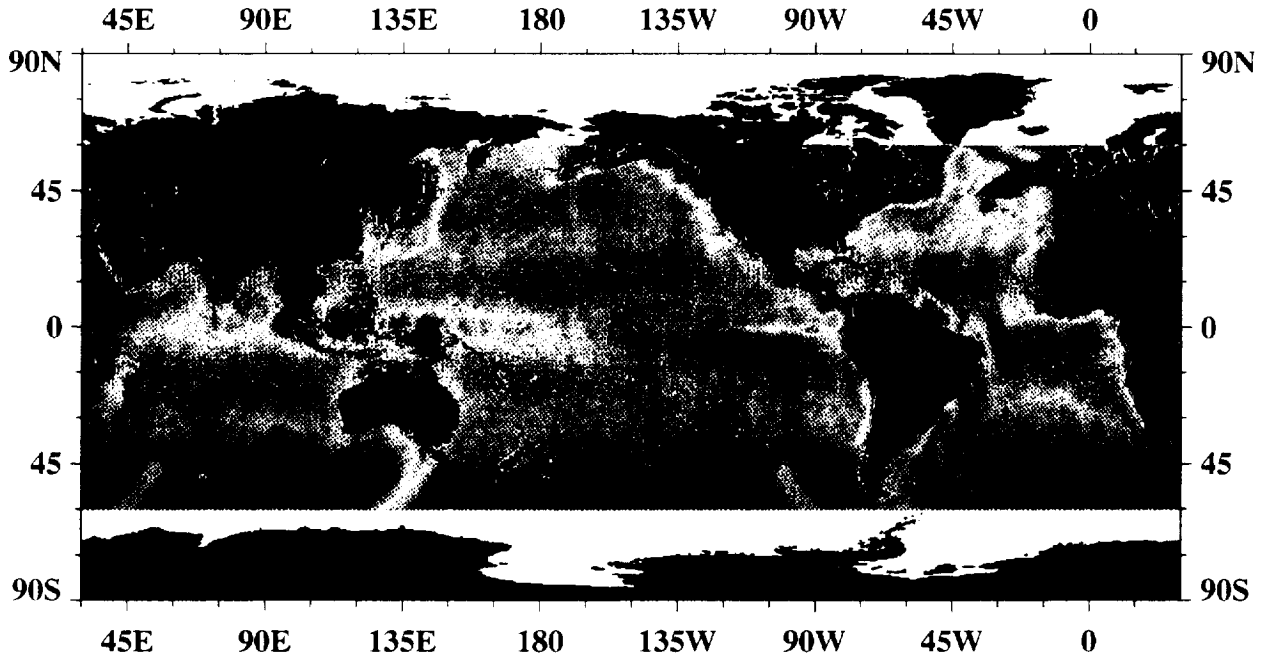

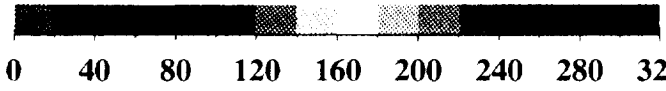

Number of ERS-1 AMI Wind Speed Values per Pixel max = 379

A8

Monthly Mean AMI Surface Wind Velocity

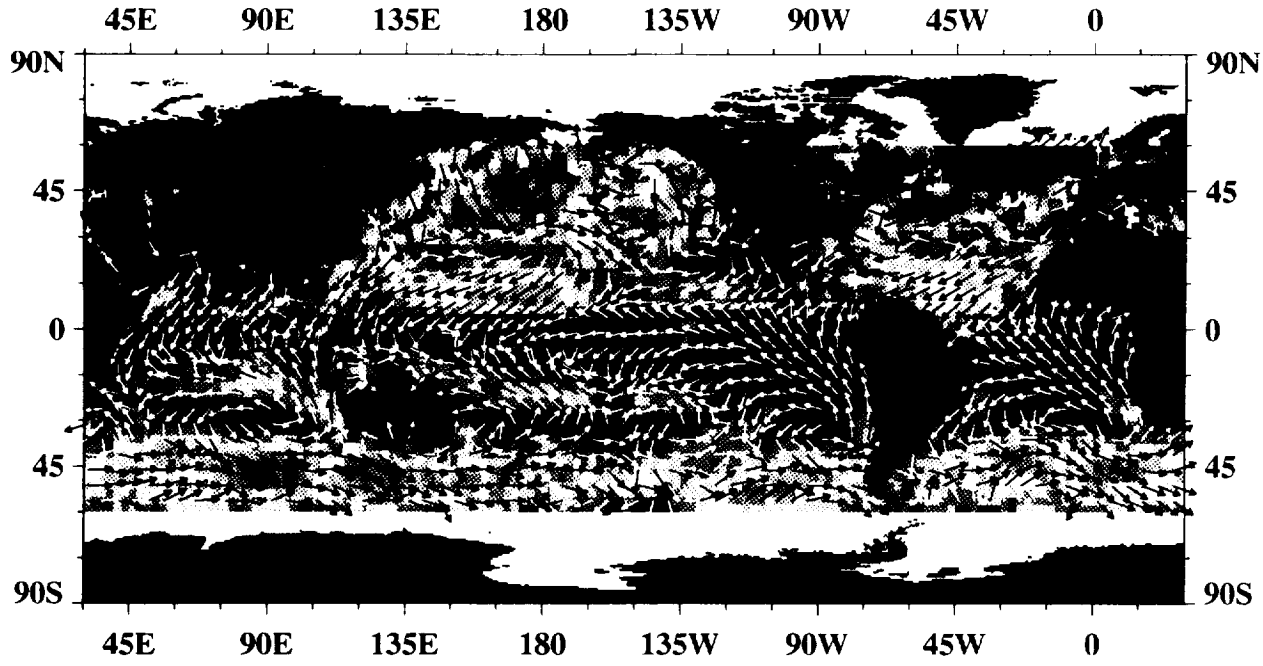

January 1993

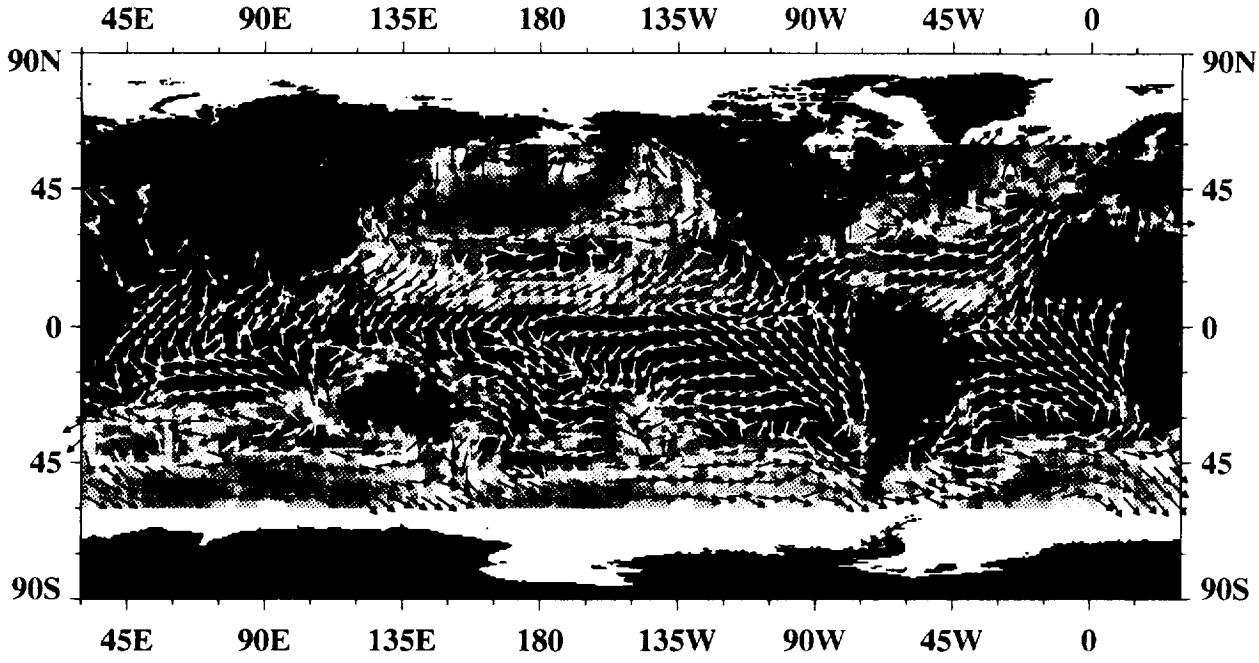

February 1993

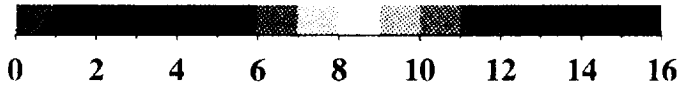

ERS-1 AMI 10 m Wind Speed, m s^{-1}

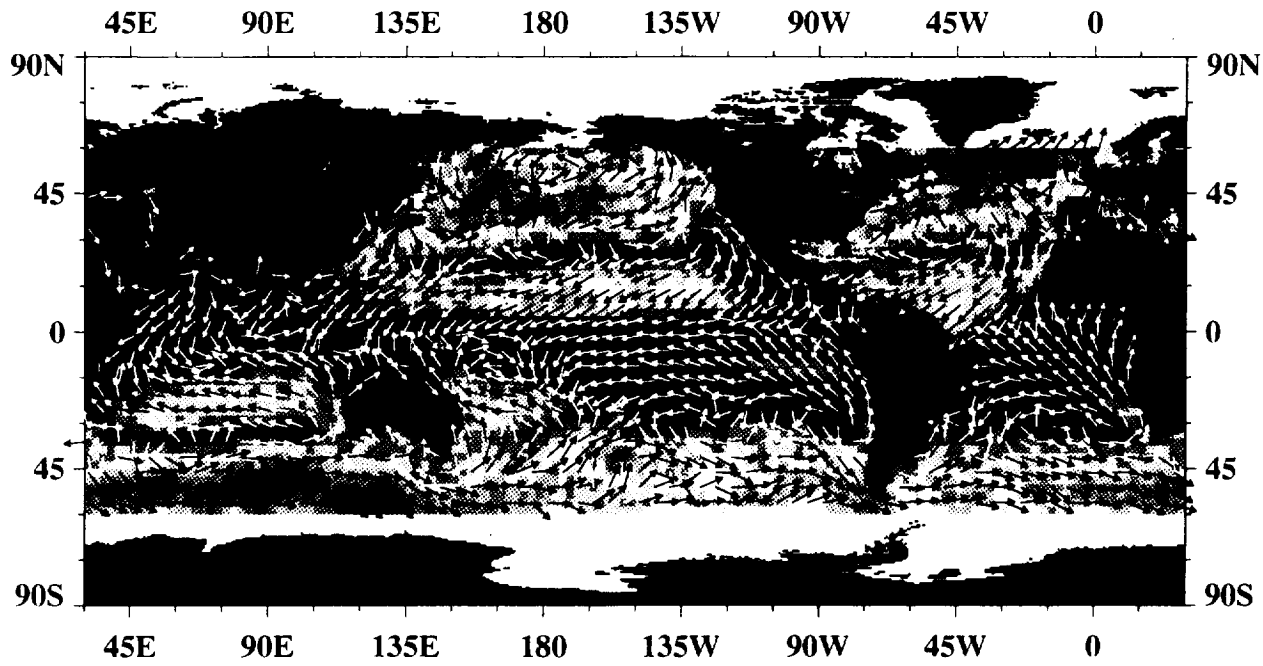

March 1993

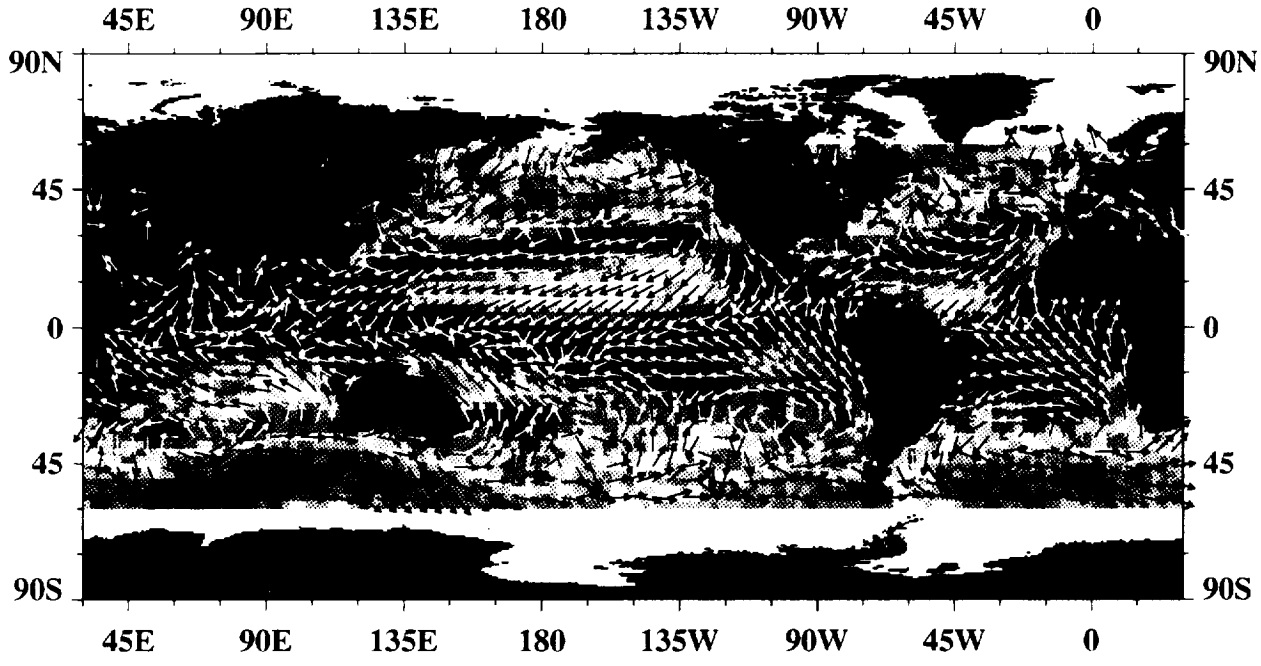

April 1993

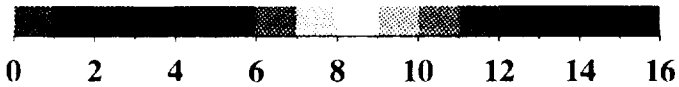

ERS-1 AMI 10 m Wind Speed, m s^{-1}

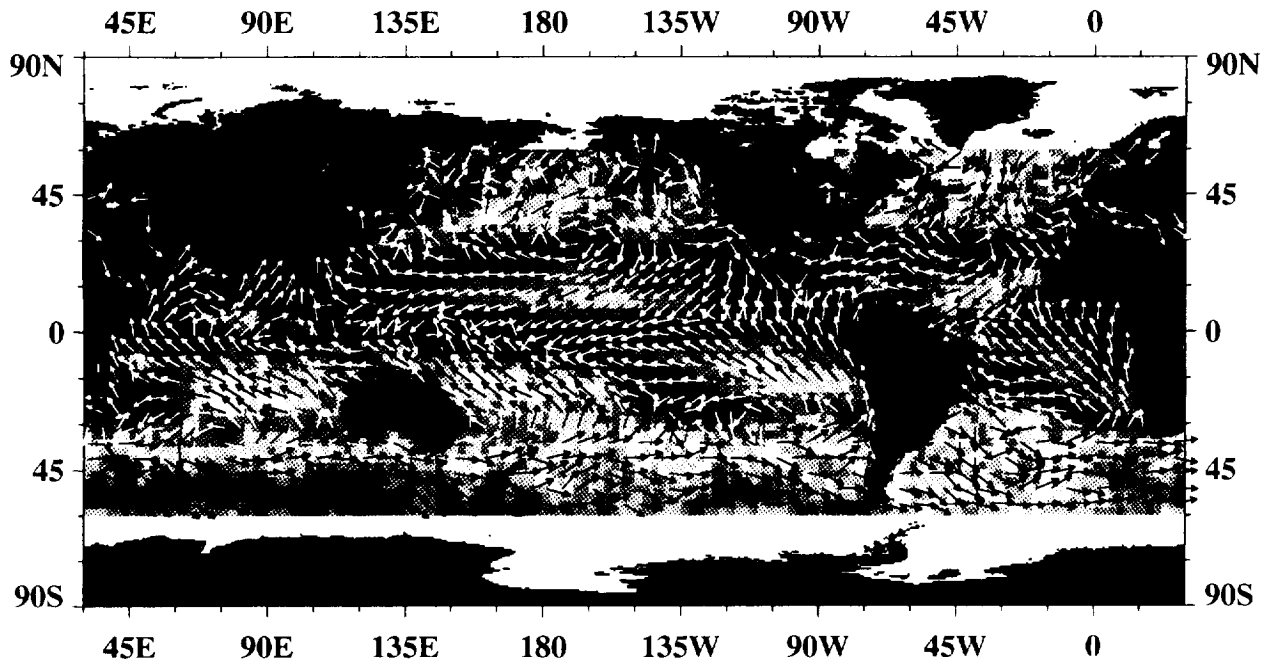

May 1993

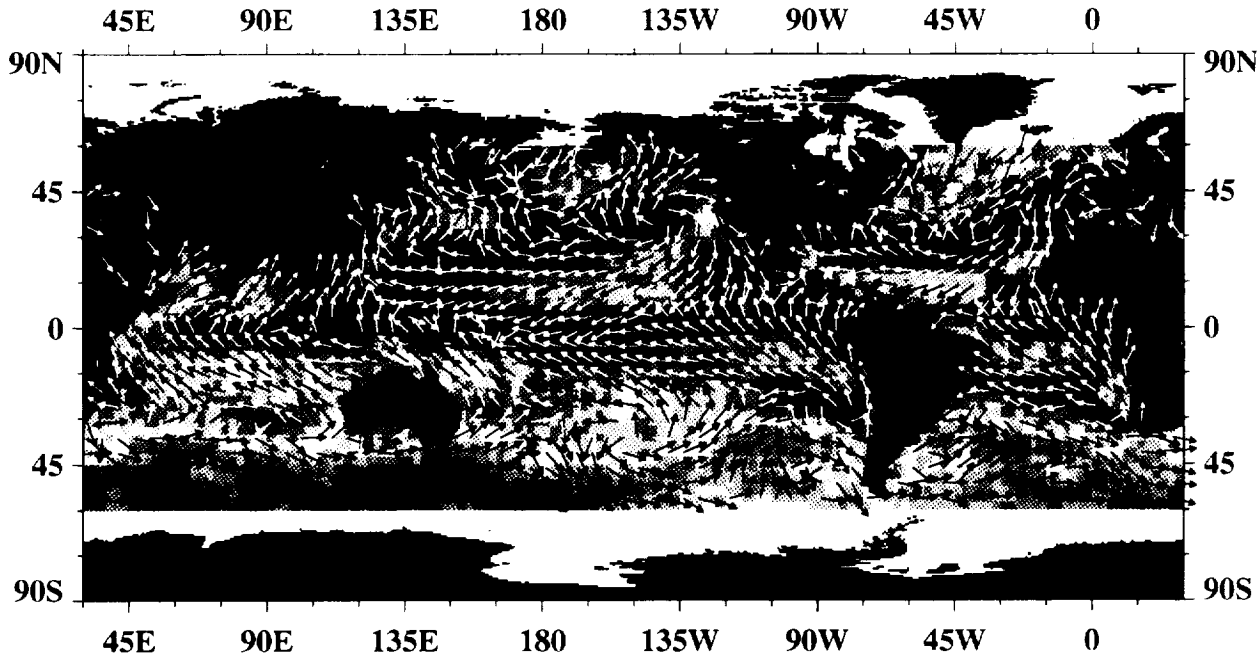

June 1993

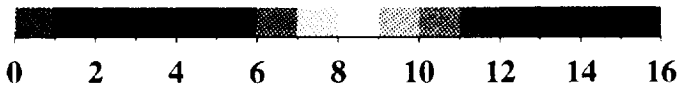

ERS-1 AMI 10 m Wind Speed, m s^{-1}

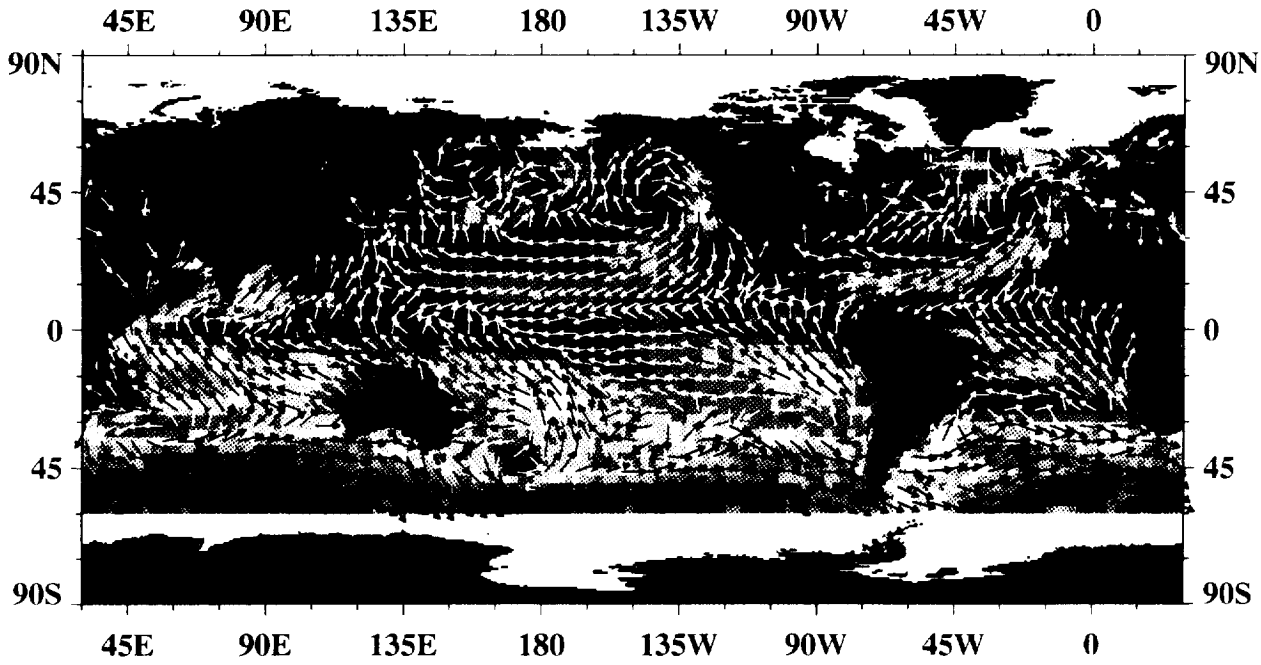

July 1993

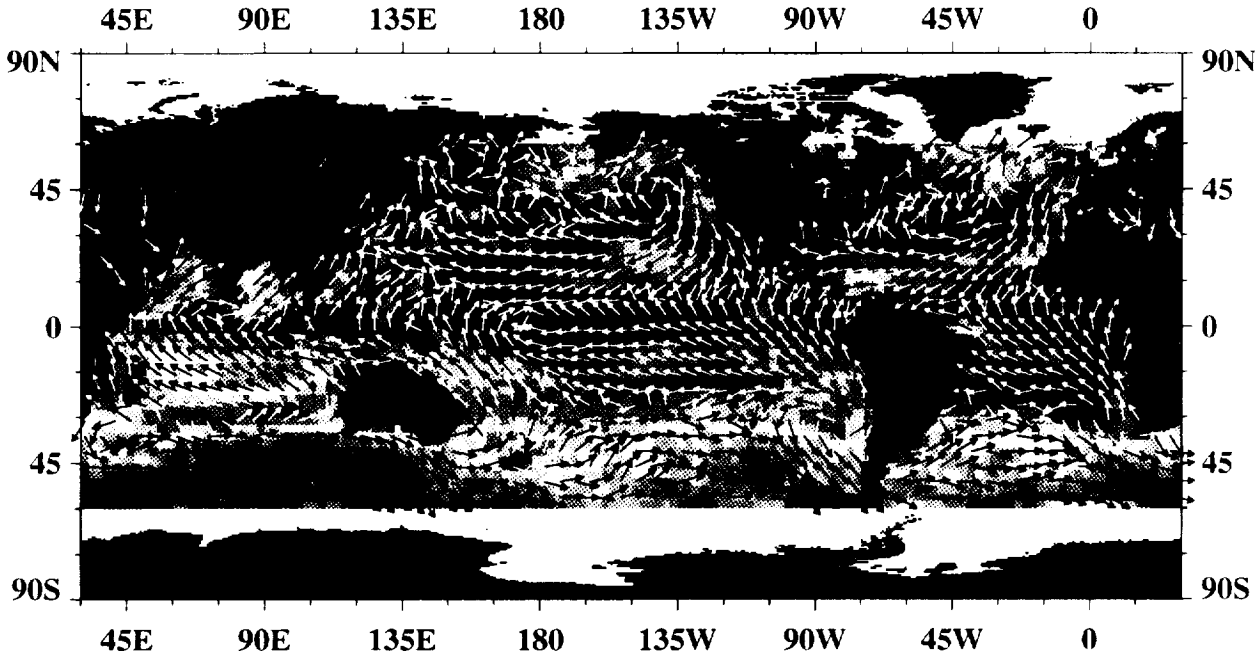

August 1993

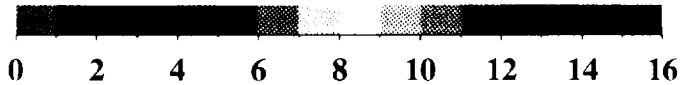

ERS-1 AMI 10 m Wind Speed, m s^{-1}

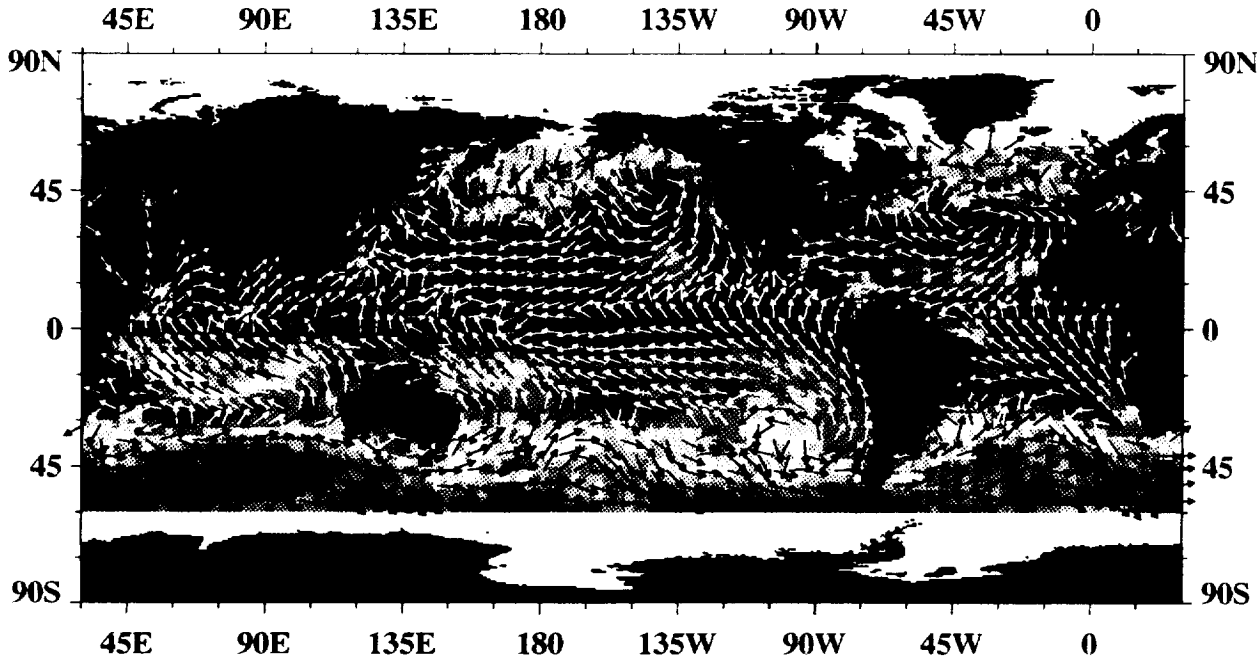

September 1993

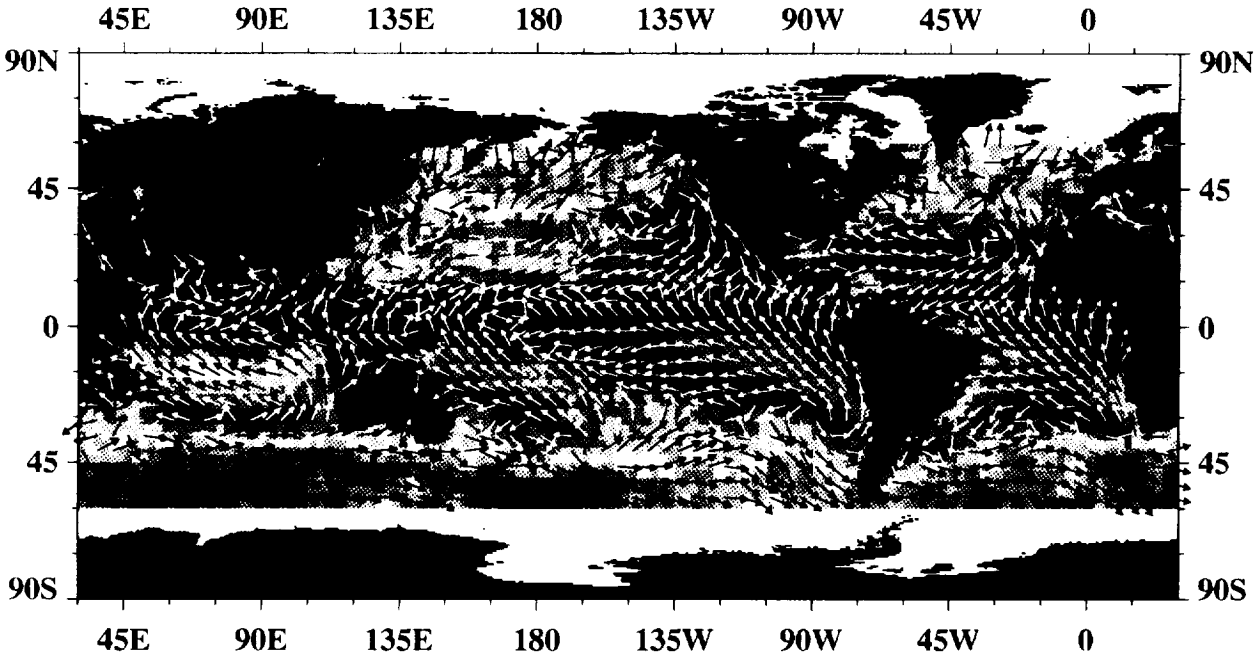

October 1993

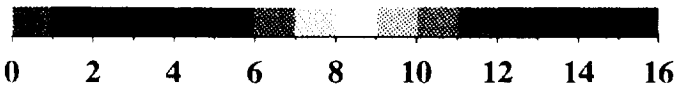

ERS-1 AMI 10 m Wind Speed, m s^{-1}

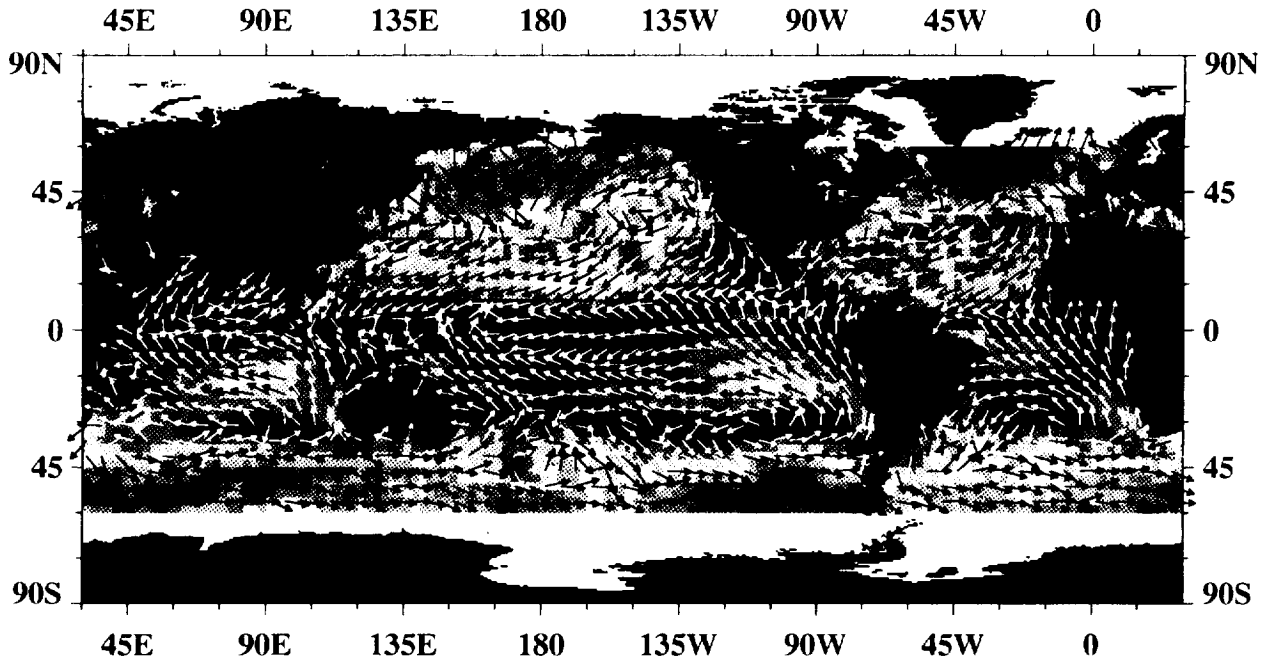

November 1993

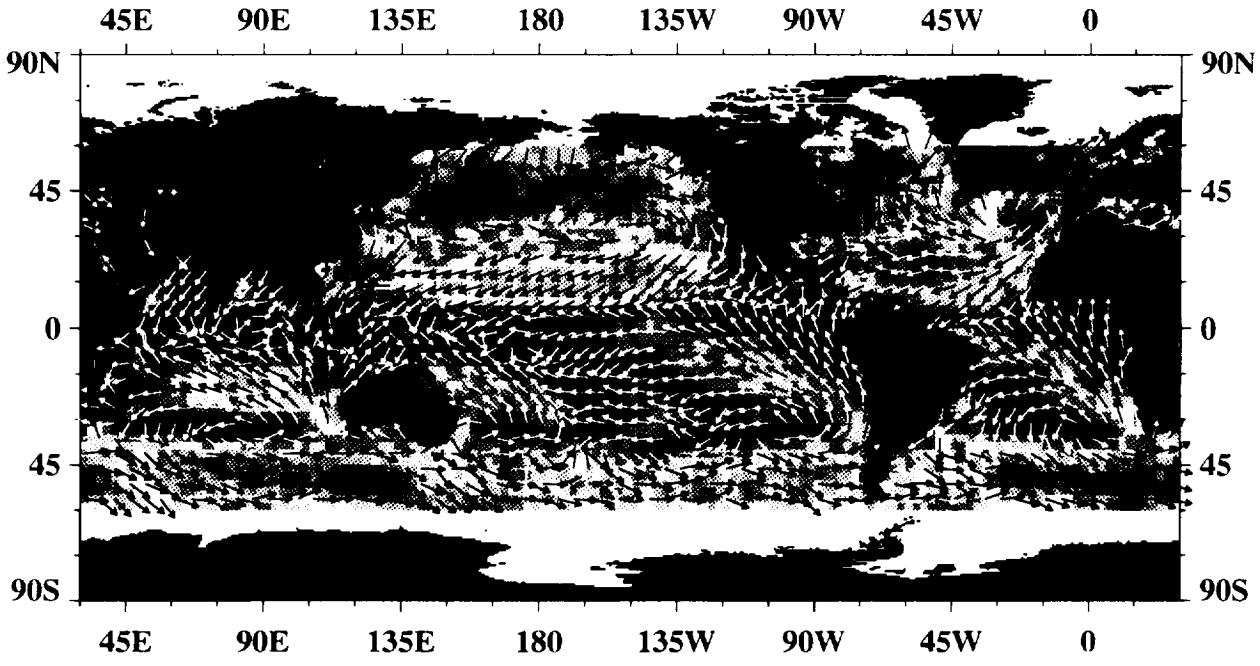

1 - 21 December 1993

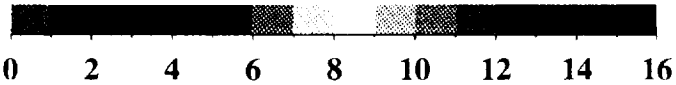

ERS-1 AMI 10 m Wind Speed, m s^{-1}

A9

Monthly AMI Sampling Distribution

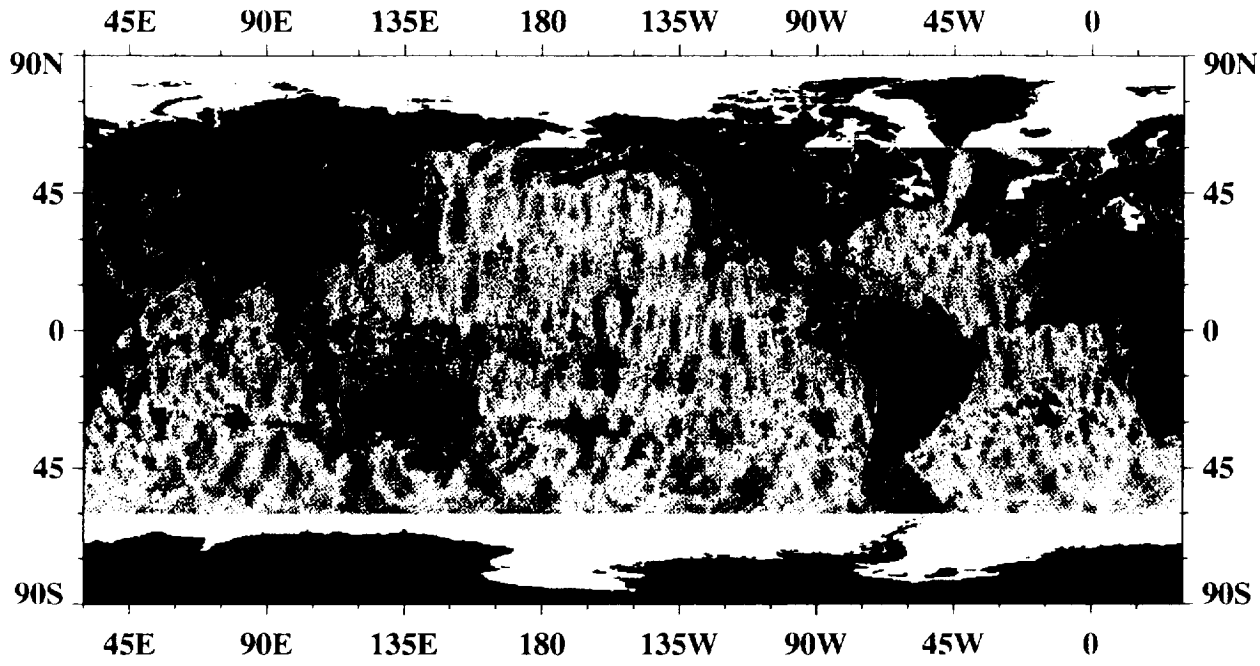

January 1993, max = 37

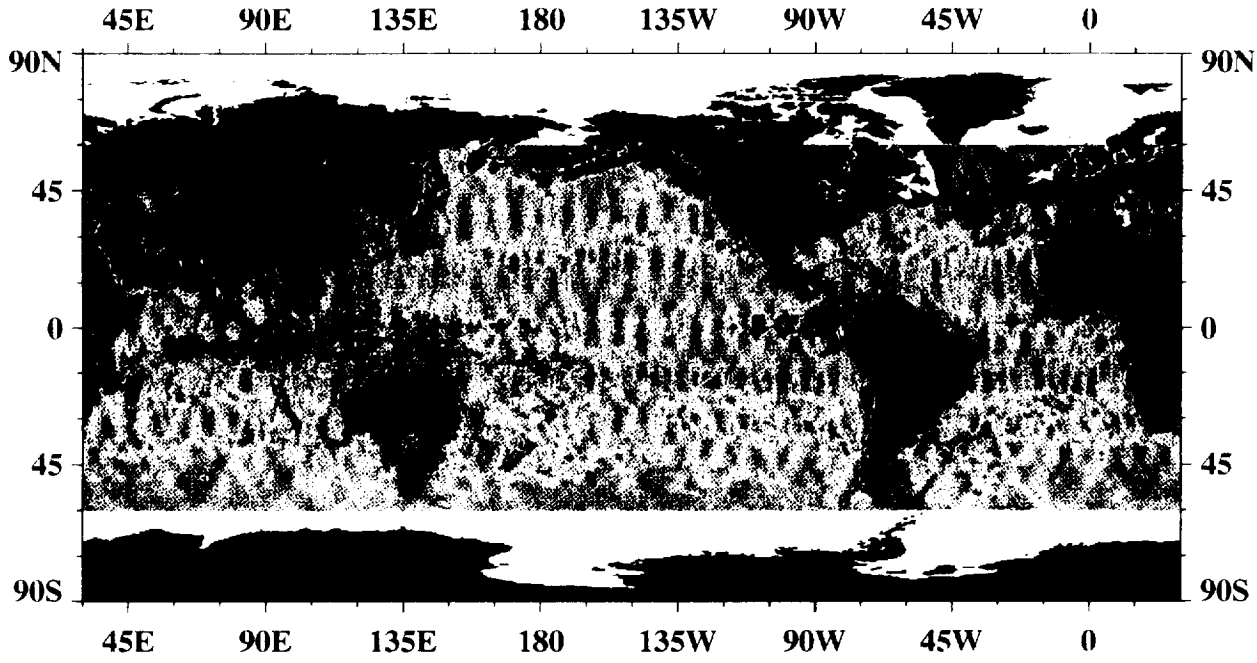

February 1993, max = 41

Number of ERS-1 AMI Wind Speed Values per Pixel

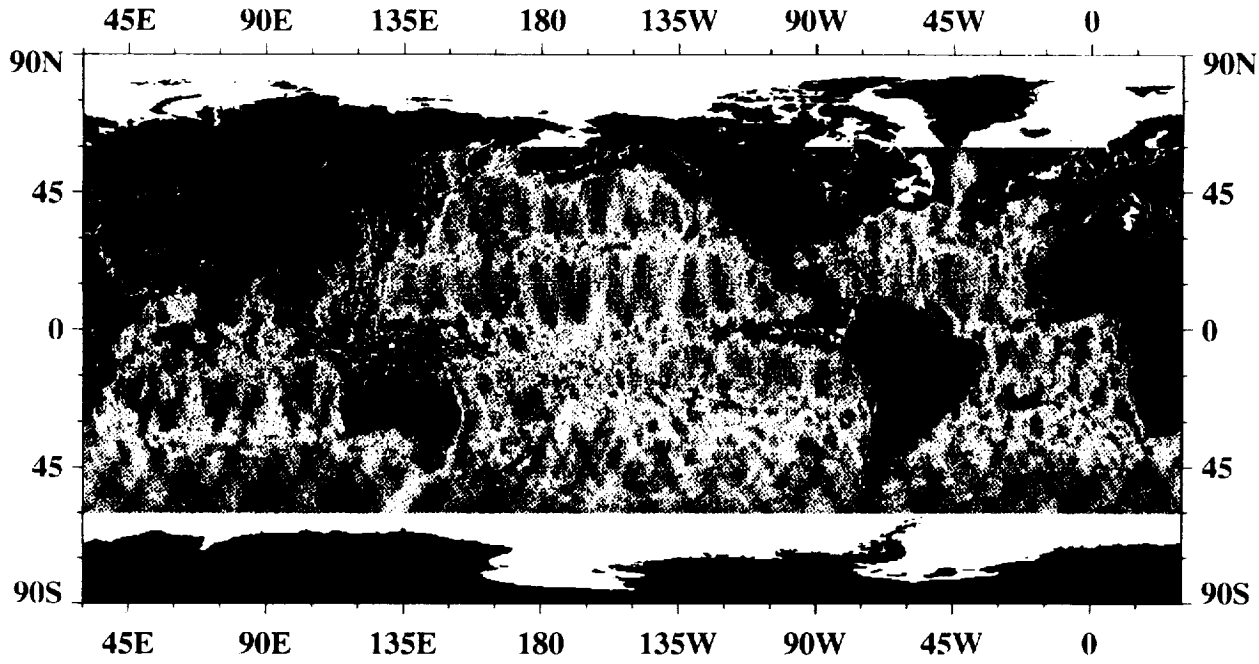

March 1993, max = 41

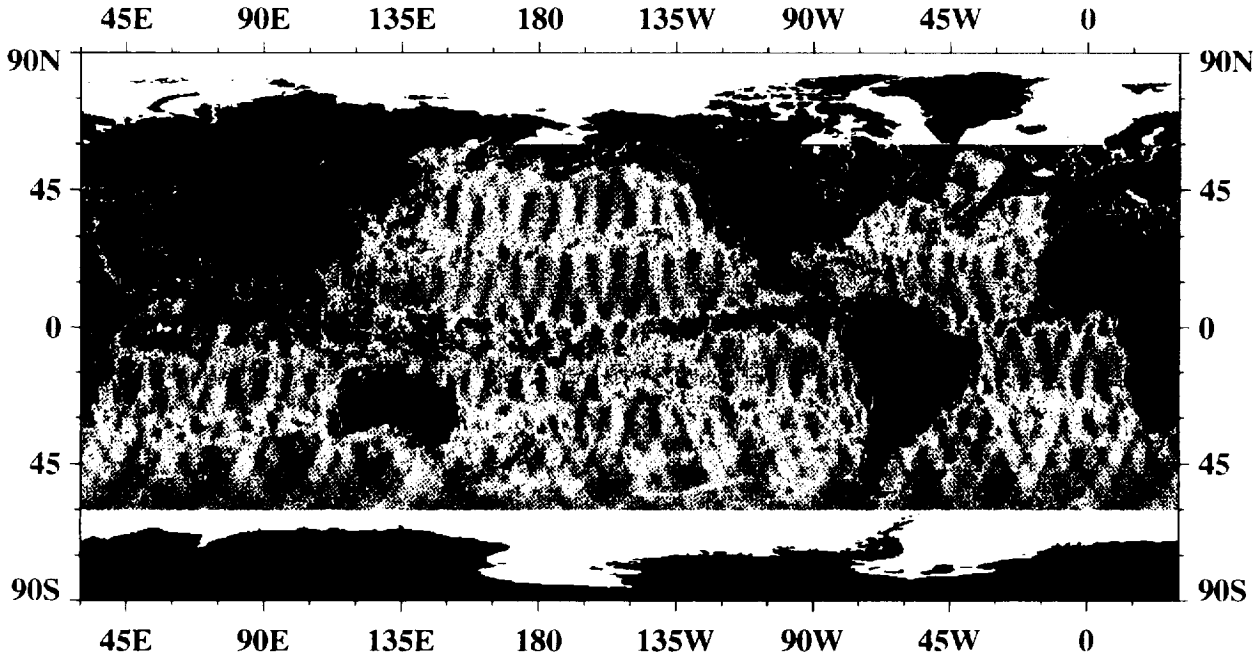

April 1993, max = 42

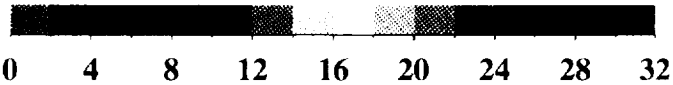

Number of ERS-1 AMI Wind Speed Values per Pixel

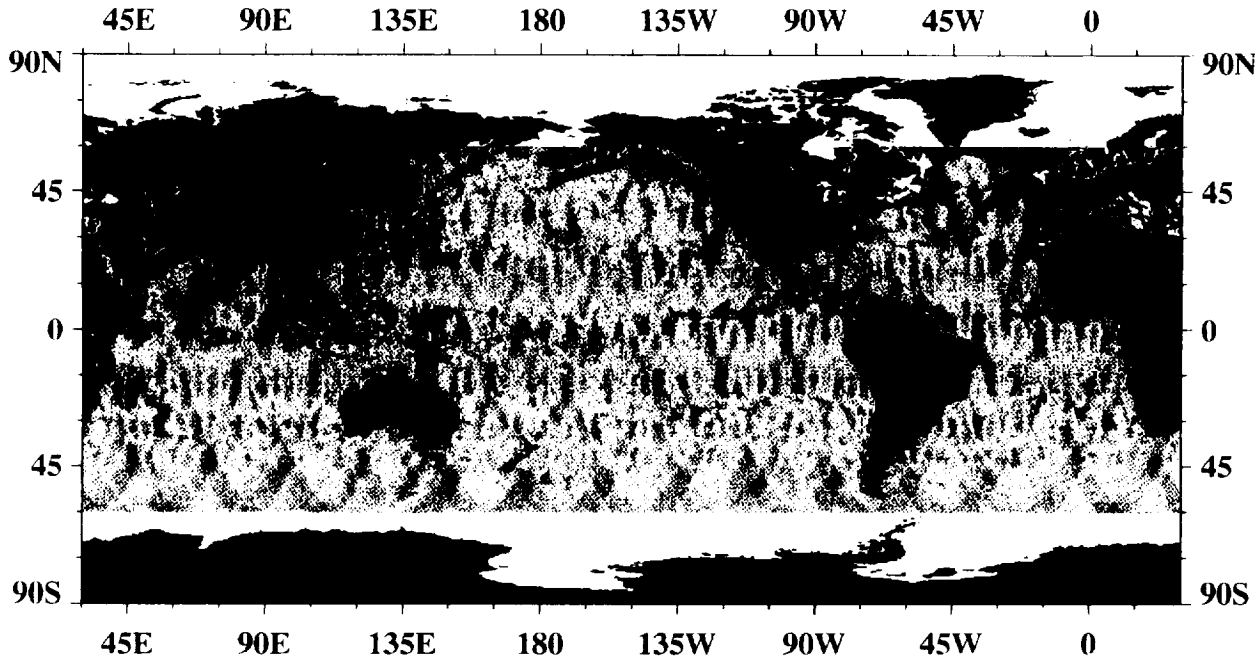

8 - 31 May 1993, max = 41

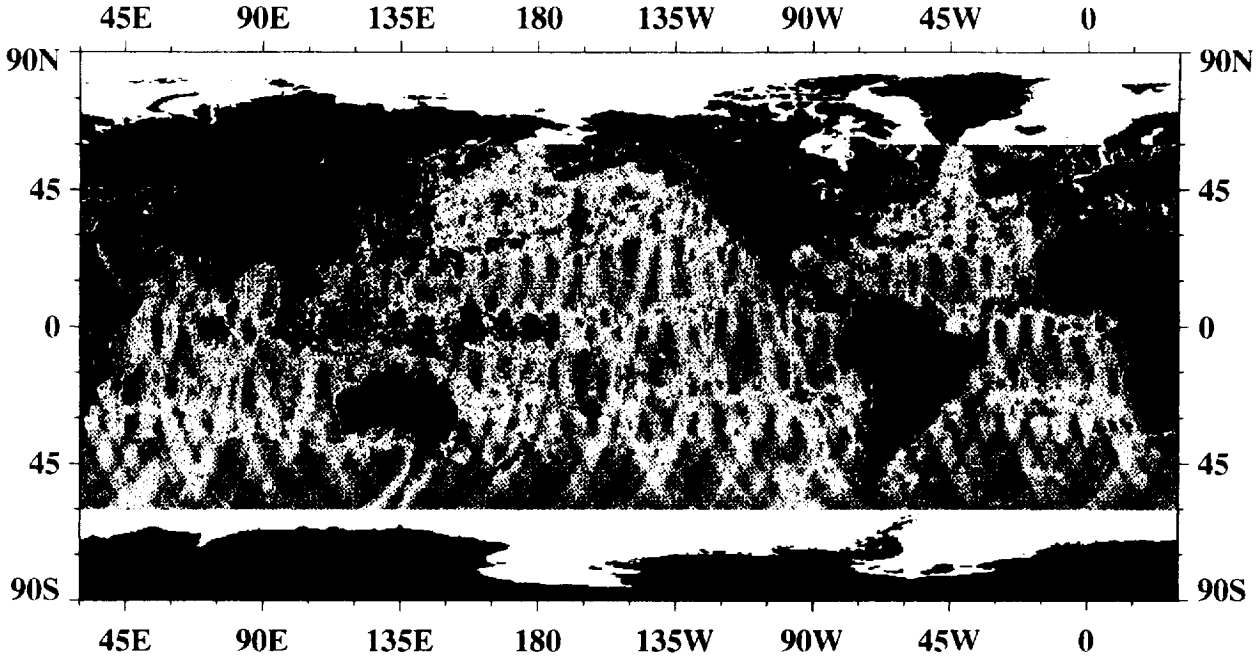

June 1993, max = 41

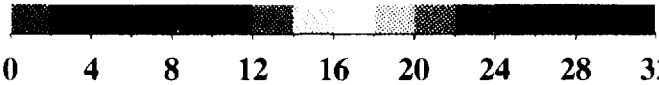

Number of ERS-1 AMI Wind Speed Values per Pixel

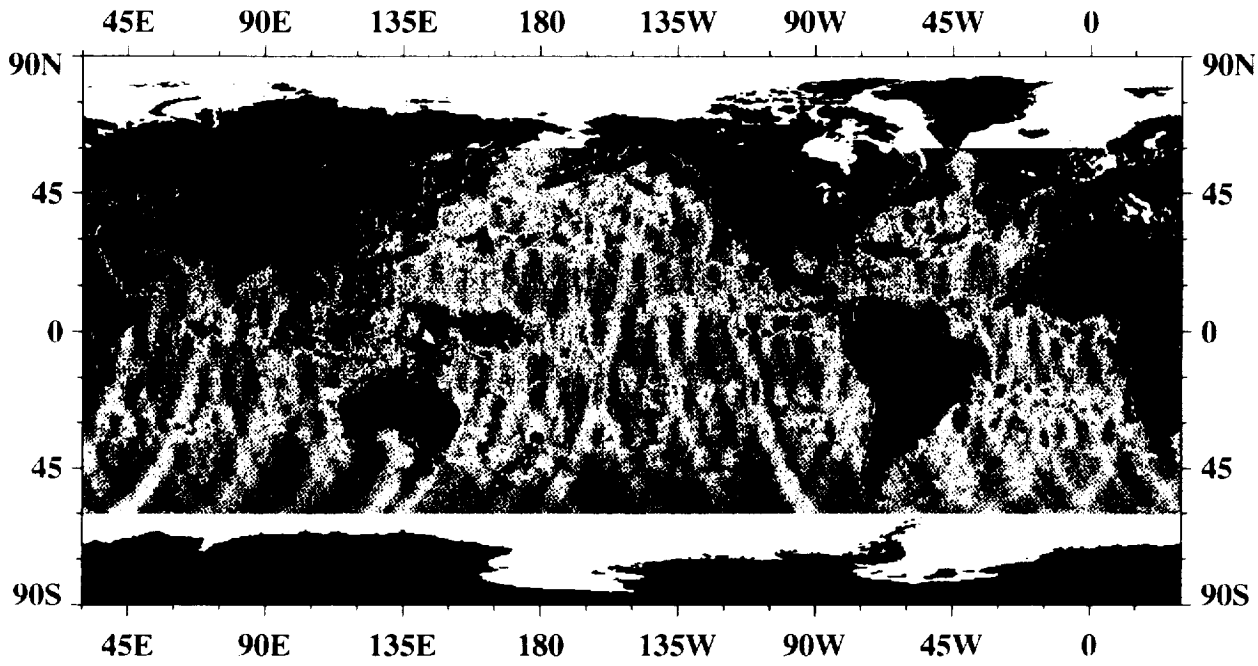

July 1993, max = 41

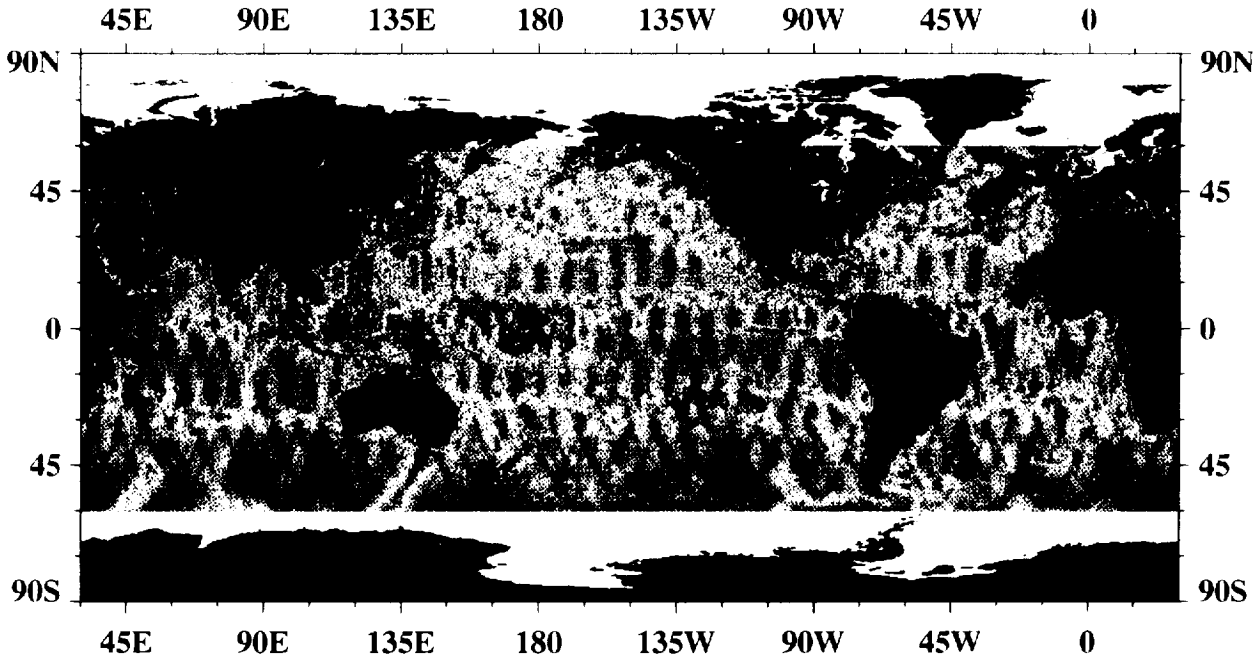

August 1993, max = 42

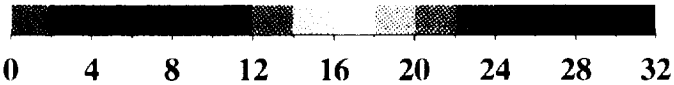

Number of ERS-1 AMI Wind Speed Values per Pixel

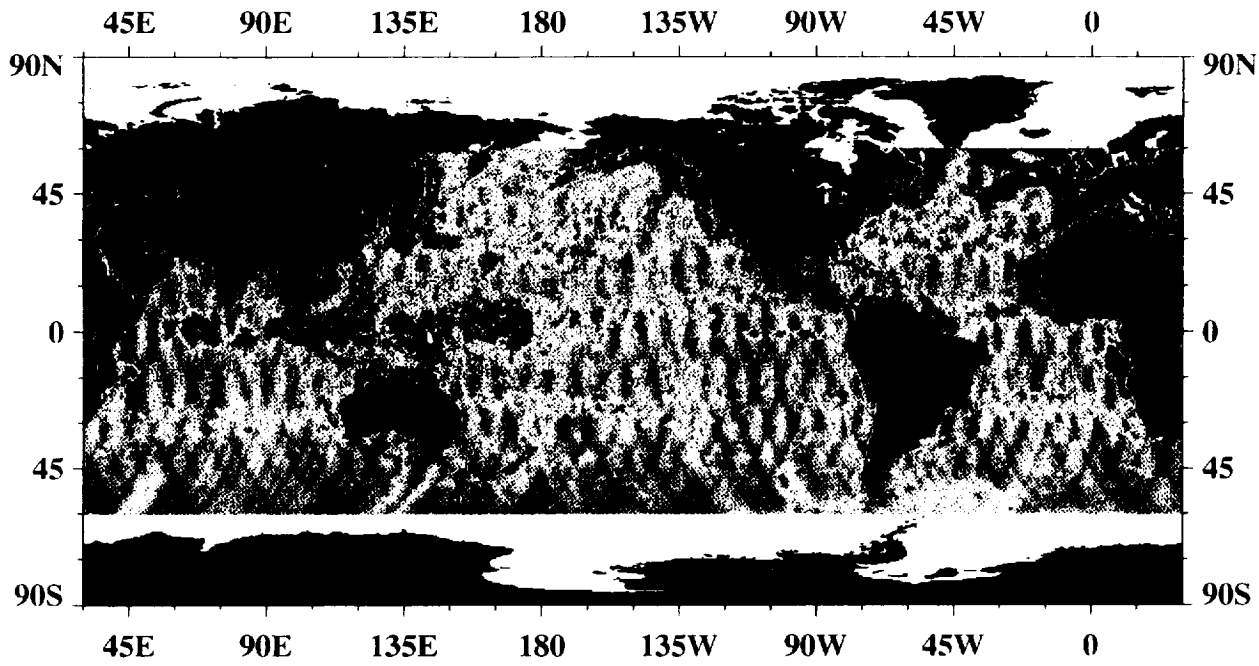

September 1993, max = 42

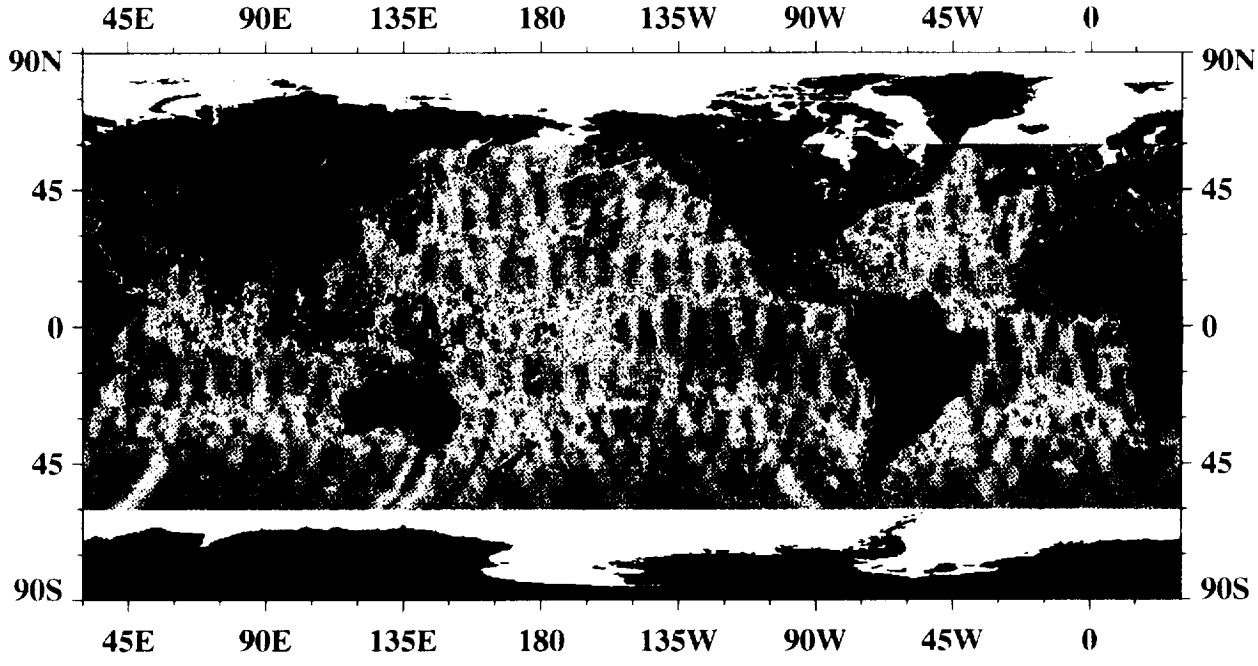

October 1993, max = 41

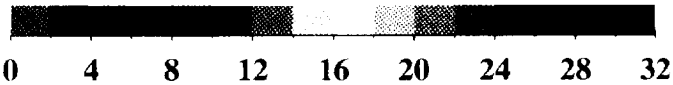

Number of ERS-1 AMI Wind Speed Values per Pixel

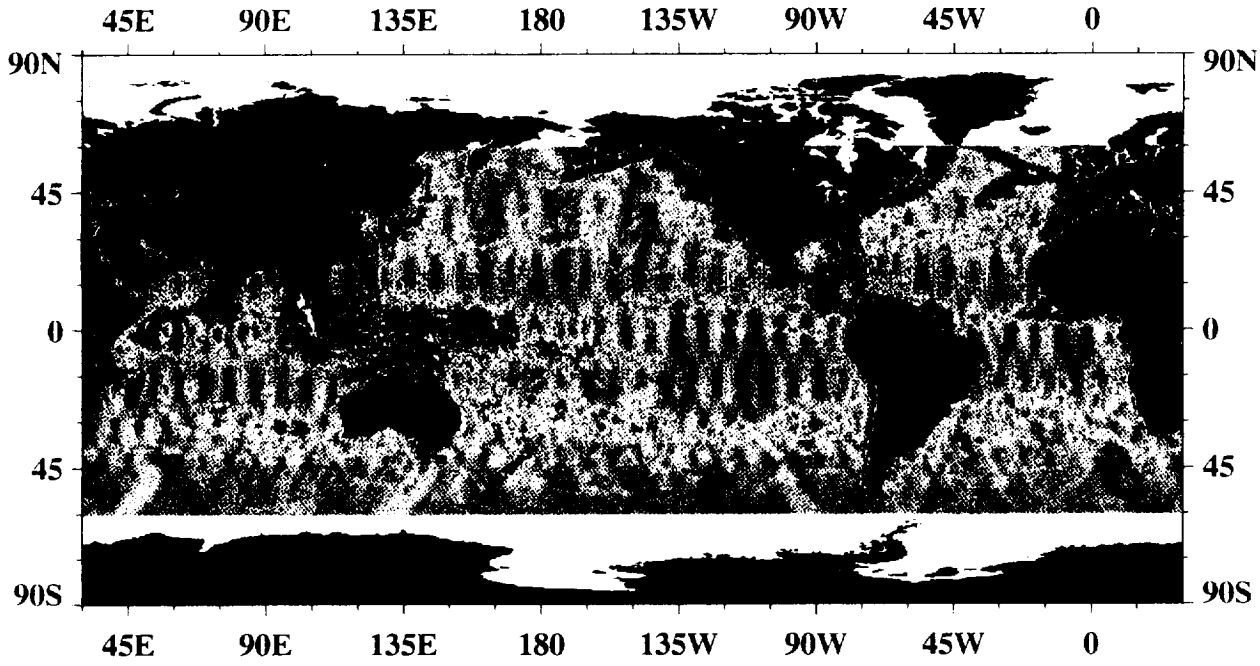

November 1993, max = 43

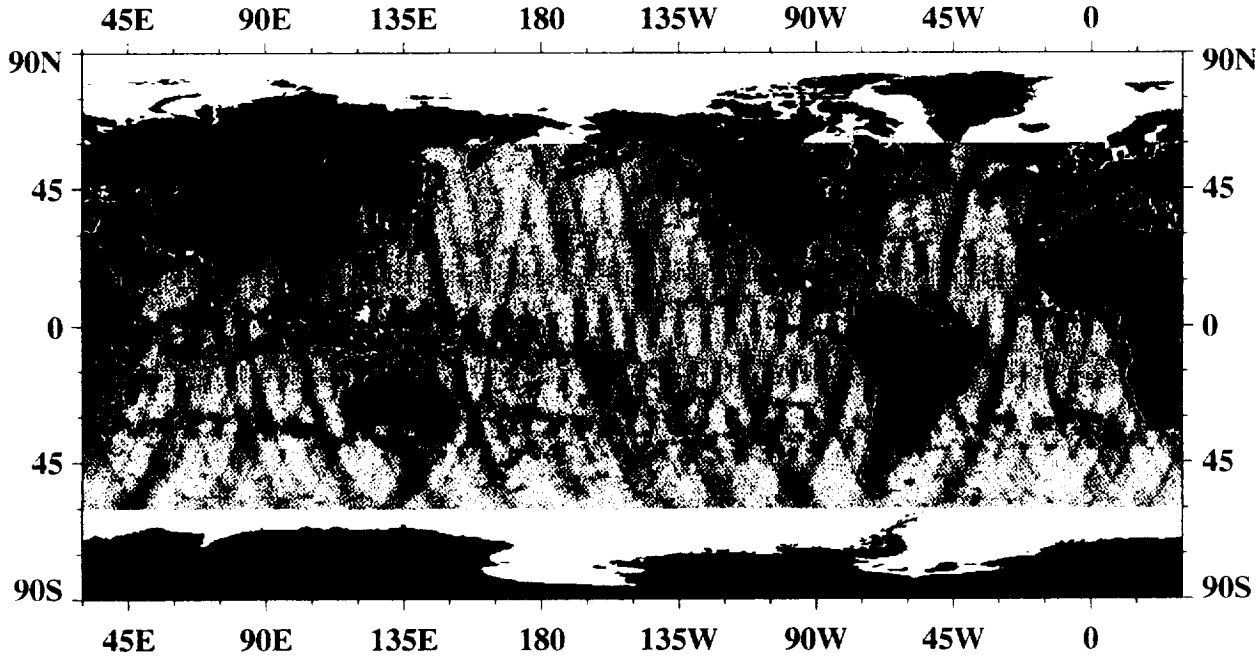

1 - 21 December 1993, max = 34

Number of ERS-1 AMI Wind Speed Values per Pixel

A10

Monthly Mean TOPEX/POSEIDON Sea Surface Height Variation

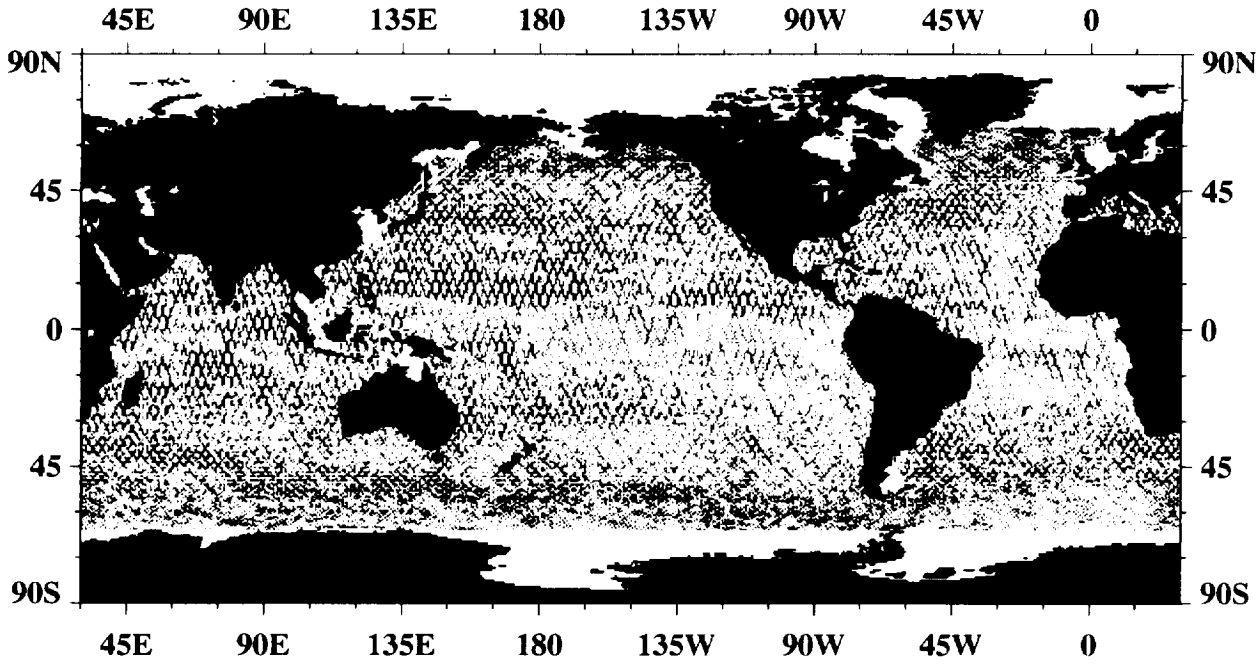

January 1993

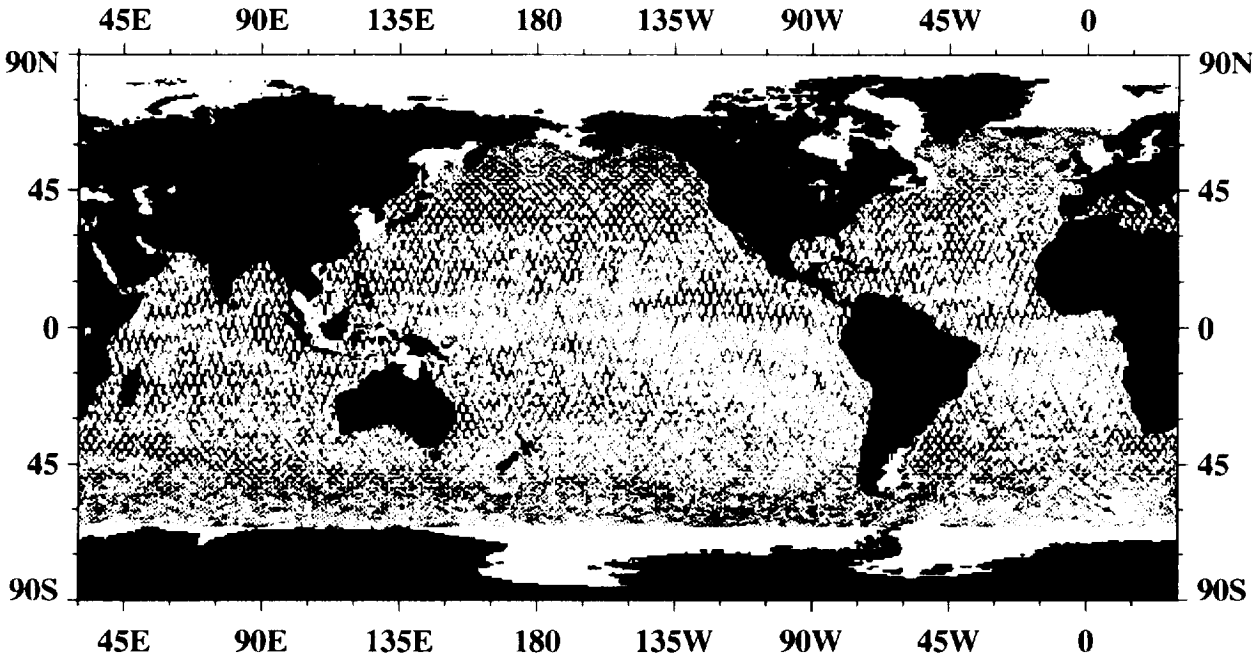

February 1993

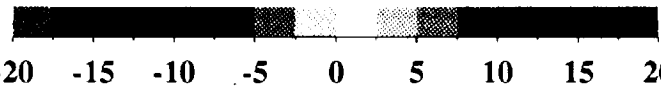

TOPEX/POSEIDON Sea Surface Height Variation Referenced to 1993 Mean, cm

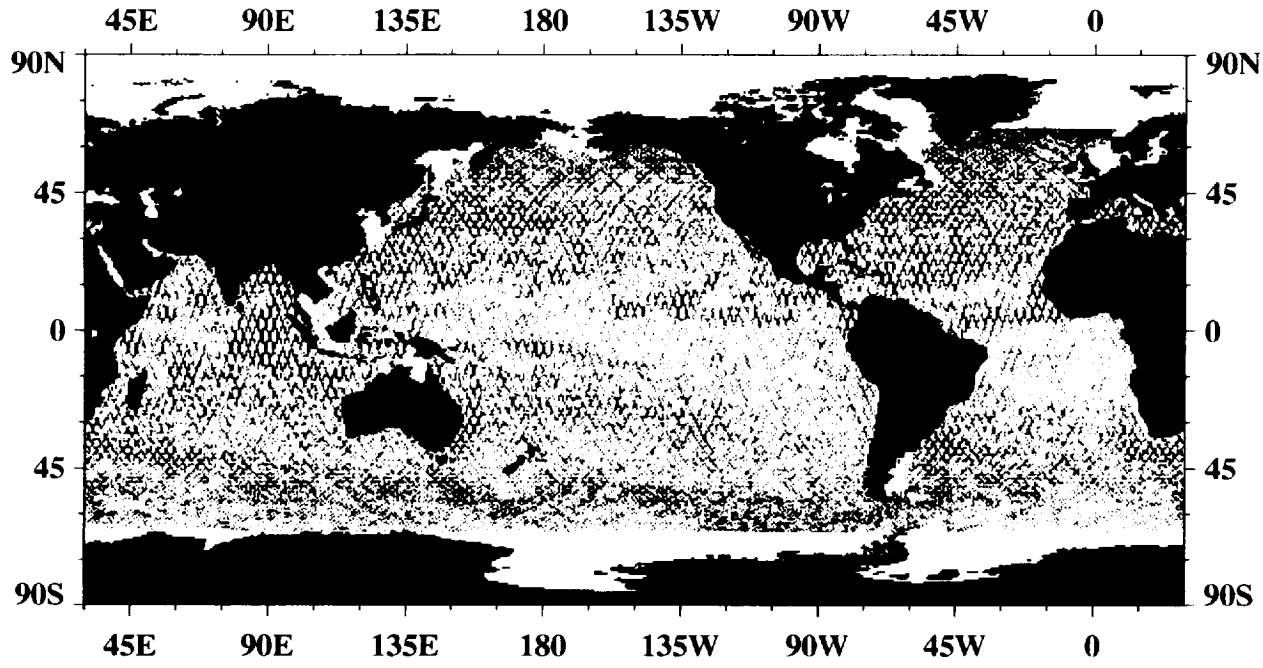

March 1993

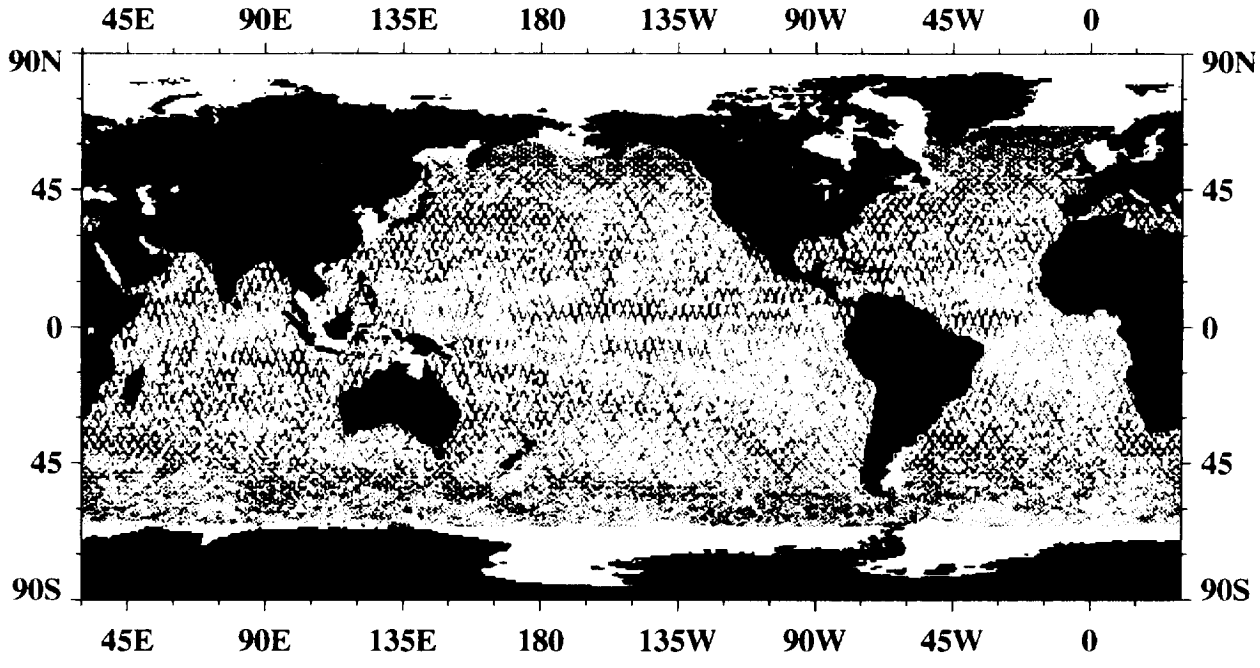

April 1993

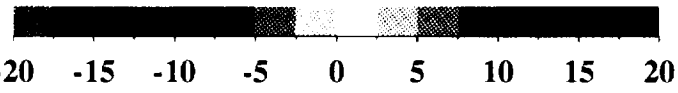

TOPEX/POSEIDON Sea Surface Height Variation Referenced to 1993 Mean, cm

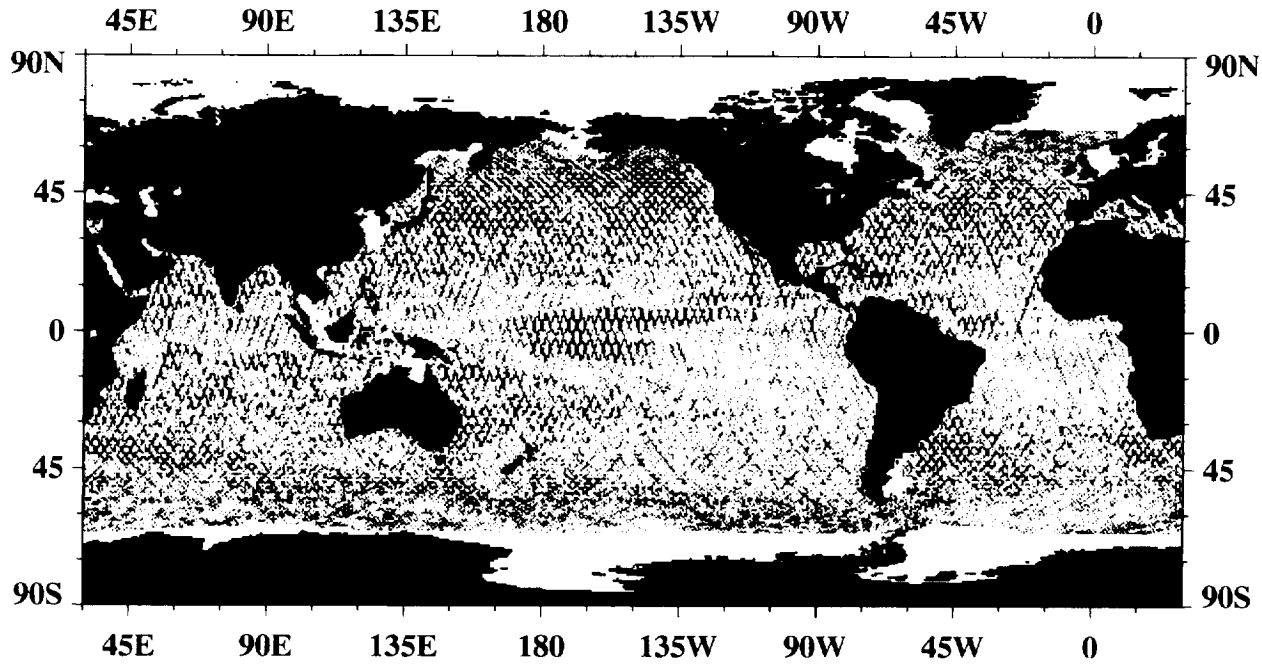

May 1993

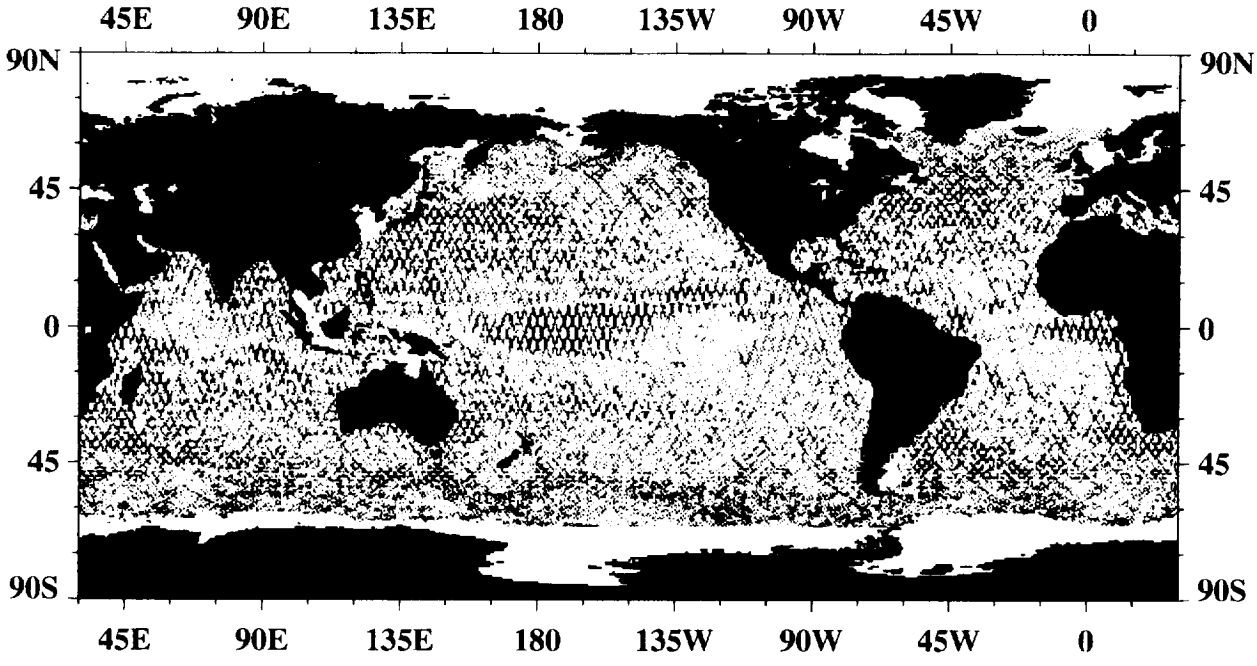

June 1993

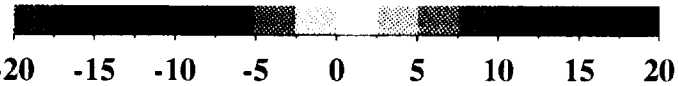

TOPEX/POSEIDON Sea Surface Height Variation Referenced to 1993 Mean, cm

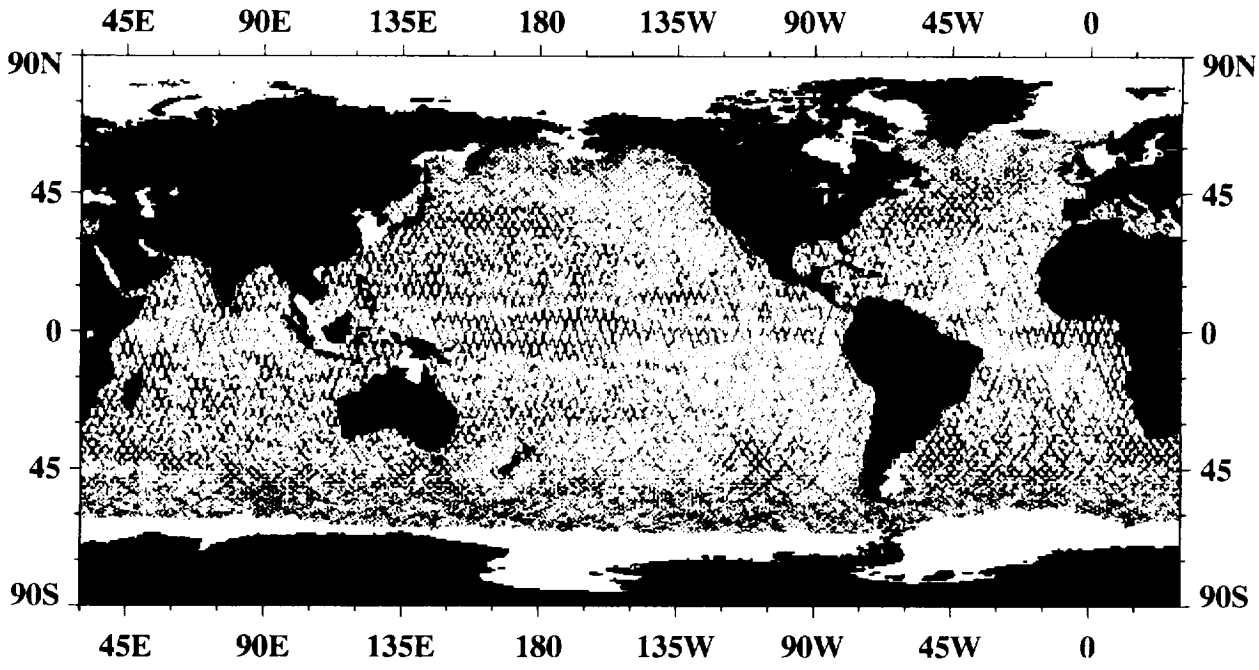

July 1993

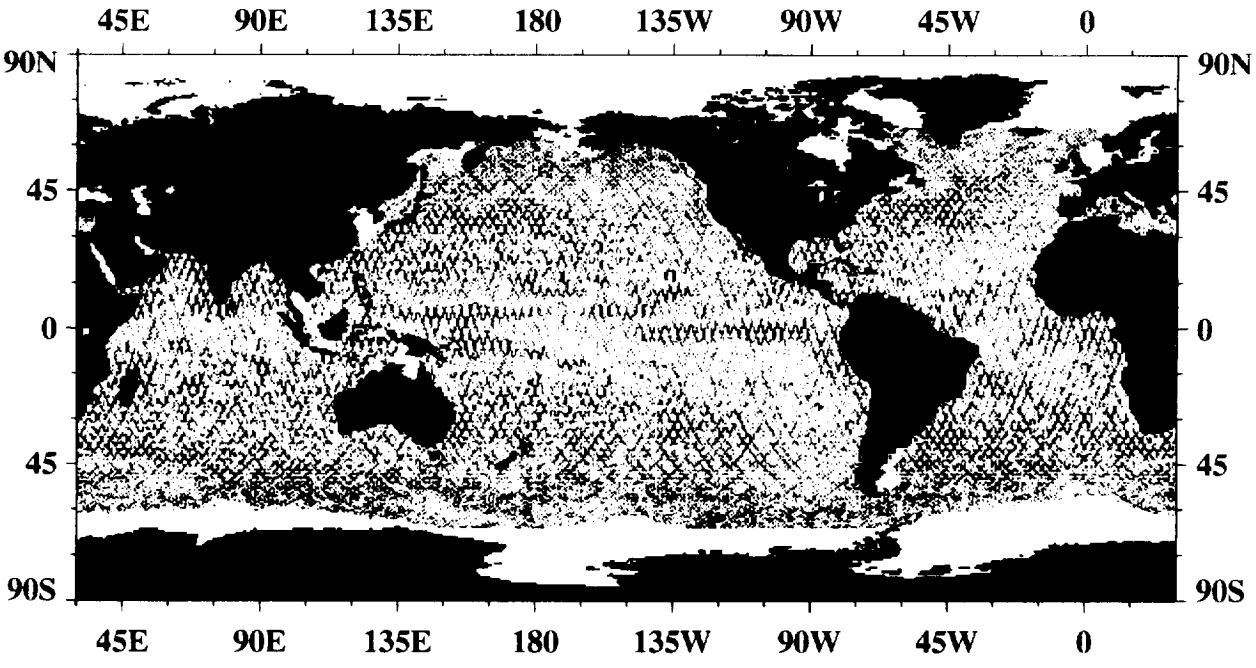

August 1993

TOPEX/POSEIDON Sea Surface Height Variation Referenced to 1993 Mean, cm

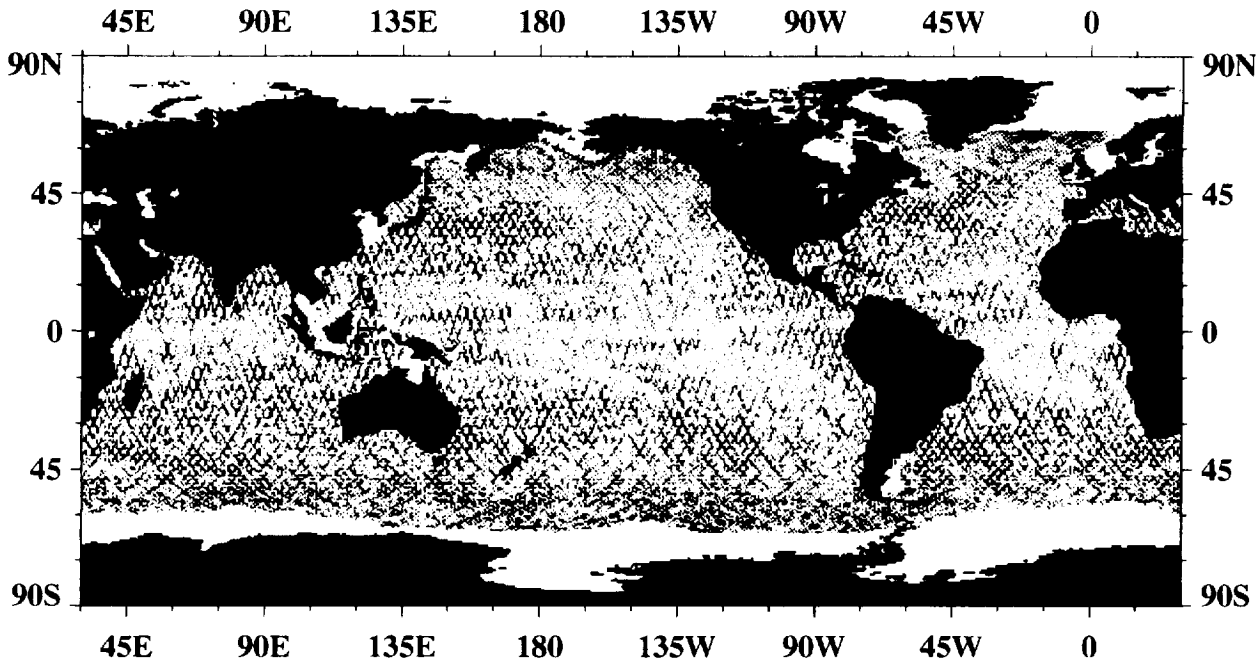

September 1993

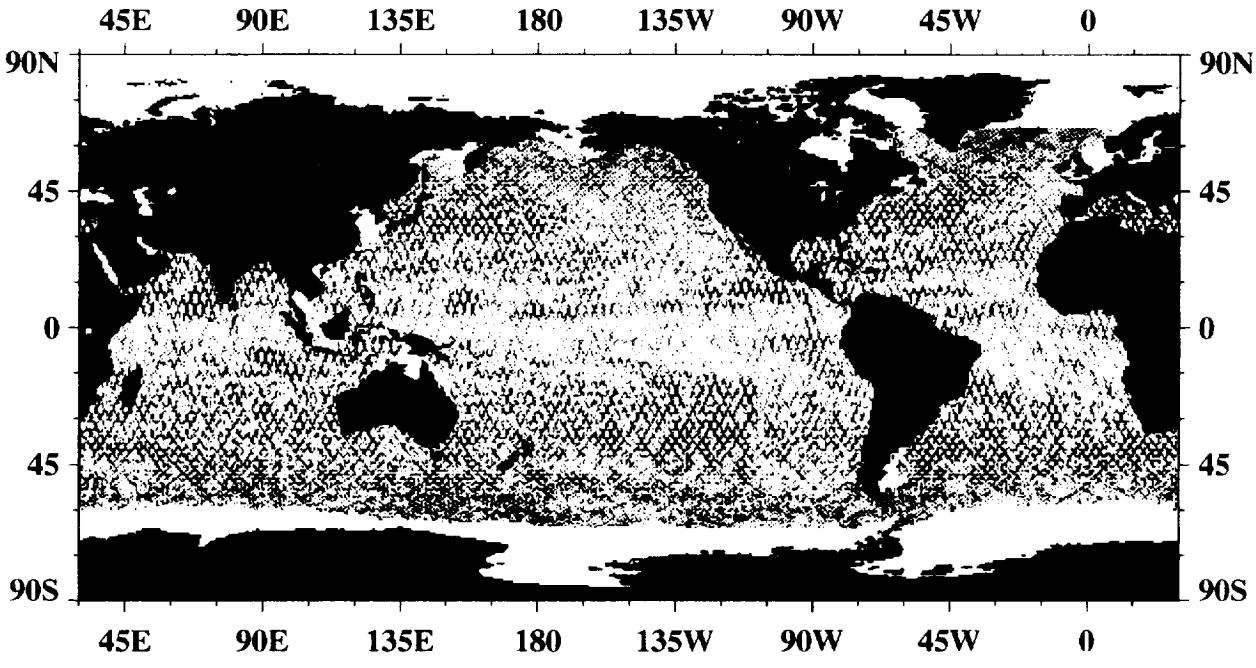

October 1993

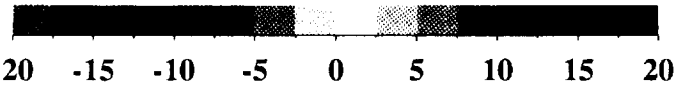

TOPEX/POSEIDON Sea Surface Height Variation Referenced to 1993 Mean, cm

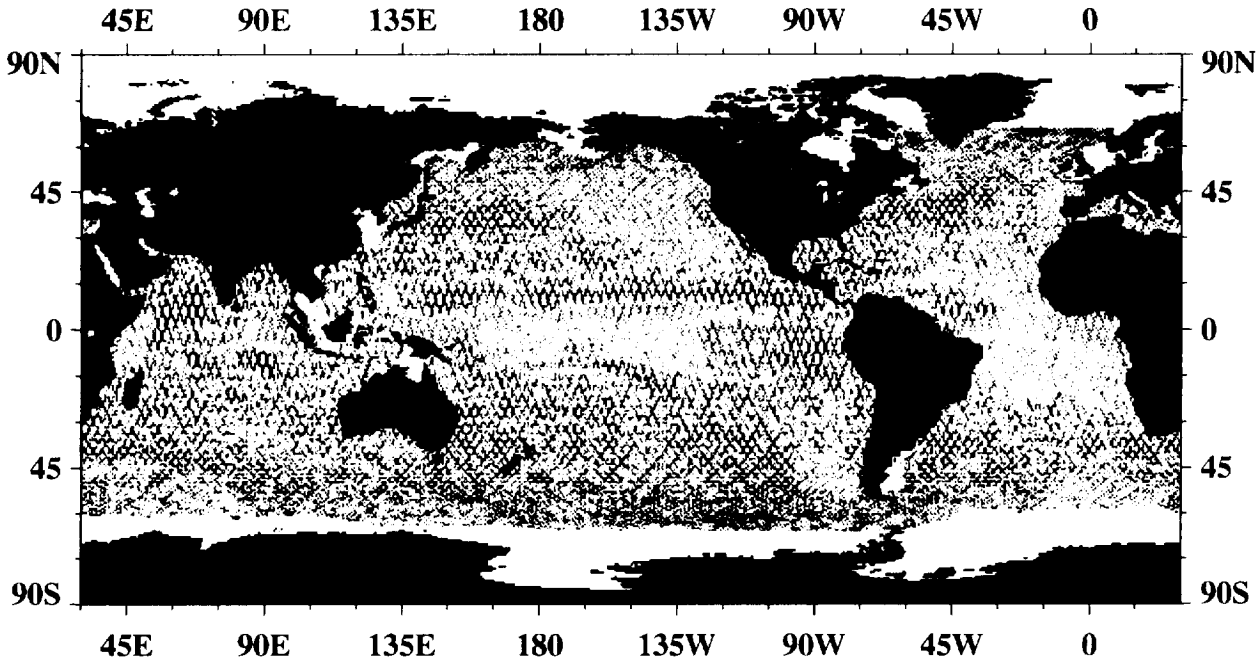

November 1993

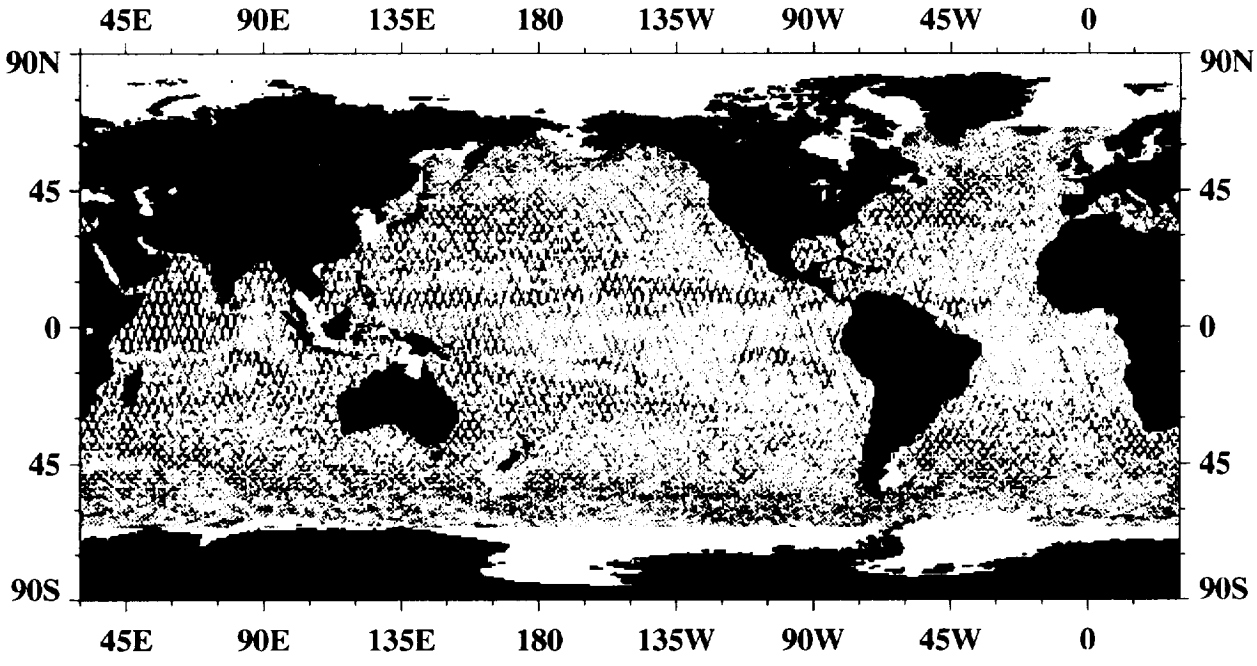

December 1993

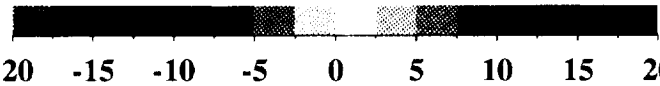

TOPEX/POSEIDON Sea Surface Height Variation Referenced to 1993 Mean, cm

A11

Monthly TOPEX/POSEIDON Sampling Distribution

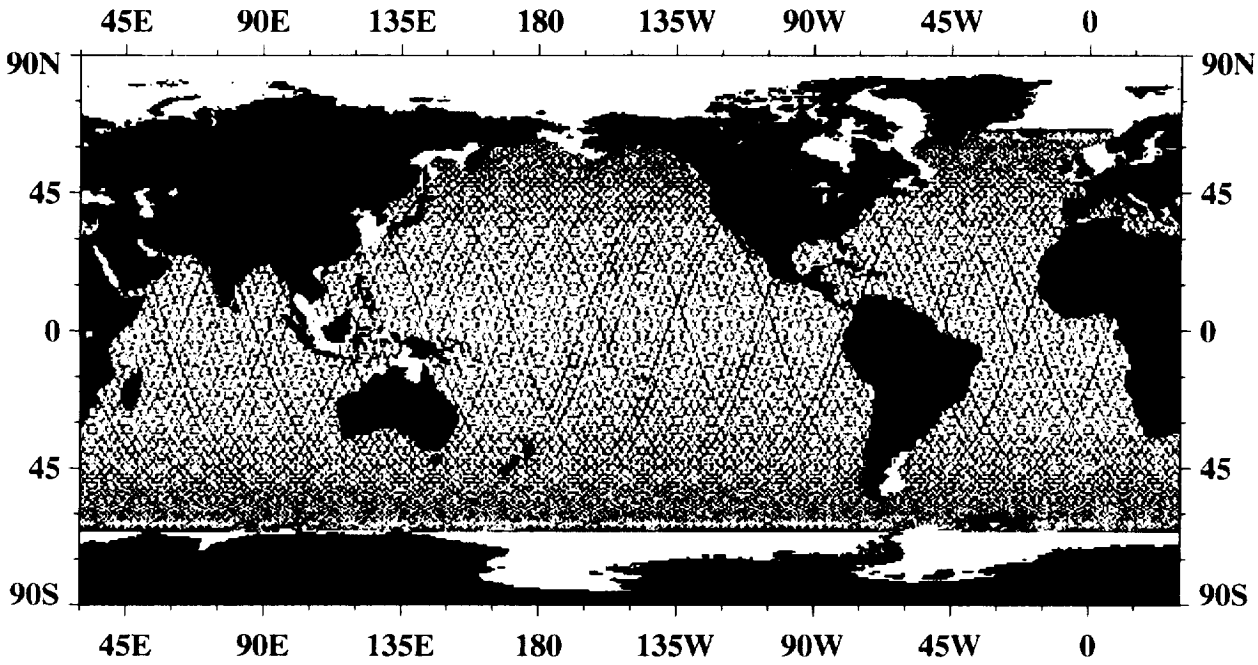

January 1993, max =111

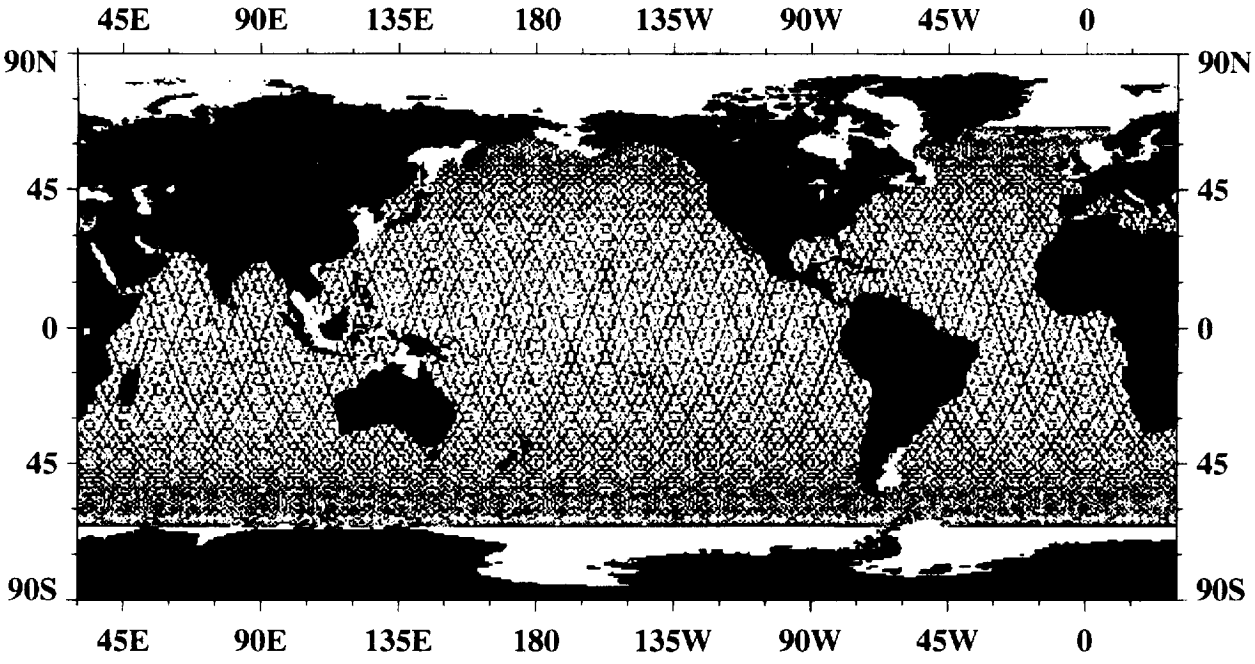

February 1993, max = 92

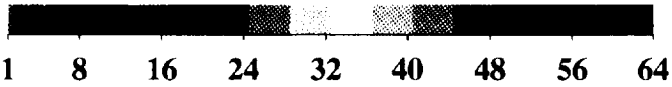

Number of TOPEX/POSEIDON Sea Surface Height Values per Pixel

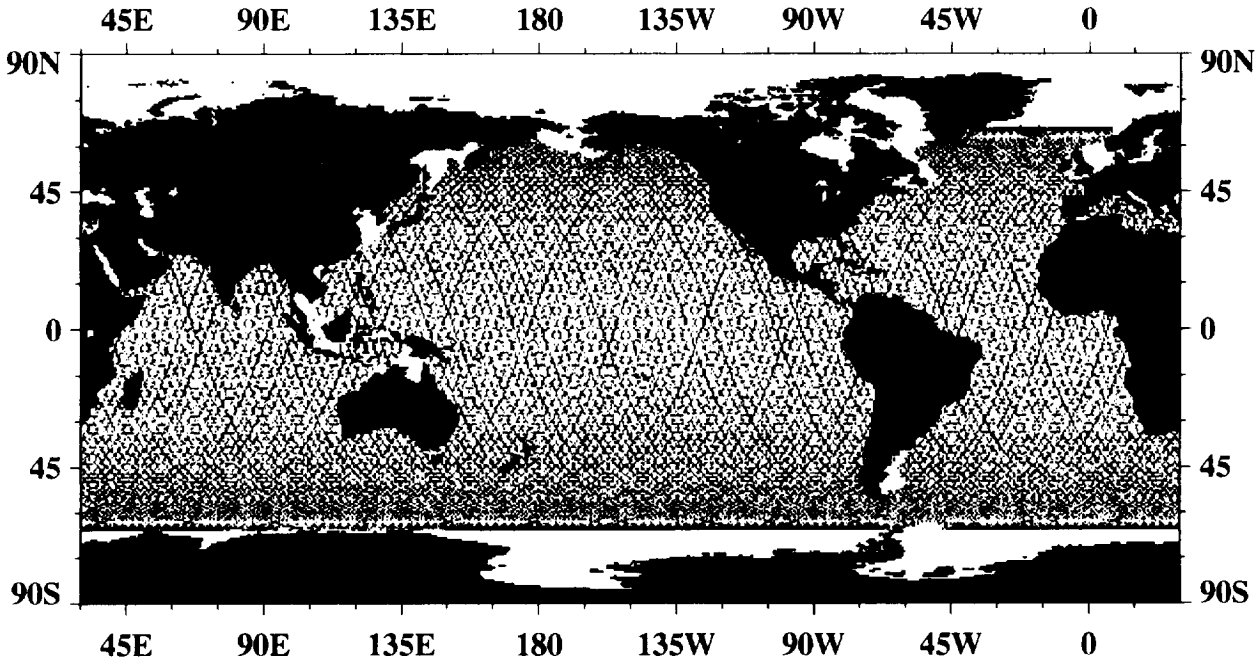

March 1993, max =112

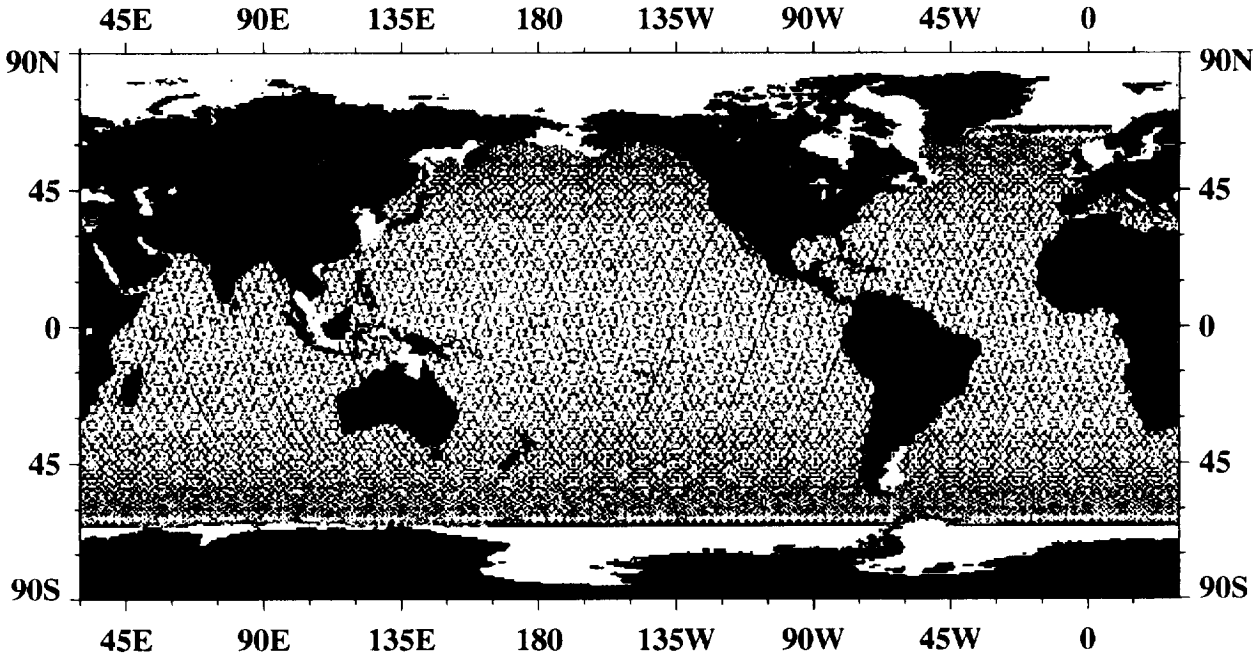

April 1993, max =103

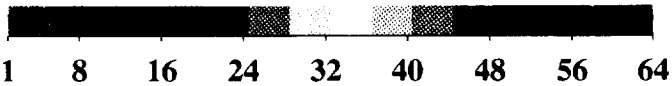

Number of TOPEX/POSEIDON Sea Surface Height Values per Pixel

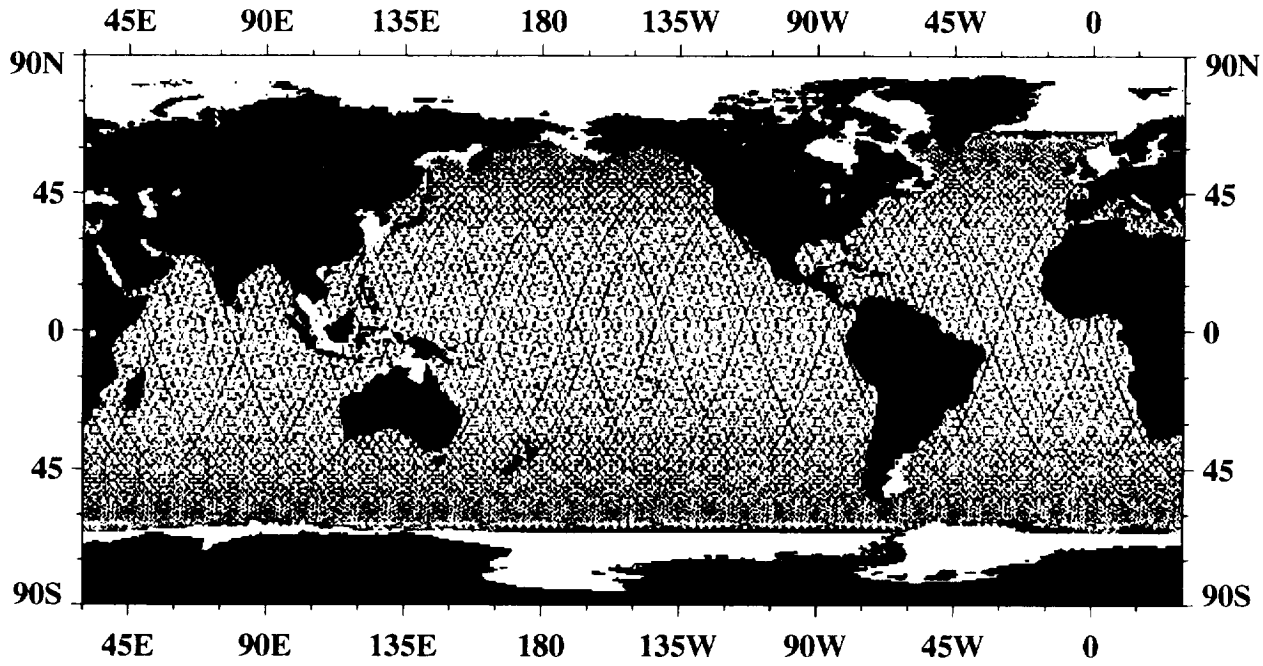

May 1993, max =112

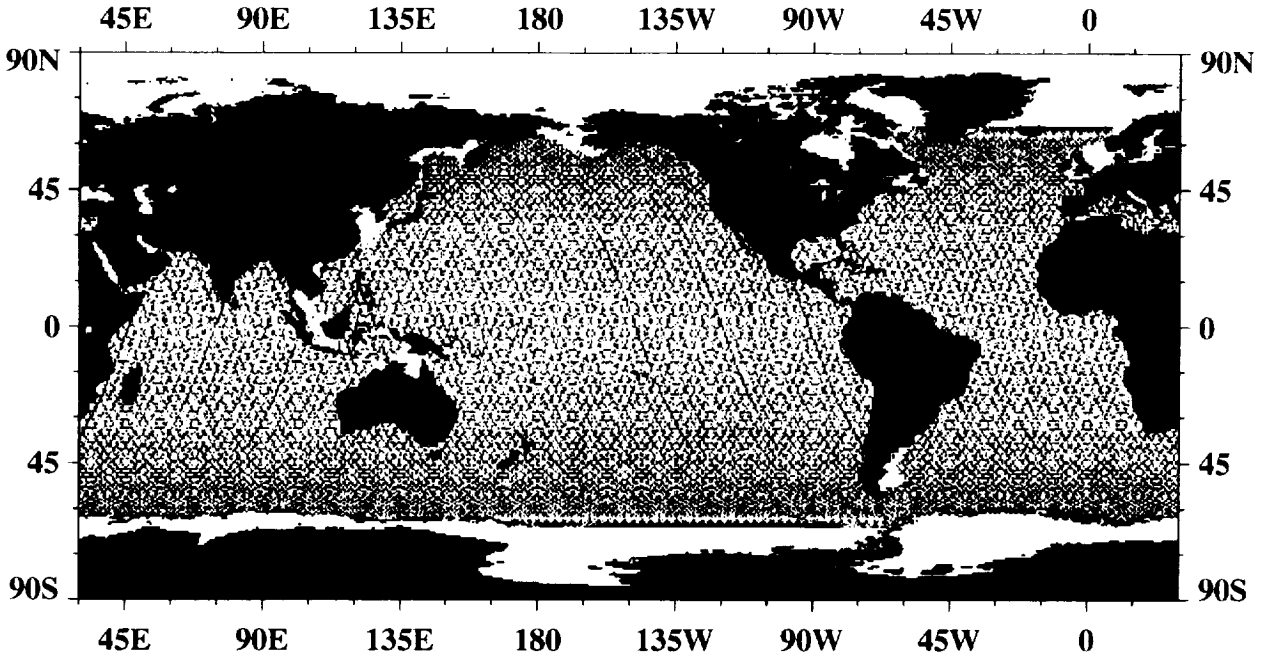

June 1993, max = 98

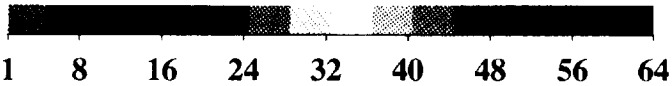

Number of TOPEX/POSEIDON Sea Surface Height Values per Pixel

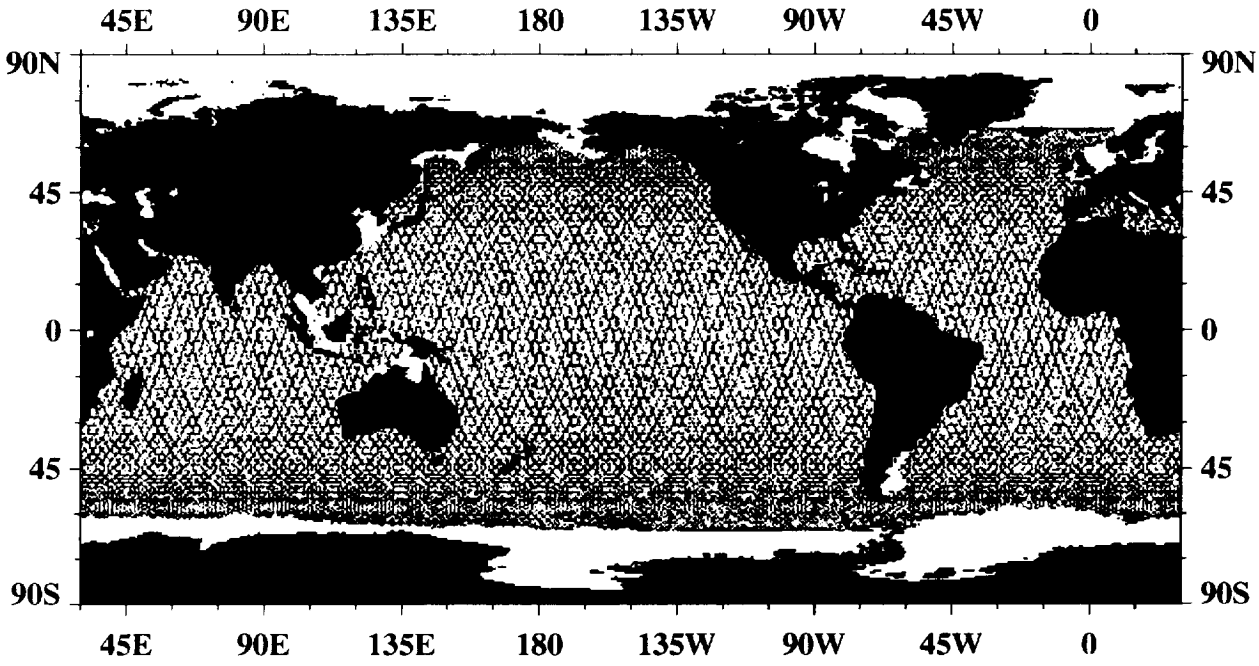

July 1993, max =112

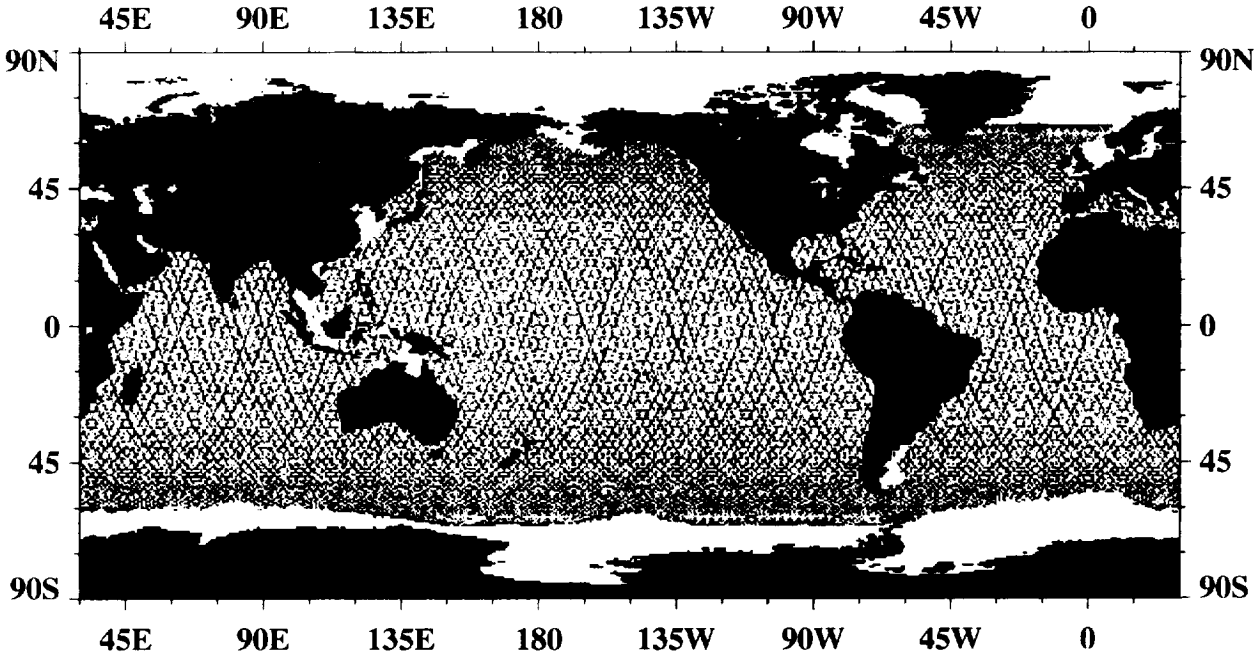

August 1993, max =106

Number of TOPEX/POSEIDON Sea Surface Height Values per Pixel

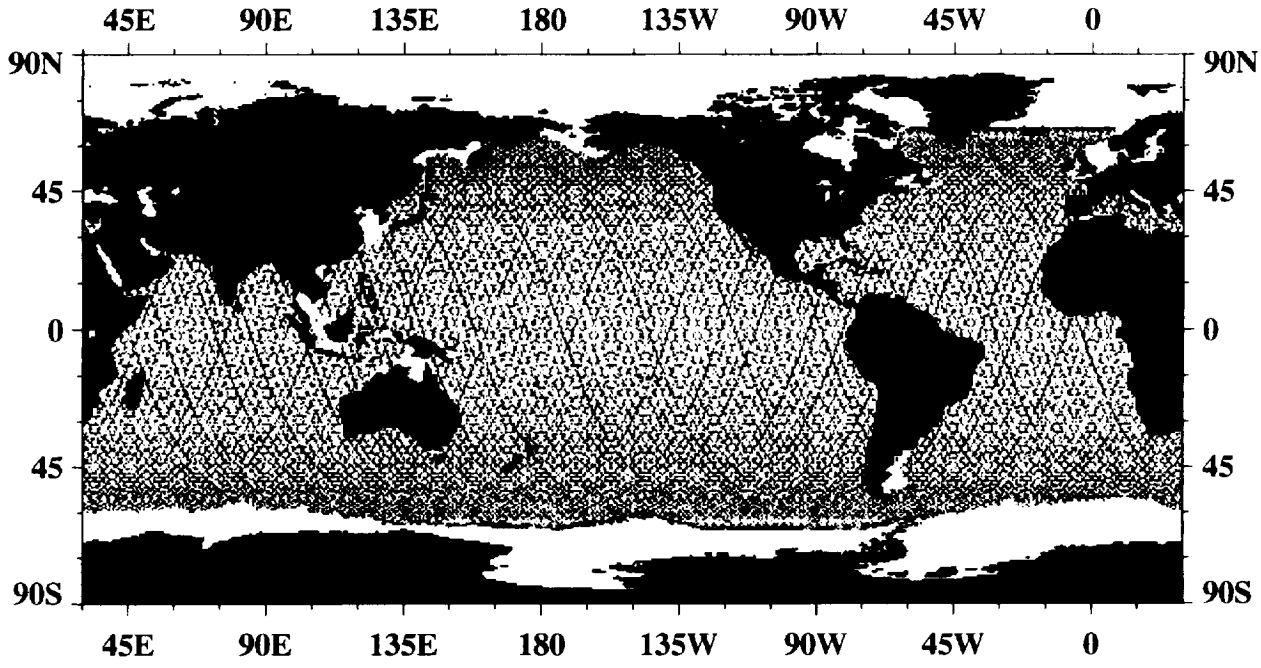

September 1993, max = 98

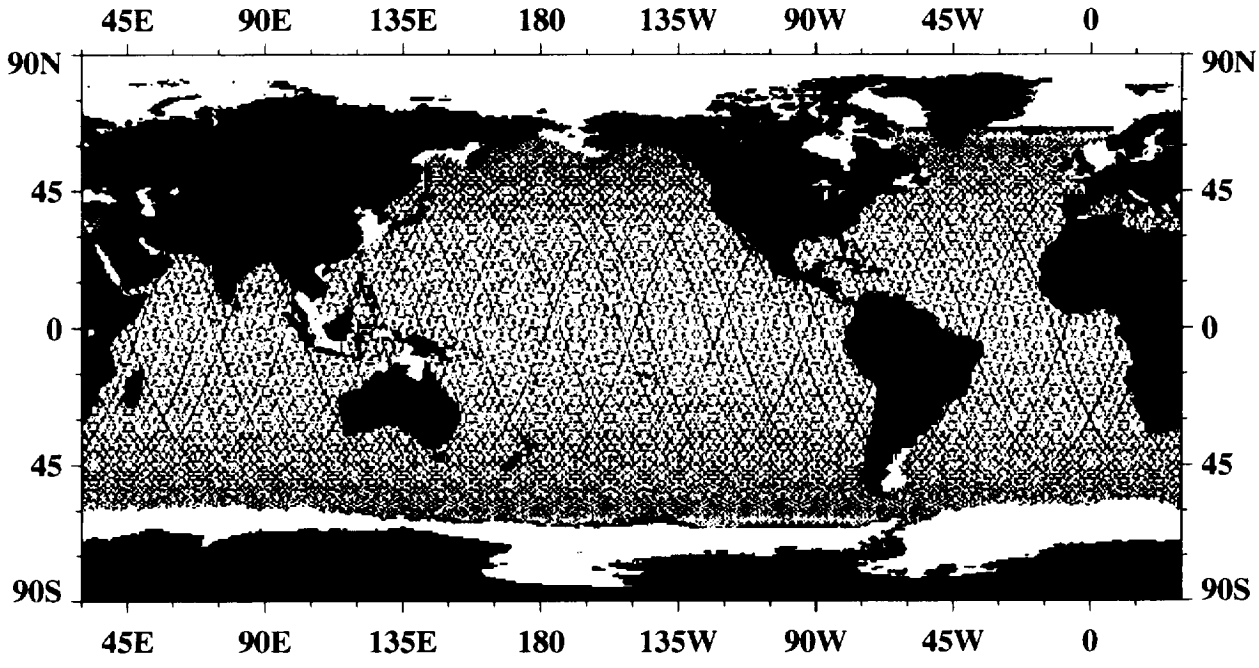

October 1993, max =106

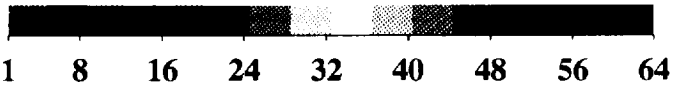

Number of TOPEX/POSEIDON Sea Surface Height Values per Pixel

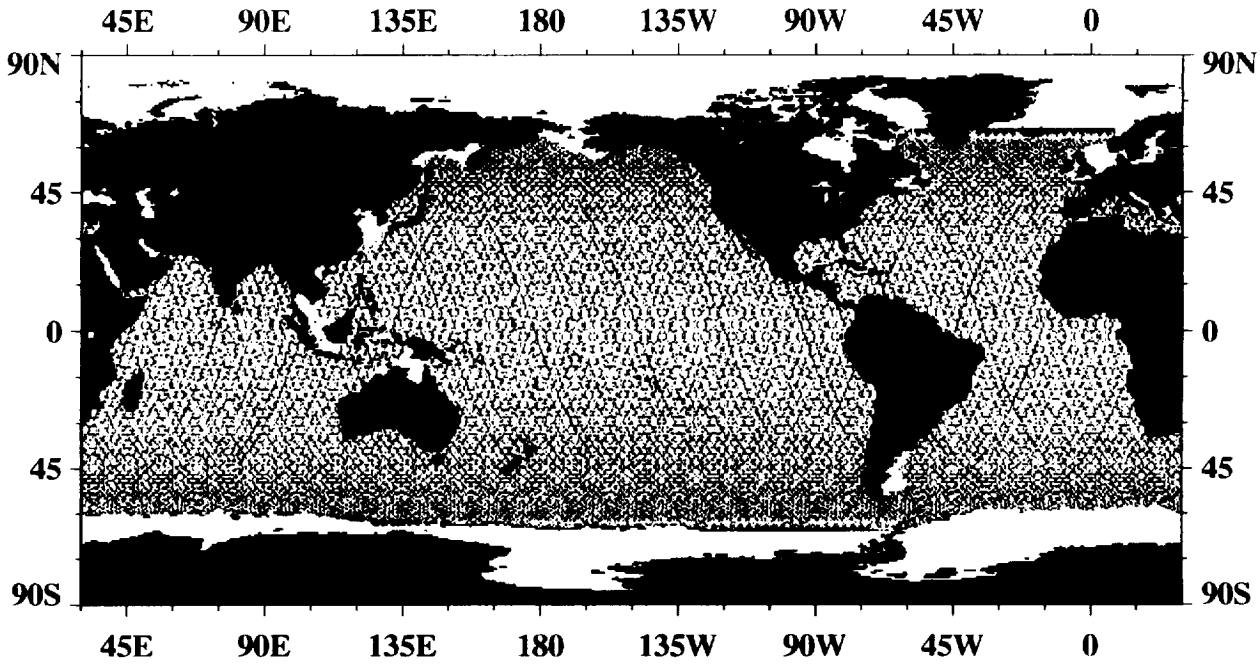

November 1993, max =102

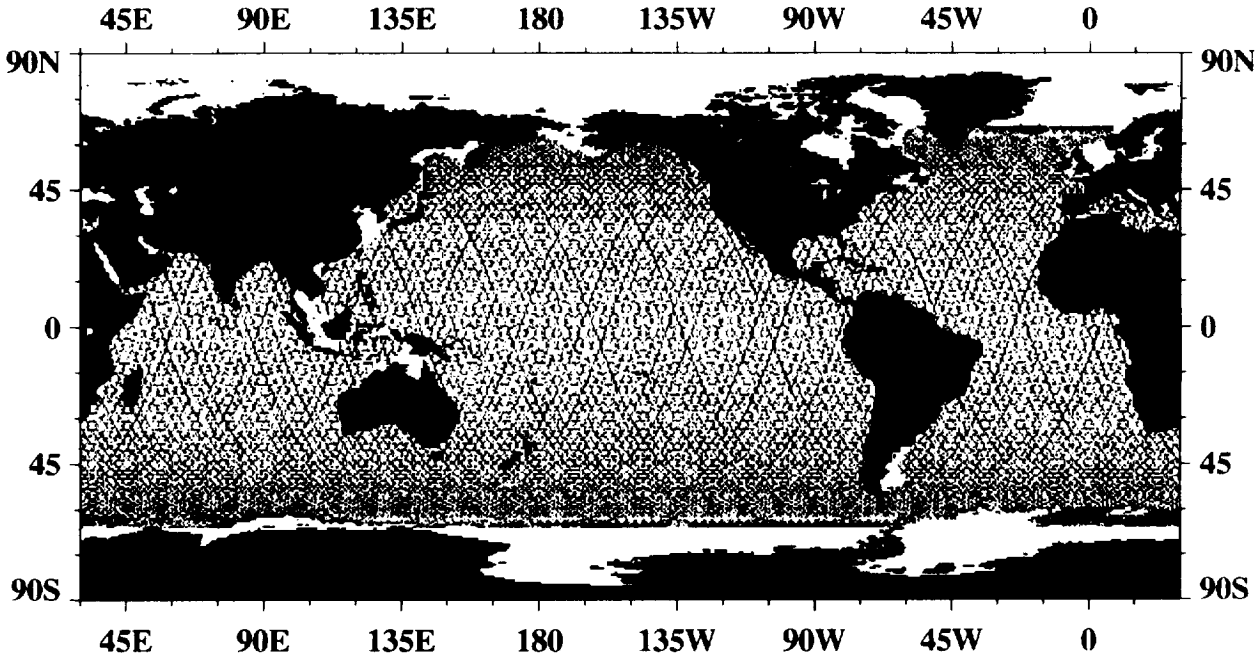

December 1993, max =111

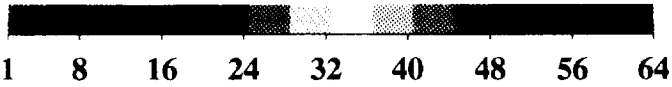

Number of TOPEX/POSEIDON Sea Surface Height Values per Pixel

A12

Annual Mean ECMWF Surface Wind Velocity

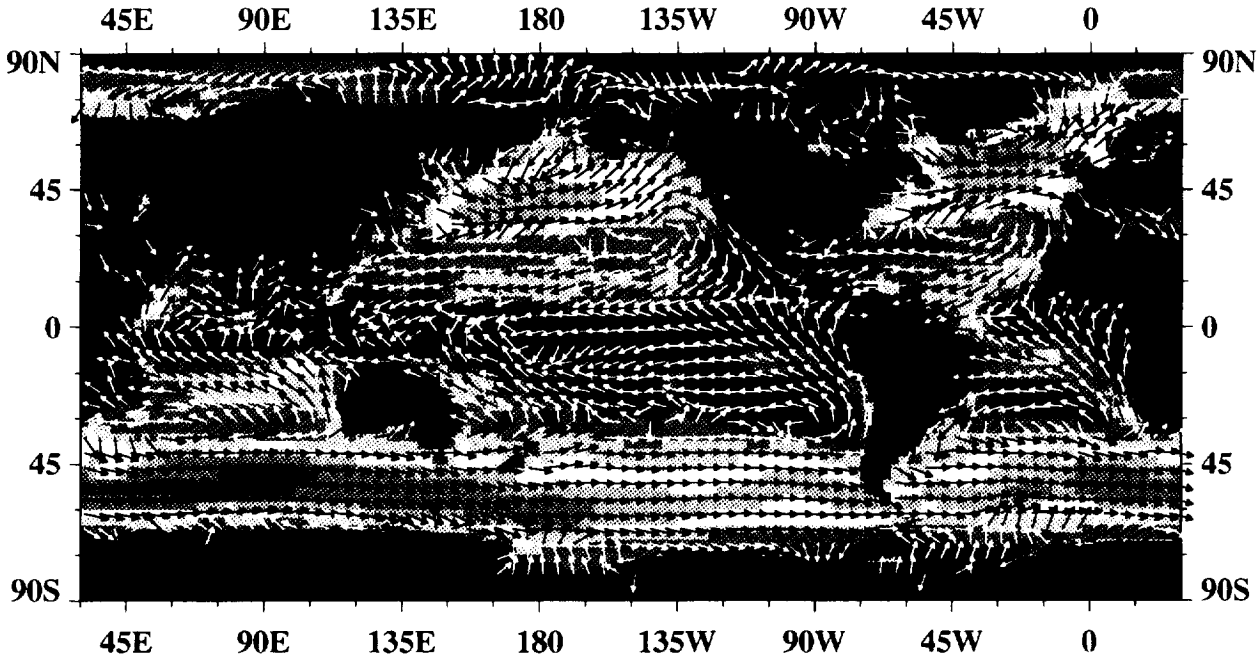

Annual Mean 1993

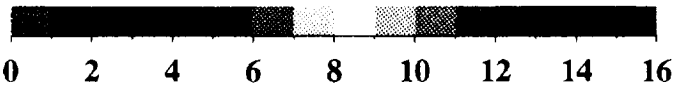

ECMWF 10 m Wind Speed, m s^{-1}

A13

Monthly Mean ECMWF Surface Wind Velocity

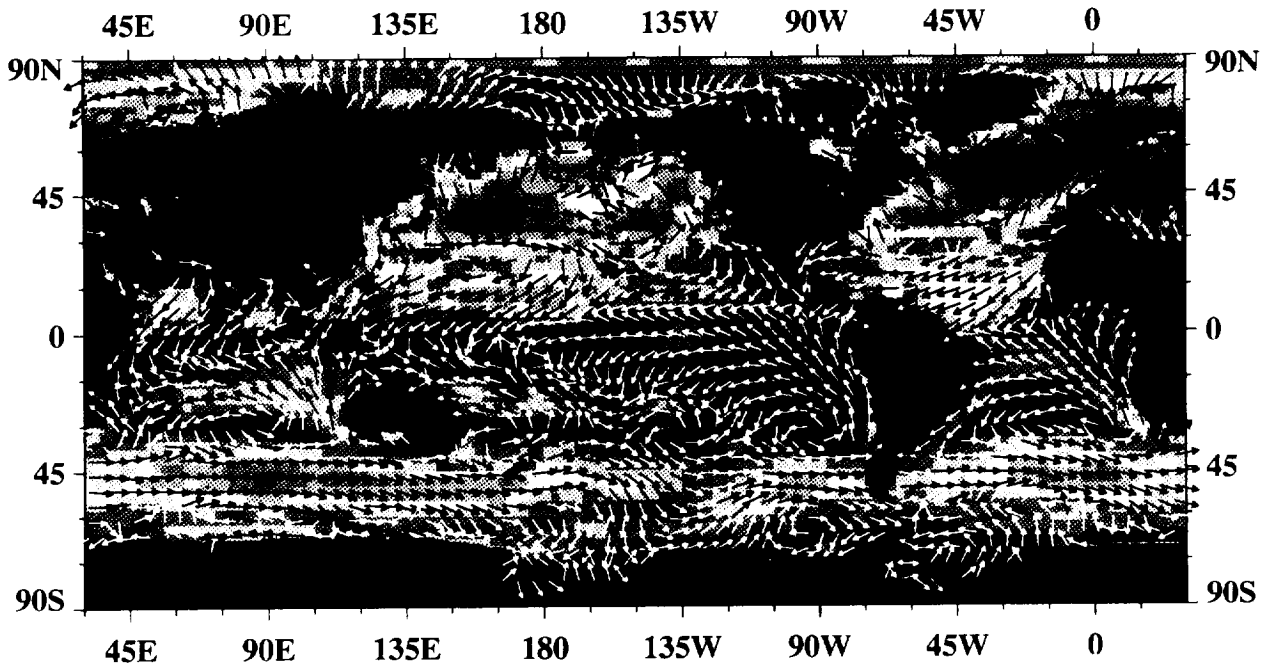

January 1993

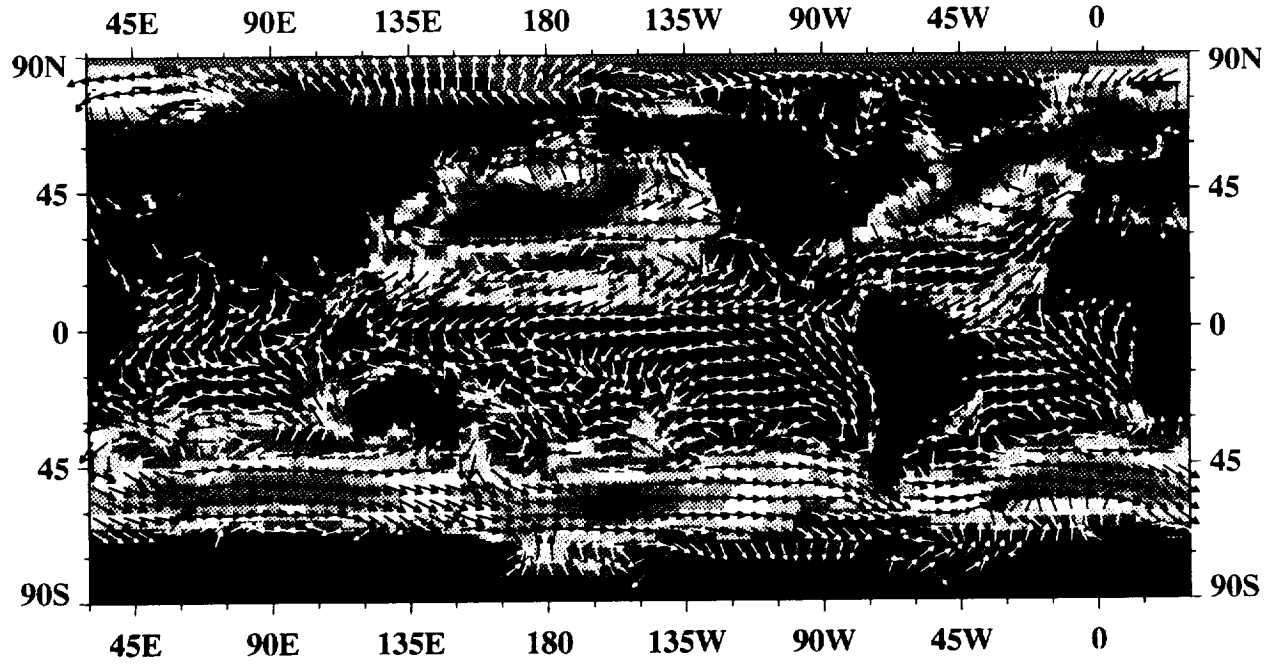

February 1993

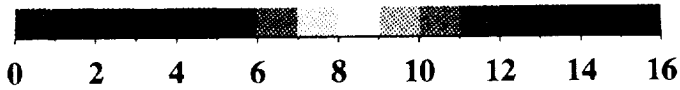

ECMWF 10 m Wind Speed, m s^{-1}

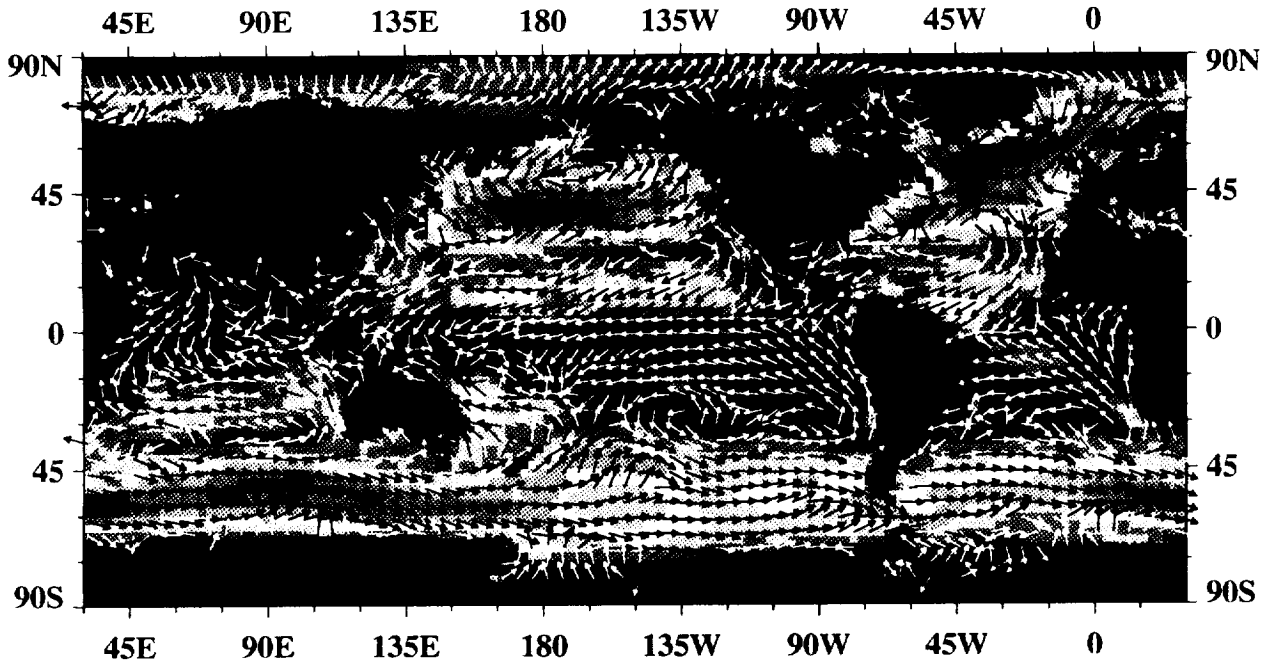

March 1993

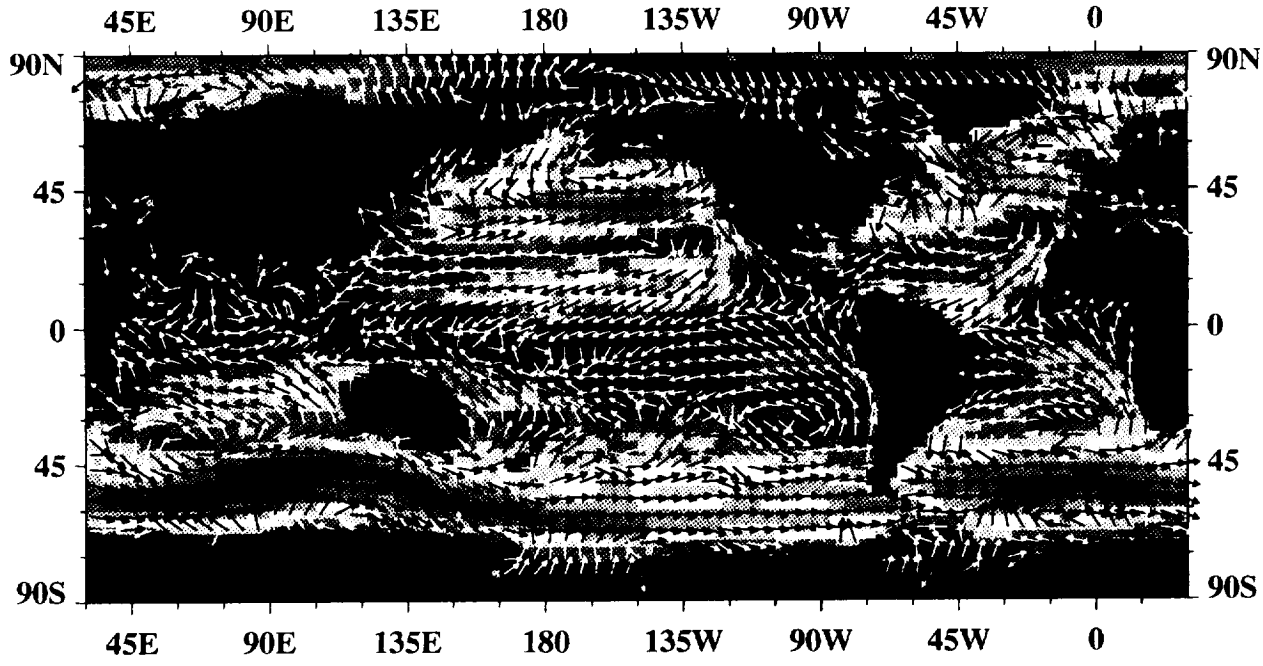

April 1993

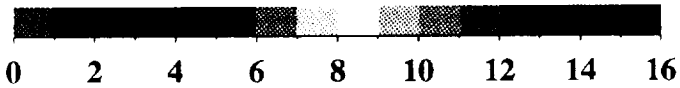

ECMWF 10 m Wind Speed, m s^{-1}

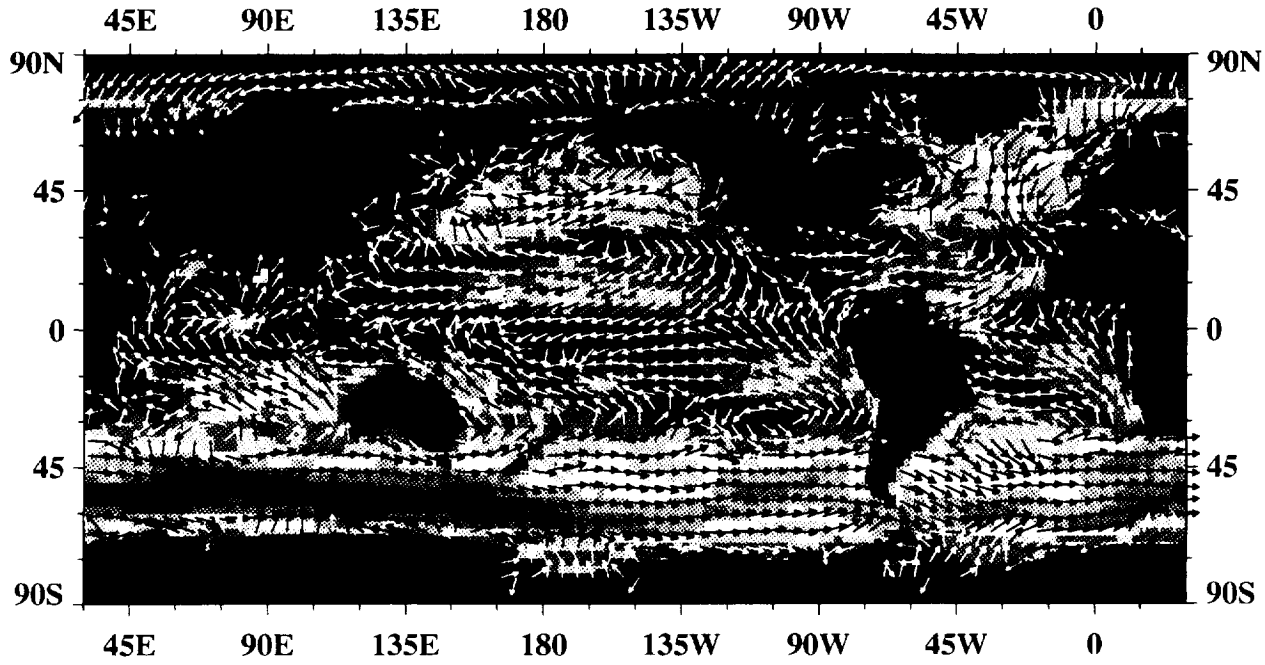

May 1993

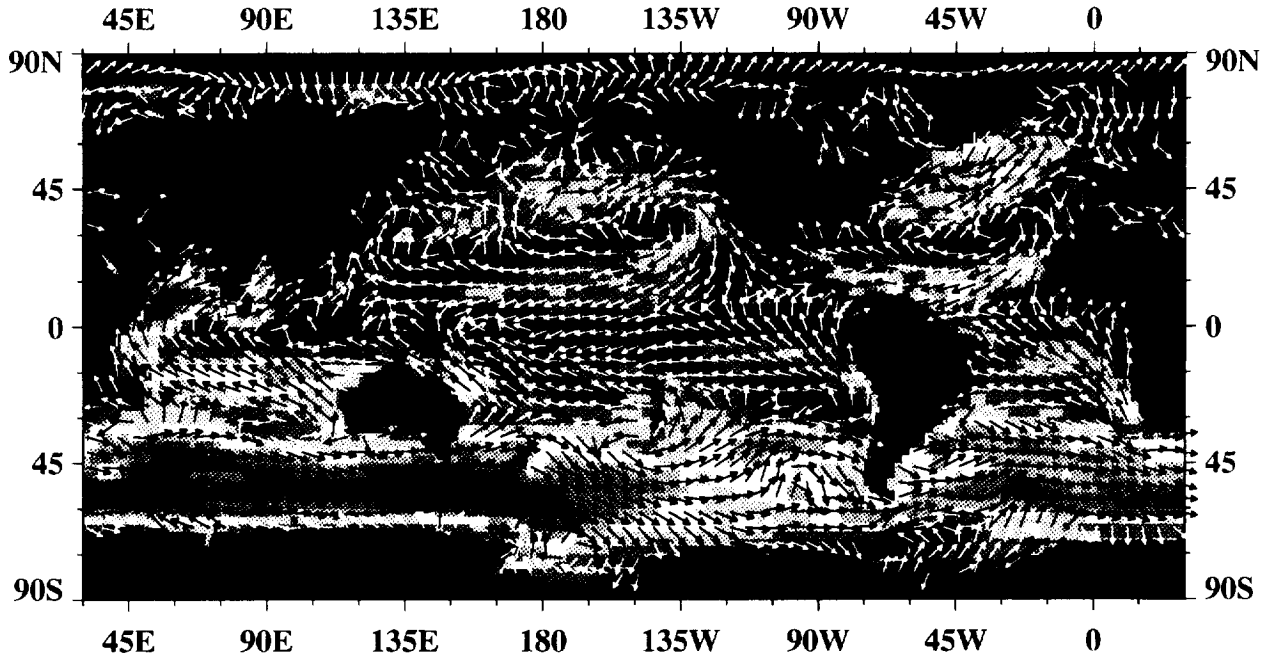

June 1993

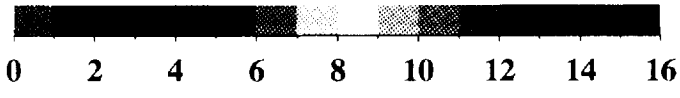

ECMWF 10 m Wind Speed, m s^{-1}

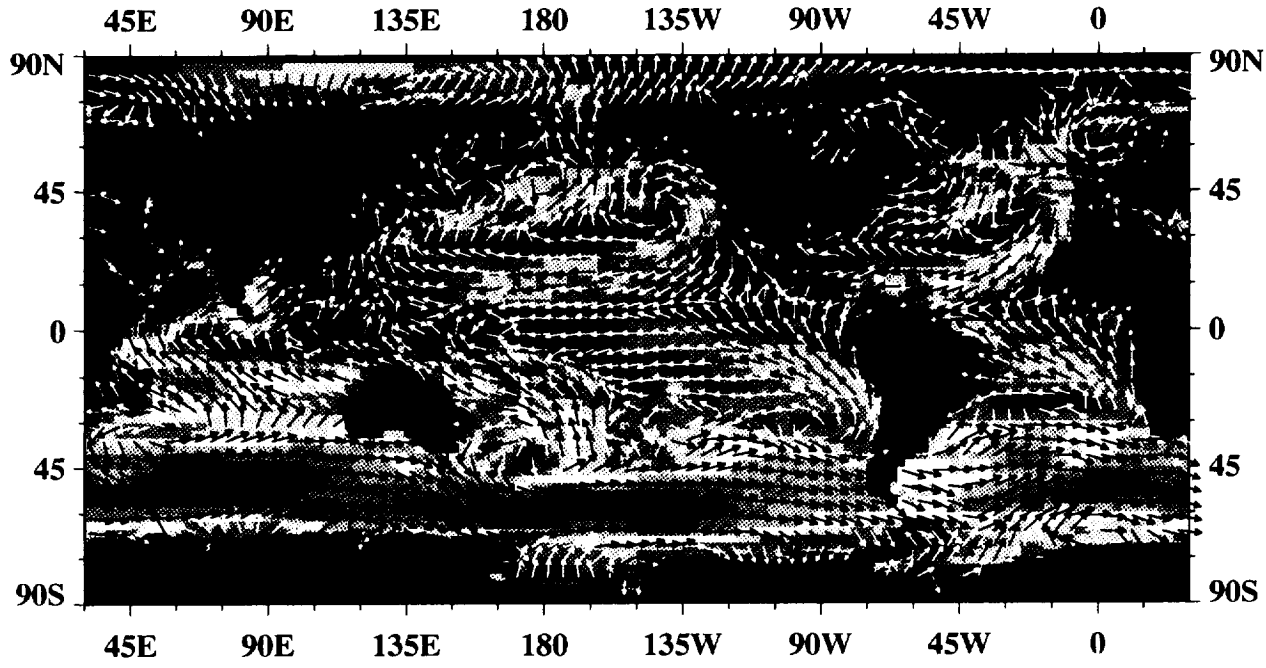

July 1993

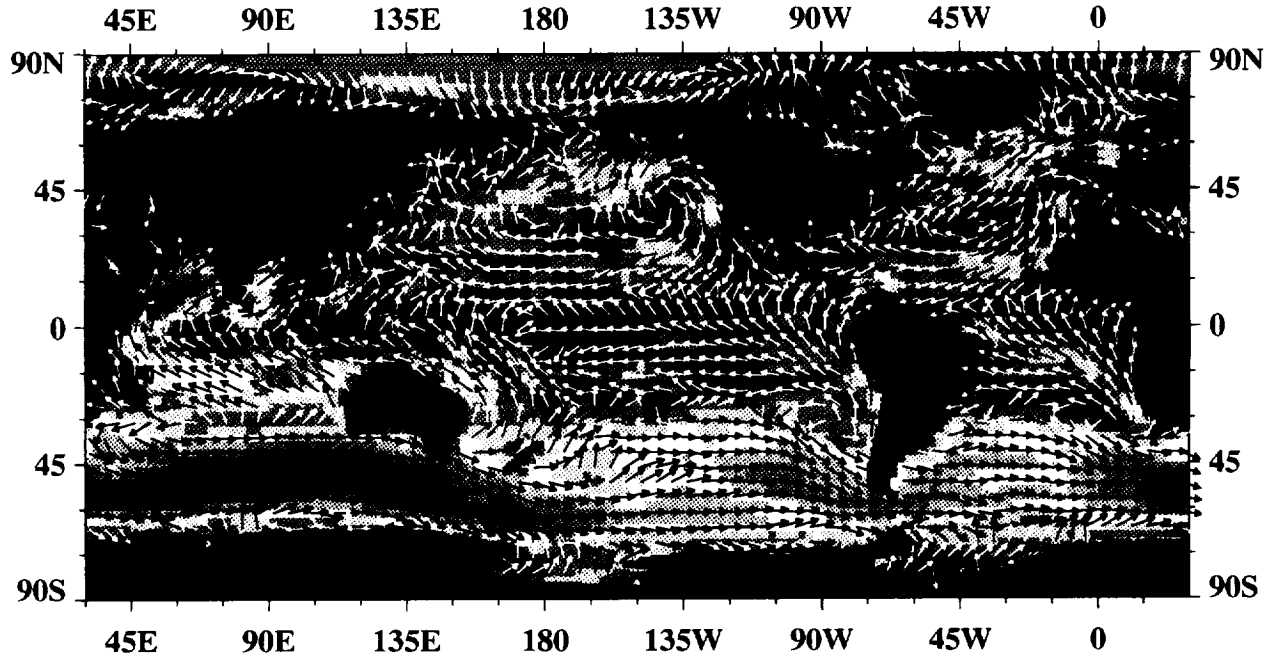

August 1993

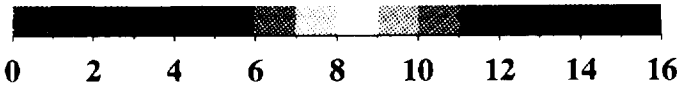

ECMWF 10 m Wind Speed, m s^{-1}

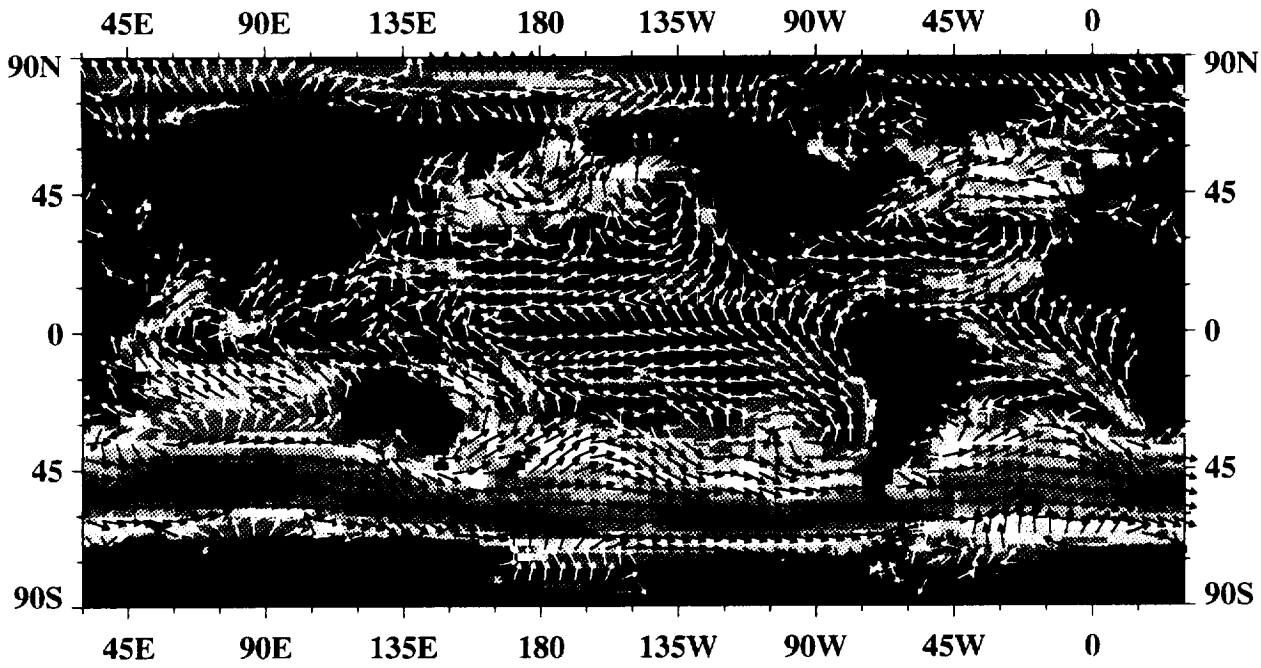

September 1993

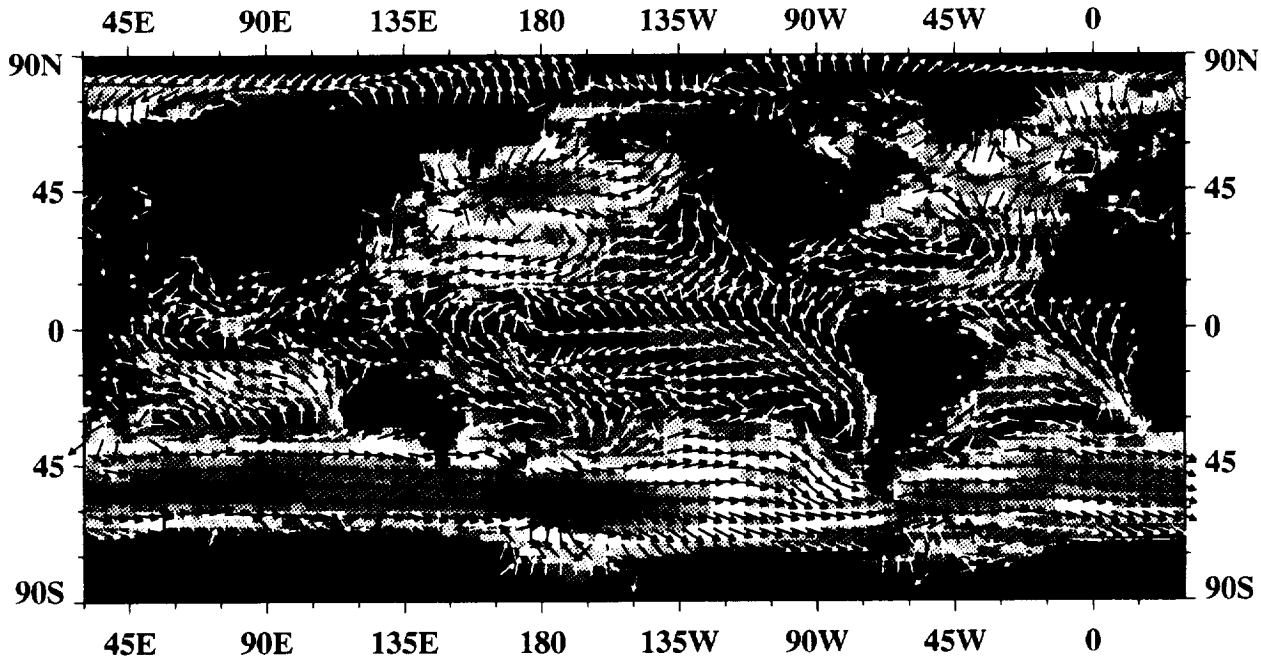

October 1993

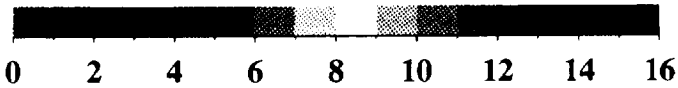

ECMWF 10 m Wind Speed, m s^{-1}

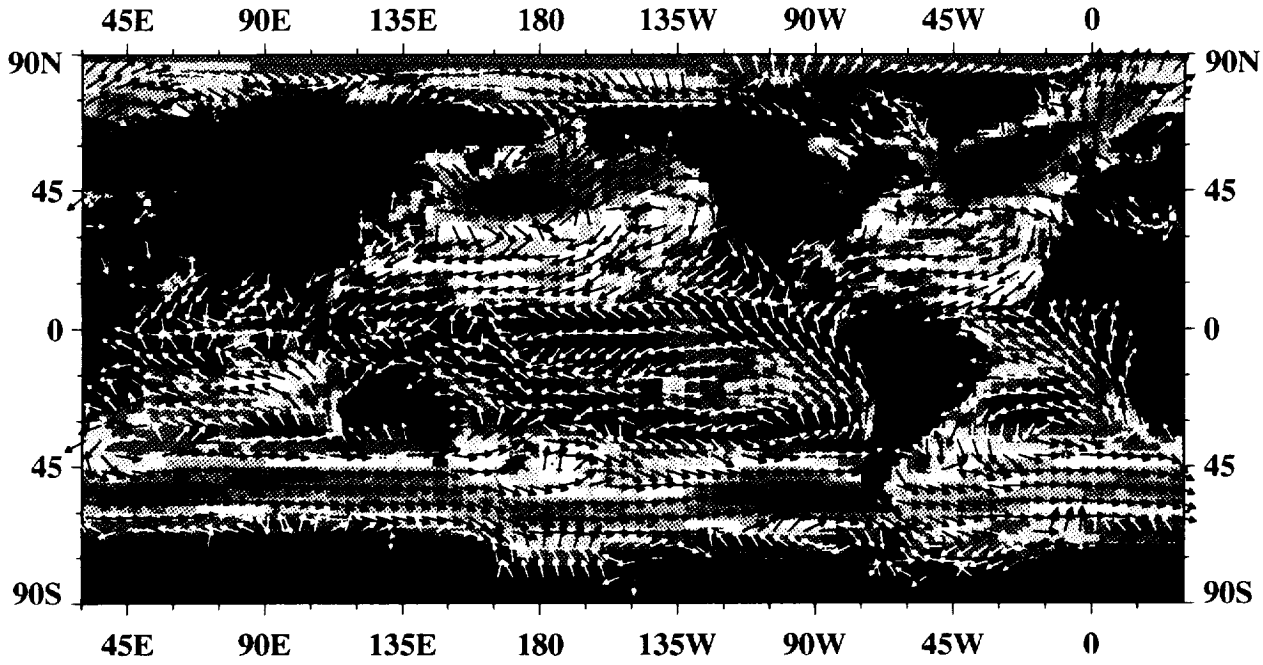

November 1993

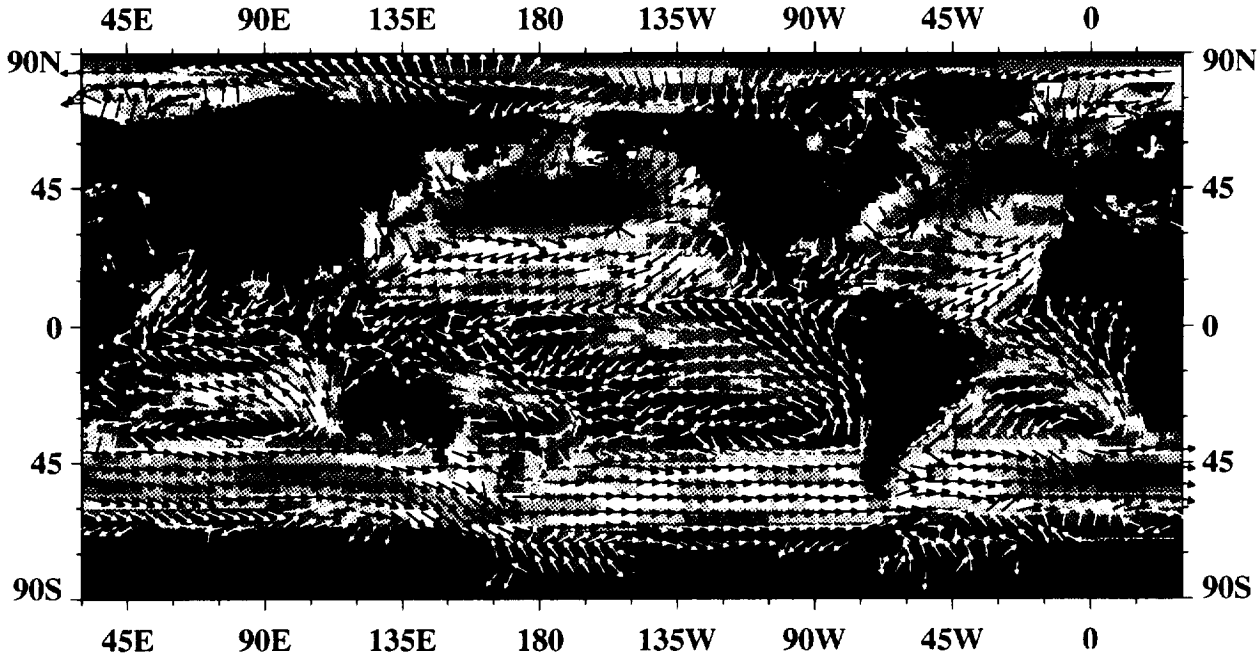

December 1993

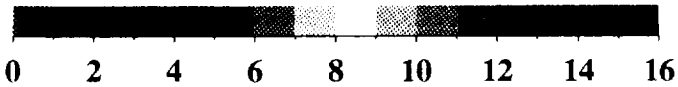

ECMWF 10 m Wind Speed, m s^{-1}

TECHNICAL REPORT STANDARD TITLE PAGE

1. Report No. JPL Pub. 95-3	2. Government Accession No.	3. Recipient's Catalog No.
4. Title and Subtitle An Atlas of Monthly Mean Distributions of SSMI Surface Wind Speed, AVHRR/2 Sea Surface Temperature, AMI Surface Wind Velocity, TOPEX/POSEIDON Sea Surface Height, and ECMWF Surface Wind Velocity During 1993		5. Report Date January 1995 6. Performing Organization Code
7. Author(s) D. Halpern, L. Fu, W. Knauss, G. Pihos, O. Brown, M. Freilich, and F. Wentz		8. Performing Organization Report No.
9. Performing Organization Name and Address JET PROPULSION LABORATORY California Institute of Technology 4800 Oak Grove Drive Pasadena, California 91109		10. Work Unit No. 11. Contract or Grant No. ~~NAS7-918~~ ~~XXXXXXXX~~ NAS7-1260 13. Type of Report and Period Covered JPL Publication
12. Sponsoring Agency Name and Address NATIONAL AERONAUTICS AND SPACE ADMINISTRATION Washington, D.C. 20546		14. Sponsoring Agency Code RF 4 BP57822260100
15. Supplementary Notes		

16. Abstract

The following monthly mean global distributions for 1993 are presented with a common color scale and geographical map: 10-m height wind speed estimated from the Special Sensor Microwave Imager (SSMI) on a United States (U.S.) Air Force Defense Meteorological Satellite Program (DMSP) spacecraft; sea surface temperature estimated from the Advanced Very High Resolution Radiometer (AVHRR/2) on a U.S. National Oceanic and Atmospheric Administration (NOAA) satellite; 10-m height wind speed and direction estimated from the Active Microwave Instrument (AMI) on the European Space Agency (ESA) European Remote Sensing (ERS-1) satellite; sea surface height estimated from the joint U.S.-France Topography Experiment (TOPEX)/POSEIDON spacecraft; and 10-m heigh wind speed and direction produced by the European Center for Medium-Range Weather Forecasting (ECMWF). Charts of annual mean, monthly mean, and sampling distributions are displayed.

17. Key Words (Selected by Author(s))	18. Distribution Statement
Geosciences and Oceanography (General) Meteorology and Climatology Physical Oceanography	Unclassified - Unlimited

19. Security Classif. (of this report)	20. Security Classif. (of this page)	21. No. of Pages	22. Price
Unclassified	Unclassified	88	